ELECTROSPUN BIOMIMETIC AND PHOTOSENSITIVE NANOFIBROUS SCAFFOLD FOR SKIN TISSUE ENGINEERING

JIN GUORUI
(Bachelor of Engineering, Harbin Institute of Technology, China)

A THESIS SUBMITTED

FOR THE DEGREE OF DOCTOR OF PHILOSOPHY

DEPARTMENT OF MECHANICAL ENGINEERING

NATIONAL UNIVERSITY OF SINGAPORE

2013

Declaration

I hereby declare that this thesis is my original work and it has been written by me in its entirety. I have duly acknowledged all the sources of information which have been used in the thesis.

This thesis has also not been submitted for any degree in any university previously.

Jin Guorui

19 August 2013

Acknowledgement

First of all, I would like to give my sincere thanks to Prof. Seeram Ramakrishna, for his tremendous encouragement and excellent supervision during my PhD study. His foresight of frontier science, his wisdom and enthusiasm, his positive attitude and hard-working spirit always inspired and encouraged me throughout my four-year research life.

My special thank is to Dr. Molamma P Prabhakaran, who has provided many valuable suggestions and patient guidance during my PhD study. Dr. Molamma helped me in my academic research whenever I needed. My special appreciation is to Dr. Susan Liao, who has provided much patient tutorship during the beginning of my PhD study. Dr. Susan Liao also helped me in my daily life whenever I needed.

My thanks are extended to all other members in the Centrer for Nanofiber & Nanotechnology Laboratory: to Ms. Charlene Wang and Mr. Teo Wee Eong who introduced me the basic methods and techniques in cell culture and electrospinning; to Mr. Kai Dan, Ms. Rajeswari Ravichandran, Ms. Su Yan, Ms. Luong TH Nguyen, Ms. Tian Lingling, Ms. Jia Lin, Ms. Shayanti Mukherjee, Mr. Nair, A. Sreekumaran, Dr. Gopal and Mr. A. Gora for their invaluable advices, discussions and suggestions. My special thanks to Ms. Zhao Jing for her kindly help, discussions during my release studies. To lab officer: Charlene Wang and for her good maintenance and great contribution to the laboratory and their timely help throughout the course of my PhD study.

And especially, I would like to express my gratitude to Prof. Tian Weiming and Mr. Li Yong who have input brilliant insights and provided great assistance in my animal study. Besides, I would like to extend my thanks to all my other friends in the lab: Wu Yongzhi, Peng Shengjie, Zhu Peining, He Liuming *et al.* for their precious friendship and help during my PhD studies.

Last, I would like to give the highest thanks to my parents and brother for their constant love, care and support during my study.

Publications

Journal Papers

1. **Guorui Jin**, Prabhakaran MP, Ramakrishna S. Photosensitive and biomimetic core-shell nanofibrous scaffolds as wound dressing. *Photochem. Photobiol. 2014 (accepted)*
2. **Guorui Jin**, Molamma P Prabhakaran, Kai Dan, Seeram Ramakrishna. Controlled release of multiple epidermal induction factors through core-shell nanofibers for skin regeneration. *Eur. J. Pharm. Biopharm. 2013*
3. **Guorui Jin**, Molamma P Prabhakaran, Dan Kai, Sathesh Kumar Annamalai, Kantha D. Arunachalam, Seeram Ramakrishna. Tissue engineered plant extracts as nanofibrous wound dressing. *Biomaterials. 2012, 34(3):724-734.*
4. **Guorui Jin**, Molamma P Prabhakaran, Kai Dan, Seeram Ramakrishna. Electrospun photosensitive nanofibers: Potential for photocurrent therapy in skin regeneration. *Photochem Photobiol Sci. 2012, 12(1):124-34.*
5. **Guorui Jin**, Molamma P Prabhakaran, Dan Kai, Seeram Ramakrishna. Electrospun Silver nanoparticles containing PLLCL nanofibers for skin tissue engineering. *J Biomater Sci Polym Ed. 2012 Jan 12*
6. **Guorui Jin**, Molamma P Prabhakaran, Seeram Ramakrishna. Mesenchymal stem cell differentiation to epidermal lineages on electrospun nanofibrous substrates for skin tissue engineering. *Acta Biomateria, 2011 Aug;7(8):3113-22*
7. **Guorui Jin**, Molamma P. Prabhakaran, Susan Liao, Seeram Ramakrishna. Photosensitive materials and potential of photocurrent mediated tissue regeneration. *J Photoch Photobio B, 2011, 102, 93-101*
8. Dan Kai, **Guorui Jin**, Molamma P Prabhakaran, Seeram Ramakrishna. Electrospun synthetic and natural nanofibers for regenerative medicine and stem cells. *Biotechnol J, 2013, 8(1):59-72.*
9. Kai Dan, Molamma P Prabhakaran, **Guorui Jin**, Seeram Ramakrishna. Biocompatibility evaluation of electrically conductive nanofibrous scaffolds for cardiac tissue engineering. *J. Mater. Chem. B, DOI: 10.1039/C3TB00151B*
10. Elham Vatankhah, Molamma P Prabhakaran, **Guorui Jin**, Seeram Ramakrishna.

Development of nanofibrous Cellulose acetate/gelatin skin substitutes for variety wound treatment applications. *J. Biomater. Appl. 2013, doi: 10.1177/0885328213486527*

11. L. Ghasemi-Mobarakeh, M.P. Prabhakarn, Preethi, **Guorui Jin** et al. Advance in electrosupun nanofibers for bone and cartilage regeneration. *J Nanosci Nanotechnol, 2012, accepted*
12. M.P. Prabhakaran, J. Venugopal, L. Ghasemi-Mobarakeh, D. Kai, **Guorui Jin**, S. Ramakrishna. Stem cells and nanostructures for advanced tissue regeneration. *Adv Polym Sci, 2011, 12, 113*
13. Dan Kai, Molamma P Prabhakaran, **Guorui Jin**, Seeram Ramakrishna. Guided orientation of cardiomyocytes on electrospun aligned nanofibers for cardiac tissue engineering. *J Biomed Mater Res B, 2011 Aug;98B(2):379-86*
14. Su Yan, Su Qianqian, Liu Wei, **Guorui Jin**, Mo Xiumei, Ramakrishna Seeram. Dual-Drug Encapsulation and Release from Core–Shell Nanofiber. *J Biomater Sci Polym Ed. 2011 Mar 18*
15. M.P. Prabhakaran, L. Ghasemi-Mobarakeh, **Guorui Jin**, S. Ramakrishna. Electrospun conducting polymer nanofibers and electrical stimulation of nerve stem cells. *J Biosci Bioeng. 2011 Nov;112(5):501-7*
16. Kai D, Prabhakaran MP, **Guorui Jin**, Ramakrishna S. Polypyrrole-contained electrospun conductive nanofibrous membranes for cardiac tissue engineering. *J Biomed Mater Res A. 2011 Dec 1;99(3):376-85*

Conferences

1. **Guorui Jin**, M.P. Prabhakaran, S. Ramakrishna. Electrospun photosensitive nanofibers promote human dermal fibroblast proliferation. Oral presented at *The 4th Asian Biomaterials Congress*, Hong Kong, 2013.
2. **Guorui Jin**, Molamma P Prabhakaran, Seeram Ramakrishna. Keratinocyte lines derived from mesenchymal stem cell on electrospun nanofibrous substrates for skin tissue engineering. *MRS-S Trilateral Conference August 2010 Singapore*.

Table of contents

Acknowledgement

Table of contents..... VI

Summary..... X

List of Tables XII

List of Figures..... XIII

List of Abbreviations XVII

Chapter 1 Introduction 1

1.1 Background 1

1.2 Motivation 2

1.3 Hypothesis and objectives 5

1.4 Research rationale and strategy 6

1.5 Work scope 8

Chapter 2 Literature Review 12

2.1 Introduction 12

2.1.1 Skin composition and functions 12

2.1.1.1 Keratinocyte maturation 14

2.1.1.2 Keratins 15

2.1.1.3 Non-keratins 18

2.1.2 Wound healing *in vivo* 18

2.2 Full-thickness skin wounds 19

2.2.1 Current treatments for full-thickness skin wounds 20

2.2.1.1 Autografts, allografts and xenografts 21

2.2.1.2 Tissue-engineered skin grafts 21

2.2.1.2.1 Commercialized tissue-engineered skin grafts 23

2.2.1.2.1.1 Dermo-Epidermal (Composite) skin substitutes 23

2.2.1.2.1.2 Dermal skin substitutes 24

2.2.1.2.1.3 Epidermal skin substitutes 25

2.2.1.2.2 Drawbacks of current commercialized skin grafts 25

2.2.2 Potential of photocurrent therapy for wound healing and skin regeneration 29

2.2.2.1 Phototherapy 29

2.2.2.2 Electrotherapy 31

2.2.2.3 Photocurrent therapy 33
2.2.3 Potential of human adipose-derived stem cells (ASCs) for skin regeneration 34
2.2.3.1 Characteristics of human ASCs 35
2.2.3.2 Contributions of human ASCs in wound healing and skin regeneration 37
2.2.4 Potential of electrospun nanofibrous scaffolds (NFS) as tissue-engineered skin grafts 38
2.2.4.1 NFS as tissue-engineered scaffolds 38
2.2.3.2 Fabrication of NFS by electrospinning 39
2.2.3.3 Electrospun NFS as tissue-engineered skin grafts 42
2.3 Summary 46
Chapter 3 Fabrication and optimization of cost-effective nanofibrous scaffolds for in vivo wound healing 47
3.1 Introduction 47
3.2 Materials and methods 49
3.2.1 Materials 49
3.2.2 Electrospinning of nanofibers 49
3.2.3 Morphology and characterization of electrospun nanofibers 50
3.2.4 Culture of HDFs 51
3.2.5 Cell proliferation 51
3.2.6 F-actin staining 51
3.2.7 Expression of collagen 52
3.2.8 Surgical procedures 52
3.2.9 Histological and immunological analyses 53
3.2.10 Statistical analysis 53
3.3 Results and discussions 53
3.3.1 Morphology and characterization 54
3.3.2 HDF proliferation on electrospun nanofibers 58
3.3.3 Cell morphology on nanofibers 60
3.3.4 Collagen expression 61
3.3.5 Wound size measurements 62
3.3.6 Histological analysis 63
3.4 Conclusion 64
Chapter 4 Stem cell epidermal differentiation on multiple epidermal induction factors encapsulated core-shell nanofibers 66

4.1 Introduction 66
4.2 Materials and Methods 68
4.2.1 Materials 68
4.2.2 Electrospinning of nanofibers 69
4.2.3 Morphology and characterization of electrospun nanofibers 70
4.2.4 Culture of ASCs on the scaffolds 71
4.2.5 Drug release study 71
4.2.6 Cell proliferation assay 72
4.2.7 Induction of ASCs towards the epidermal lineage 72
4.2.8 Immunostaining analysis of differentiated ASCs 73
4.2.9 Morphology of differentiated ASCs 73
4.2.10 Statistical analysis 74
4.3 Results and discussion 74
4.3.1 Morphology, chemical and mechanical characterization of electrospun nanofibers 75
4.3.2 Drug release study 80
4.3.3 ASCs proliferation on electrospun nanofibers 81
4.3.4 Induced epidermal morphology 81
4.4 Conclusion 85
Chapter 5 Electrospun photosensitive nanofibers for photocurrent therapy in skin regeneration 87
5.1 Introduction 87
5.2 Materials and Methods 89
5.2.1 Materials 89
5.2.2 Electrospinning of PCL/P3HT nanofibers 89
5.2.3 Characterization 89
5.2.4 Human dermal fibroblast culture 90
5.2.5 Light stimulation 90
5.2.6 F-actin staining 92
5.2.7 Expression of collagen 92
5.2.8 Statistical analysis 92
5.3 Results and discussion 92
5.3.1 UV-vis spectra 92
5.3.2 Morphology and characterization 93
5.3.3 Photovoltaic study 96

5.3.4 Light stimulation 97
5.3.5 F-actin staining 102
5.3.6 Collagen expression 103
5.4 Conclusions 105
Chapter 6 Electrospun biomimetic and photosensitive core-shell nanofibrous scaffolds for skin regeneration 106
6.1 Introduction 106
6.2 Materials and Methods 108
6.2.1 Materials 108
6.2.2 Electrospinning of nanofibers 108
6.2.3 Characterization of electrospun nanofibers 109
6.2.4 Light stimulation conditions 109
6.2.5 Culture of HDFs and proliferation 110
6.2.6 *In vitro* wound healing on Gel/PLLCL/P3GF(cs) nanofibrous scaffold 111
6.2.7 Epidermal differentiation of ASCs on photosensitive scaffolds 111
6.2.8 Immunostaining analysis of differentiated ASCs 111
6.2.9 Statistical analysis 112
6.3 Results and discussion 112
6.3.1 Morphology, chemical and mechanical characterization of electrospun nanofibers 113
6.3.2 Light stimulative effect 116
6.3.3 *In vitro* wound healing 117
6.3.4 Epidermal differentiation of ASCs on photosensitive core-shell nanofibers 119
6.4 Conclusion 121
Chapter 7 Conclusions and Recommendations 123
7.1 Main conclusions 123
7.2 Recommendations for future work 124
Reference 127

Summary

Burn injuries, chronic wounds (venous, pressure and leg ulcers), excision of skin and tumors are the main forms of skin damage. The full-thickness skin loss caused by these damages is not adequately addressed by current methods of wound coverage. Split-thickness skin autografts still represent the “gold standard” treatment to resurface the deep wounds. However, in patients with very large total body surface area wounds, insufficient donor sites for autografting complicate wound closure, which can compromise recovery, increase the risk of invasive wound infection and mortality. Tissue engineering has emerged as a new and promising field for the treatment of skin lesions, combining scaffolds, cells and biomolecular signals, such as growth factors. The tissue engineered skin grafts are being applied to overcome the problem of insufficient autografts. However, a critical issue of tissue engineered scaffold is the ex *vivo* cell expansion which is required to obtain sufficient numbers of the needed cells, while preserving the cells' normal phenotype and functionality within a short time. Interestingly, light and electrical stimulations were found to promote cell proliferation. In this project, it is hypothesized that tissue-engineered skin grafts composed of cost-effective and biodegradable nanofibrous scaffolds (NFS) enriched with growth factor, photosensitive polymer and adipose-derived stem cells (ASCs) can promote wound healing and skin regeneration in acute full-thickness skin wounds.

Composite gelatin/poly(L -lactic acid)–co-poly(ε-caprolactone) (Gel/PLLCL) nanofibers with four different weight ratios of gelatin:PLLCL (w/w) of 80:20 [Gel/PLLCL(80)], 70:30 [Gel/PLLCL(70)], 60:40 [Gel/PLLCL(60)] and 50:50 [Gel/PLLCL(50)] were successfully fabricated with electrospinning technique. It demonstrated that the Gel/PLLCL(60) naonfibers which had small pore size, proper mechanical properties both in wet and dry conditions and higher cell proliferation was the optimized nanofibrous scaffold for skin tissue engineering. The wound healing performance of Gel/PLLCL(60) was further evaluated *in vivo*. A faster wound healing and better reepithelialization were achieved by using the cost-effective Gel/PLLCL(60) NFS.

A few major epidermal induction factors (EIF) were successfully incorporated into polymeric core-shell nanofibers and the results of the release studies demonstrated that the core-shell nanofibers achieved sustained release without burst release. The differentiation potential of ASCs into epidermal lineage on core-shell NFS was confirmed and the expression of early and intermediate epidermal differentiation markers was observed. With sustained release of EIF from core-shell nanofibers, the percentage of epidermally differentiated ASCs on core-shell nanofibers (62%) was significantly higher than that on EIF blended nanofibers (43%).

The optimized photosensitive poly(3-hexylthiophene) (P3HT) containing poly(ε-caprolactone) (PCL) nanofibrous scaffolds were fabricated by electrospinning. Photocurent generation in electrospun PCL/P3HT nanofibers was confirmed. Fibroblast proliferation on PCL/P3HT and PCL nanofibrous scaffolds under light stimulation was studied and the results suggestted that fibroblasts cultured on PCL/P3HT after light stimulation had better proliferation and morphology than fibroblasts cultured on electrospun PCL nanofibers. Electrospun PCL/P3HT nanofibrous scaffold was capable of supporting cell proliferation and favoring cell ECM secretion.

Epidermal growth factor (EGF) and photosensitive polymer P3HT were encapsulated into electrospun core-shell NFS. Fibroblast proliferation was significantly improved on EGF encapsulated nanofibers and photosensitive P3HT in the core-shell nanofibers can further promoted fibroblast proliferation under light stimulation. Keratinocyte-like ASCs were only found on the light stimulated EGF and P3HT encapsulated core-shell nanofibers. The expression of early epidermal differentiation markers was observed. Moreover, this core-shell nanofibrous scaffold was found to accelerate *in vitro* wound healing. Therefore, the biomimetic and photosensitive core-shell nanofibers could be a novel scaffold applied in photocurrent therapy for wound healing and skin construction. Our study sheds light on a novel way for wound healing - photocurrent therapy.

List of Tables

Table 1.1 Overview of project scope.

Table 2.1 Keratin markers expressed in different human epithelial types [52].

Table 2.2 Examples of current commercialized tissue-engineered skin substitutes with associated advantages and disadvantages.

Table 2.3 Phototherapy applied in the field of wound healing.

Table 2.4 Immunophenotype of passaged human ASCs [152].

Table 2.5 Effect of changing electrospinning process parameters on the resultant fiber morphology [171].

Table 3.1 Tensile properties of the electrospun nanofibers in both dry and wet conditions.

Table 4.1 Tensile properties of the electrospun nanofibers.

Table 6.1 Tensile properties of the electrospun nanofibers.

List of Figures

Fig. 2.1 Structure of skin [46].

Fig. 2.2 The structures of stratified epidermis [53].

Fig. 2.3 Number of journal publications in tissue engineering.

Fig. 2.4 Schematic illustration of photocurrent stimulation in regenerative medicine [134].

Fig. 2.5 Multilineage differentiation potential for adipose-derived stem cells [160].

Fig. 2.6 The scheme of electrospinning system [14].

Fig. 3.1 **Characterizations of electrospun nanofibers. a**. SEM morphology of Gel/PLLCL/(80), Gel/PLLCL/(70), Gel/PLLCL/(60), Gel/PLLCL/(50) and PLLCL nanofibers. **b**. Water contact angle for electrospun nanofibers. **c**. FTIR spectra of Gel/PLLCL/(80), Gel/PLLCL/(70), Gel/PLLCL/(60), Gel/PLLCL/(50) and PLLCL nanofibers. **d**. Morphological changes of Gel/PLLCL/(80), Gel/PLLCL/(70), Gel/PLLCL/(60) and Gel/PLLCL/(50) nanofibers after degradation in PBS for 5, 10 and 15 days.

Fig. 3.2 Typical stress-strain curves of random Gel/PLLCL/(80), Gel/PLLCL/(70), Gel/PLLCL/(60), Gel/PLLCL/(50) and PLLCL nanofibrous scaffolds in dry and wet conditions.

Fig. 3.3 HDFs proliferation on electrospun Gel/PLLCL/(80), Gel/PLLCL/(70), Gel/PLLCL/(60), Gel/PLLCL/(50) and PLLCL nanofibers. *Significant against cell proliferation on PLLCL at $p \leq 0.05$; $^{\blacklozenge}$Significant against cell proliferation on Gel/PLLCL/(80), Gel/PLLCL/(70) and Gel/PLLCL/(50) nanofibers.

Fig. 3.4 SEM images of HDFs on Gel/PLLCL/(60), PLLCL and TCP.

Fig. 3.5 Dual immunocytochemical analysis for the expression of F-actin, vinculin and the merged images showing the dual expression of both F-actin and vinculin on electrospun Gel/PLLCL/(60), PLLCL nanofibers and TCP.

Fig. 3.6 Collagen staining on nanofibrous scaffolds: (A) Gel/PLLCL(60), (B) PLLCL and (C) TCP.

Fig. 3.7 Wound size measurements and appearances at different time points. (I) Percentages of unepithelialized wound area in different groups from day 1 to 14. (II) Appearances of wounds in different groups on days 0 and 10.

Fig. 3.8 Hematoxylin and eosin staining in different groups on days 5 and 10. Scale bars: 200 mm (low magnification), 100 mm (high magnification). F, fibrinous debris; N, neutrophils; C, capillary; S, sebaceous gland; E, epithelialization.

Fig. 4.1 **Characterizations of electrospun nanofibers.** SEM morphology of (A) Gel/PLLCL/EIF(cs), (B) Gel/PLLCL/EIF(b), (C) Gelatin/PLLCL and (D) PLLCL nanofibers. TEM micrographs of (E) Gel/PLLCL/EIF(cs), (F) Gel/PLLCL/EIF(b) and fluorescence microscopic images of (G) Gel/PLLCL/EIF(cs) with FITC-dextran in the core, (H) Gel/PLLCL/EIF(b) with FITC-dextran stained all over the fibers. (I) FTIR spectra of Gel/PLLCL/EIF(cs), Gel/PLLCL/EIF(b), Gelatin/PLLCL and PLLCL nanofibers. (J) Stress-strain curve of the electrospun nanofibers.

Fig. 4.2 Release profiles of electrospun nanofibers and their effect on proliferation of ASCs. (A) Morphological changes of Gel/PLLCL/EIF(cs), Gel/PLLCL/EIF(b), Gelatin/PLLCL and PLLCL nanofibers after degradation in PBS for 5, 10 and 15 days. (B) Release profiles of EGF from Gel/PLLCL/EIF(cs) and Gel/PLLCL/EIF(b). (C) ASCs proliferation on electrospun Gel/PLLCL/EIF(cs), Gel/PLLCL/EIF(b), Gelatin/PLLCL and PLLCL nanofibers. *Significant against cell proliferation on PLLCL at $p \leq 0.05$; ◆ Significant against cell proliferation on Gel/PLLCL/EIF(b) and Gelatin/PLLCL nanofibers.

Fig. 4.3 Protein expression and cell morphology studies. (A) Laser scanning confocal microscope (LSCM) image of undifferentiated ASCs stained with CD 105 on TCP and SEM image showing the cell morphology, observed on day 15. (B) Two dimensional immunostaining images show the expression of Ker 10, filaggrin and the merged image on electrospun Gel/PLLCL/EIF(cs), Gel/PLLCL/EIF(b) at 60 × magnification. (C) Three dimensional immunostaining images show a filamentous cytoplasmic distribution of Ker 10 (red) and filaggrin (green). (D) SEM images of epidermally differentiated ASCs on Gel/PLLCL/EIF(cs) and Gel/PLLCL/EIF(b); undifferentiated ASCs on Gelatin/PLLCL, PLLCL and TCP.

Fig. 4.4 Dual immunocytochemical analysis for the expression of Ker 10, CD 105 and merged image showing the dual expression of both CD 105 and Ker 10 on (A-D) Gel/PLLCL/EIF(cs); (E-H) Gel/PLLCL/EIF(b); (I-L) Gelatin/PLLCL; (M-P) PLLCL and (Q-T) TCP at 20 × magnification.

Fig. 5.1 Schematic explanation of the method used for light irradiation on cell-scaffold constructs. PCL (white) and P3HT containing nanofibrous scaffolds (purple) were put in 24 well plates and directly located under LED.

Fig. 5.2 UV-Visible absorption spectra of pure PCL, PCL/P3HT(2), PCL/P3HT(10), and PCL/P3HT(20) solutions dispersed in chloroform and methanol (75/25 v/v). The concentration of each solution was 9 % (w/v).

Fig. 5.3 SEM images of electrospun (A) PCL/P3HT(2), (B) PCL/P3HT(10), (C)

PCL/P3HT(20) and (D) PCL nanofibers and pore size distribution of i) PCL/P3HT(2), ii) PCL/P3HT(10), iii) PCL/P3HT(20) and iv) PCL nanofibers.

Fig. 5.4 PL spectra for PCL, PCL/P3HT(2), PCL/P3HT(10) and PCL/P3HT(20) under excitation beam of 380 - 400 nm.

Fig. 5.5 (A) J-V graph of the PCL/P3HT(2), PCL/P3HT(10) and PCL/P3HT(20) photosensitive scaffolds measured under 1 Sun conditions. (B) the resonant structures, (i) aromatic and (ii) quinoid, of poly (3-alkylthiophenes) chains.

Fig. 5.6 (A) HDF proliferation on electrospun PCL, PCL/P3HT(2), PCL/P3HT(10) and PCL/P3HT(20) nanofibrous scaffolds stimulated (S) compared to HDF proliferation on electrospun PCL/P3HT(2), PCL/P3HT(10), PCL/P3HT(20) and PCL nanofibrous scaffolds non-stimulated (NS) by MTS assay. *Significant against cell proliferation on TCP (NS) at $p \leq 0.05$; ◆Significant against cell proliferation on PCL/P3HT(2) (S) at $p \leq 0.05$. #Significant against cell proliferation on PCL/P3HT(20) (S) at $p \leq 0.05$. ※ Significant against cell proliferation on PCL/P3HT(10) (NS) at $p \leq 0.05$. ▼Significant against cell proliferation on PCL/P3HT(10) and PCL (S) at $p \leq 0.05$. ☆Significant against cell proliferation on PCL/P3HT(10) and PCL (NS) at $p \leq 0.05$. (B) Growth rate of cells on stimulated PCL/P3HT(2), PCL/P3HT(10), PCL/P3HT(20), PCL and TCP with respect to the non-stimulated scaffolds on day 2, day 4 and day 6.

Fig. 5.7 SEM images of HDFs on electrospun (A) PCL/P3HT(10) (S), (B) PCL (S), (C) TCP (S), (D) PCL/P3HT(10) (NS), (E) PCL (NS) and (F) TCP (NS).

Fig. 5.8 Signal pathway involved in light stimulation induced cell proliferation (Black line) and photocurrent induced cell proliferation (Green dotted line).

Fig. 5.9 Laser scanning confocal microscopic (LSCM) micrographs of HDFs grown on (A) PCL/P3HT(10) (S), (B) PCL (S), (C) TCP (S), (D) PCL/P3HT(10) (NS), (E) PCL (NS) and (F) TCP (NS), expressing F-actin.

Fig. 5.10 Collagen staining on fibroblasts on nanofibrous scaffolds: A) PCL/P3HT(10) (S), (B) PCL (S), (C) TCP (S), (D) PCL/P3HT(10) (NS), (E) PCL (NS) and (F) TCP (NS).

Fig. 6.1 Characterizations of electrospun nanofibers. a. SEM morphology of Gel/PLLCL/P3GF(cs), Gel/PLLCL/GF(cs) , Gel/PLLCL and PLLCL nanofibers. b. TEM morphology of core-shell nanofibers. c. FTIR spectra of Gel/PLLCL/P3GF(cs), Gel/PLLCL/GF(cs), Gel/PLLCL and PLLCL nanofibers. d. Water contact angle of electrospun nanofibers.

Fig. 6.2 Stress-strain curve of electrospun Gel/PLLCL/P3GF(cs), Gel/PLLCL/GF(cs), Gel/PLLCL and PLLCL nanofibers.

Fig. 6.3 HDF proliferation on electrospun Gel/PLLCL/P3GF(cs), Gel/PLLCL/GF(cs), Gel/PLLCL and PLLCL nanofibrous scaffolds stimulated (S) compared to HDF proliferation on electrospun Gel/PLLCL/P3GF(cs), Gel/PLLCL/GF(cs), Gel/PLLCL and PLLCL nanofibrous scaffolds non-stimulated (NS) by MTS assay. *Significant against cell proliferation on PLLCL (NS) at $p \leq 0.05$. $^{\Delta}$Significant against cell proliferation on Gel/PLLCL/P3GF(cs) (NS) and Gel/PLLCL/GF(cs) (NS) at $p \leq 0.05$. $^{\#}$Significant against cell proliferation on Gel/PLLCL/P3GF(cs) (NS) at $p \leq 0.05$.$^{\blacklozenge}$Significant against cell proliferation on Gel/PLLCL/GF(cs) (S) at $p \leq 0.05$.

Fig. 6.4 *In vitro* wound healing on stimulated and non-stimulated Gel/PLLCL/P3GF(cs) nanofibrous scaffold for 9 days.

Fig. 6.5 Dual immunocytochemical analysis for the expression of Ker 10, CD 105 and merged image showing the dual expression of both CD 105 and Ker 10 on stimulated Gel/PLLCL/P3GF(cs), Gel/PLLCL/GF(cs) nanofibers and non-stimulated Gel/PLLCL/P3GF(cs), Gel/PLLCL/GF(cs) nanofibers at 20 × magnification.

Fig. 7.1 Photograph of a scaffold of radially aligned nanofibers directly deposited on the ring collector [310].

List of Abbreviations

Ab: Antibody

AFM: Atomic Force Microscope

ASCs: Adipose derived stem cells

ATR-FTIR: Attenuated Total Reflectance-Fourier Transform Infrared

BM-MSCs: Bone Marrow-derived Mesenchymal Stem Cells

BSA: Bovine Serum Albumin

CK: Cytokeratin

Coll: Collagen

DAPI: 4',6-diamidino-2-phenylindole, dihydrochloride

DMEM: Low Glucose Dulbecco's Modified Eagle's Medium

DMSO: Dimethyl sulfoxide

ECM: Extracellular Matrix

EGF: Epidermal Growth Factor

EGFR: Epidermal Growth Factor Receptor

EIF: Epidermal induction factors

FBS: Fetal Bovine Serum

FDA: Food and Drug Administration

FGF: Fibroblast Growth Factor

FITC: Fluorescein-isothiocyanate

GAG: Glycosaminoglycans

Gel: Gelatin

HDF: Human Dermal Fibroblasts

H&E: Hematoxylin and Eosin

Ker 10: Keratin 10

KGF: Keratinocyte growth factor

LLLT: Low level laser therapy

NFS: Nanofibrous scaffold

P3HT: Poly (3-hexylthiophene)

PCL: Poly (ε-caprolactone)

PDGF: platelet-derived growth factor

PLLA: Poly (L -lactic acid)

PLLCL: Poly (L -lactic acid-co-ε-caprolactone)

SC: Stem cell

TGF: Transforming growth factor

Chapter 1

Introduction

1.1 Background

Skin is the largest organ of the body, serving primarily as a protective barrier against the environment [1, 2]. It also helps to prevent body dehydration and constitutes a physical barrier, limiting the penetration of potentially harmful agents to internal organs. The skin has a three-layer structure composed of epidermis, dermis and hypodermis [3, 4]. The epidermis, the superficial layer, is mainly composed of keratinocytes [5, 6], providing a barrier against infection and moisture loss. The dermal layer, situated below the epidermis, is responsible for the elasticity and mechanical integrity of the skin. It contains vascularized extracellular matrix (ECM) rich in collagen, elastin and glycosaminoglycans [4, 6]. The hypodermis, located below the dermis, is mainly composed of adipose tissue and collagen, and mainly acts as an energy source [3, 5, 6]. However, when the skin is damaged, it will lose its integrity and barrier function. According to WHO, 300,000 deaths are annually attributed to burn injuries, while 6 million patients worldwide suffer from burns every year. Additionally, more than 6 million individuals suffer from chronic skin ulcers. In the USA alone, more than 3 million patients suffer from chronic wounds [3, 7]. In Singapore, average annual burn admissions from 1997 to 2003 were 288 with a range from 188 to 348. This represents a incidence rate of 0.07 per 1000 population (on average) for burn injury in the city of Singapore [8]. Acute large full-thickness skin wounds not only cause an immediate loss of wound coverage, but also initiate physiological instability and give rise to various complications. Insufficient autologous grafts greatly impede wound closure in patients with large area wounds, and then lead to infection and low mortality [9]. As a result, the development of tissue engineered skin replacements is greatly motivated by the need for permanent wound closure in full-thickness wounded patients [10].

Tissue-engineered skin graft is an attractive alternative substitute for clinicians to use for the healing of full-thickness skin wounds because they can overcome certain disadvantages of using autografts like insufficient donor supply and size mismatches. The application of biomimetic scaffolds and culturing skin cells (keratinocytes, hair follicle cells and fibroblasts *etc.*) in the scaffold is the current approach in designing skin tissue engineered substitutes. Many commercialized tissue-engineered skin grafts are available on market (Table 2.2). They offer advantages of resurfacing large wound area, supporting host fibroblast infiltration (Permacol^{TM}, OrCel®, Integra®) and improving granulation tissue deposition (Apligraf®) *etc*. However, a critical issue of tissue engineered scaffold is the ex *vivo* cell expansion that is required to obtain sufficient numbers of the needed cells, while preserving the cells' normal phenotype and functionality within a short time. What's more, the high cost and short shelf time limit the application of the current tissue engineered skin grafts. All of these deficiencies in current treatments for full-thickness skin wounds lead to an urgent necessity for the development of a novel tissue-engineered skin graft incorporating a bioactive molecular and abundant safe cell source in combination with a cost-effective, biodegradable and functional scaffold with appropriate mechanical properties.

1.2 Motivation

The composition of the native extracellular matrix (ECM) is a complex mixture of structural and functional proteins, glycosaminoglycans, glycoproteins and bioactive factors arranged in a unique, tissue specific three-dimensional architecture [11]. The native ECM contains fibrils ranged from tens of nanometers to micrometers in scale. The organized structure of these matrix fibrils guides tissue morphogenesis and remodeling. In addition, matrix fibrils serve as "depots" for the storage of bioactive factors for the regulation of cell migration, proliferation, and differentiation [12].

Research on the construction of synthetic mimics of ECM has profound implications in the field of regenerative medicine and tissue engineering [13]. Advances in tissue engineering techniques have sparked interests in making scaffolds with biocompatible and/or biodegradable polymer nanofibers. The non-woven polymeric architecture of

nanofibrous scaffolds (NFS) mimics the nano-scale protein fiber meshwork in native ECM. The large surface area-to-volume ratio of NFS favors cell adhesion, proliferation, migration and differentiation [14]. For skin graft application, the high porosity of NFS provides more structural space for accommodation of migrating and proliferating cells and enables efficient nutrient delivery, gas exchange and waste excretion, while the small pore size of NFS can protect the wound from bacterial penetration [15]. Additionally, polymeric NFS are usually strong in tensile strength, so they can retain structural integrity and prevent wound contraction when surgeon handles and implants it into the defect site of the host [16]. The most efficient and easy way to fabricate NFS at a large scale is electrospinning due to its easy setup and operation. Moreover, electrospun NFS has interconnected pores and large surface area to volume ratio [17]. The main component of native skin ECM, collagen I has been successfully electrospun into NFS and this collagen NFS was shown to have great biocompatibility both *in vitro* and *in vivo* [18-20]. However, the poor mechanical properties and high cost limit the application of collagen in wound healing. Compared with collagen, gelatin, which is derived from collagen by controlled hydrolysis, is cheaper and does not show antigenicity under physiological conditions [21, 22]. Moreover, gelatin is biodegradable, biocompatible and displays many integrin binding sites for cell adhesion, migration, proliferation and differentiation due to the abundant Arg–Gly–Asp (RGD) sequences in its amino acid chain [16, 23].

In addition to mimic the component of native ECM with cost-effective proteins, core-shell nanofibers incorporated with bioactive factors of ECM could be a better biomimetic scaffold for wound healing. The controlled release of bioactive factors can be realized via core-shell nanofibers and core-shell nanofibers can also protect the biological agents from the harsh environments [24]. Incorporation of such growth factors and bioreagents in biocompatible and biodegradable nanofibers can be a potential alternative to regulate cell proliferation, migration and differentiation, thus enhancing skin tissue regeneration by providing adequate signaling and concentration of growth factors.

Researches in phototherapy and electrotherapy have inspired the studies in making scaffolds with functional polymer nanofibers for wound healing. Phototherapy, using low intensity radiation in the visible or near-infrared region, whether from a laser or a light emitting diode (LED), can be beneficial in a number of clinical situations, from pain remission to wound healing. Phototherapy is gaining recognition for the immediate relief of acute and chronic pain, for treating inflammatory conditions, and for the promotion of wound healing. At the inflammatory phase, a cellular modulation occurs with a decrease in cell inflammation [25] and an increase in the release of growth factors [26], initiating the proliferative phase. In the second phase, neovascularization is enhanced by photo-stimulation of endothelial cells [27]; increased proliferation of fibroblasts and collagen deposit [28, 29] also contribute towards granulated tissue formation and the ensuing closing of the wound. In addition, weak electrical current stimulation was found to promote wound healing by 20% per week [30]. Meanwhile, electrical stimulation (ES) can improve the survival of skin flaps *in vivo* [31] and significantly shorten the time of wound closure [32], epithelialization [33] fibroblast proliferation [34]. As phototherapy and electrotherapy have shown positive results in wound healing, the combination of these two therapies (photocurrent therapy) could be more helpful in skin regeneration. The photovoltaic polymer poly (3-hexylthiophene) (P3HT) is the most promising candidate for photocurrent therapy. When light irradiates on photosensitive polymer P3HT containing fibers, electrons are generated in the photosensitive polymer molecules and when the electrons flow in the fibers, an electrical current is formed. This photocurrent generated in the P3HT containing fibers could be a new way for treatment of skin wounds

Besides working on developing biomimetic and functional scaffolds for tissue engineering, researchers also combine the assist of stem cells to realize tissue regeneration. ASCs display immunosuppressive properties, allogeneic cell treatment can be foreseen to overcome unsatisfactory results with autologous cell therapy for regenerative medicine [35, 36]. Therefore, adipose tissue represents an abundant, practical, and appealing source of donor tissue for autologous and allogeneic cell replacement [37, 38]. Moreover, due to the capability of multipotential differentiation and

secretion of growth factors, ASCs will have a great contribution in wound healing. ASCs can be easily obtained from liposuction of human adipose tissue; can be cultured on a large scale [39-41]. The ability of ASCs to promote angiogenesis, to secrete growth factors and to differentiate into multiple cell types, could create a viable skin substitute. ASCs are known to significantly reduce the wound size and accelerate the re-epithelialization process via promoting the proliferation of human dermal fibroblasts (HDF) [42].

In this project, we utilized electrospinning technique to fabricate cost-effective core-shell structured nanofibrous scaffolds which encapsulated bioactive factor and photosensitive polymer and we further studied the feasibility of the resultant nanofibers/stem cell composites as skin grafts to promote wound healing and skin regeneration.

1.3 Hypothesis and objectives

Hypothesis

Electrospun cost-effective core-shell structured nanofibrous scaffolds which encapsulate bioactive factor and photosensitive polymer, promote wound healing and skin regeneration in full-thickness skin wounds.

a) Cost-effective natural polymer like gelatin can be electrospun into nano-scale architectures in tissue-engineered skin grafts with appropriate mechanical stability to resemble the natural ECM structure and accelerate *in vivo* wound healing.

b) Sustained release of multiple epidermal induction factors (EIF) from core-shell structured nanofibrous scaffold can be achieved. ASCs will differentiate into epidermal lineage on this multiple EIF encapsulated core-shell NFS.

c) Biodegradable synthetic polymer and photosensitive polymer like P3HT can be blended for co-electrospinning to provide the photosensitive skin grafts with the ability of promoting human dermal fibroblast proliferation under light stimulation.

d) Epidermal growth factor (EGF) and P3HT encapsulated core-shell nanofibers can promote cell proliferation, meanwhile assist ASC epidermal differentiation and facilitate wound healing.

Objectives

- Electrospin cost-effective NFS as skin grafts, find out the optimized NFS and apply this scaffold to realize fast wound healing *in vivo*.

- Confirm the epidermal differentiation potential of ASCs by inducing ASCs into epidermal lineage *in vitro* through manipulating the biochemical, environmental and physical conditions on an EIF encapsulated core-shell nanofiberous scaffold.

- Utilize electrospinning technique to fabricate photosensitive polymer P3HT blended nanofibrous scaffold and irradiate the cell-scaffold composite by light-emitting diode to achieve an efficient proliferation of human dermal fibroblasts.

- Demonstrate the feasible application of EGF and P3HT encapsulated photosensitive core-shell NFS as skin grafts to promote fibroblast proliferation, wound healing and skin regeneration.

1.4 Research rationale and strategy

A cost-effective NFS were fabricated by electrospining technique using PLLCL blended with natural polymer gelatin. The NFS were demonstrated a faster wound closure *in vivo* in a mouse model compared with control groups. The cost-effective NFS were further improved by encapsulating EGF and photosensitive polymer (P3HT), using coaxial electrospinning. Fibroblast proliferation was significantly improved on EGF and P3HT encapsulated core-shell NFS under light stimulation. Keratinocyte-like ASCs were only found on the light stimulated EGF and P3HT encapsulated core-shell nanofibers. We

confirmed that the biomimetic and photosensitive core-shell nanofibers could be a novel scaffold applied in photocurrent therapy for wound healing and skin construction. To the best of our knowledge, we are the first to apply photosensitive scaffold combained with light stimulation in skin tissue engineering and evaluate their capability in promoting skin reconstruction and regeneration. Thus, our study will inspire more research opportunities to explore the mechanism beneath the promising outcomes.

The Rationale of using EGF and P3HT encapsulated core-shell nanofibrous scaffold/ASCs composites as skin graft for the treatment of full-thickness skin wounds in this study are:

- ASCs have the potential to improve skin regeneration by differentiating into the phenotypes of damaged skin cells and/or enhancing repair by creating microenvironment that promotes the regeneration of local cells (such as HDF).

- The sustained release of EGF from core-shell NFS will promote cell proliferation and guide ASCs epidermal differentiation

- Photo and electrical stimulation can promote wound healing. The photocurrent generated in photosensitive P3HT containing core-shell NFS will promote cell proliferation under light stimulation.

- The non-woven polymeric architecture of NFS mimics the nano-scale protein fiber meshwork in native ECM. Its high surface area-to-volume ratio is efficient for cell adhesion, proliferation, migration and differentiation.

- The NFS has a high porosity for efficient nutrient delivery, gas exchange and waste excretion after transplantation into wounded skin**.**

- The small pore size of the nanofiber skin graft inhibits the bacterial entry.

- NFS gradual biodegradation profile allows the new skin tissue to regenerate and reduces immunological responses.

1.5 Work scope

In this dissertation, a detailed literature review is presented in Chapter 2 that includes the wound healing process, current treatments for full-thickness skin wounds, properties and potentials of electrospun photosensitive NFS for wound healing and skin regeneration. Table 1.1 summarizes the project scopes from chapter 3 to chapter 6. Conclusions for this thesis and recommendations for future work are described in Chapter 7.

Table 1.1 Overview of project scope.

Hypothesis	**Objective**	**Descriptions**	**Thesis**
(1) Biodegradable synthetic polymer and cost-effective natural protein like gelatin can be blended for co-electrospinning to provide the skin grafts with appropriate mechanical stability and biomolecular cell recognition signals for cell-scaffold interactions.	Find out the optimized gelatin containing NFS and confirm the promoting wound healing ability of the NFS *in vivo*.	(1) The solutions with different content of gelatin: PLLCL in blend (80:20, 70:30, 60:40 and 50:50 wt%) were electrospun into NFS and the NFS were further characterized for its morphology, diameter, chemical composition and degradable properties *etc*. (2) The mechanical properties of these NFS were studied both in dry and wet conditions. The comparative proliferation of HDF on	Chapter 3

		these NFS was evaluated by cell proliferation assay. (3) The wound healing capability of the optimized gelatin and PLLCL blended NFS was evaluated studied *in vivo*.	
(1) Coaxial electrospinning can be used to fabricate nano-scale architectures in tissue-engineered skin grafts to encapsulate multiple bioactive factors to resemble the natural ECM. (2) The burst release can be restrained or eliminated by using core-shell structured NFS. (3) ASCs will differentiate into epidermal lineage under the guidance of the sustained release of EIF from the core-shell NFS.	Utilize coaxial electrospinning technique to fabricate multiple epidermal induction factors (EIF) encapsulated core-shell NFS. Realize sustained release of EIF from core-shell NFS. Confirm the epidermal differentiation potential of ASCs on EIF encapsulated core-shell NFS.	(1) PLLCL blended with gelatin core-shell NFS were electrospun to encapsulate EIF and the NFS were further characterized for its morphology, diameter, chemical composition, mechanical and degradable properties *etc*. (2) The release of EGF from the core-shell NFS was studied for 15 days. (3) ASCs were induced into keratinocyte-like cells with expression of epidermal differentiation markers by the induction of released EIF.	Chapter 4

Biodegradable synthetic polymer and photovoltaic polymer like P3HT can be blended for co-electrospinning to provide the photosensitive skin grafts with appropriate mechanical stability for cell-scaffold interactions.	Demonstrate the capability of the optimized photosensitive NFS composites as skin grafts to promote cell proliferation under light irradiation.	(1) The solutions with different content of PCL: P3HT in blend (150 : 2, 150 : 10 and 150 : 20 wt%) were electrospun into NFS and the NFS were further characterized for its morphology, diameter and chemical composition properties *etc*. (2) The photosensitive property and photocurrent generation of these NFS were studied. (3) The comparative proliferation of HDF on these NFS with or without light stimulation was evaluated by cell proliferation assay.	Chapter 5
(1) Core-shell NFS encapsulated both EGF and P3HT can be fabricated by coaxial electrospinning. (2) Higher proliferation of HDFs on this photosensitive core-shell NFS under light	(1) Demonstrate the capability of the photosensitive core-shell NFS composites as skin grafts to promote cell	(1) The core-shell NFS were electrospun to encapsulate EGF and P3HT. The photosensitive core-shell NFS were further characterized	Chapter 6

stimulation will be achieved. (3) ASCs will differentiate into epidermal lineage under the guidance of sustained release of EGF from the core-shell NFS and light stimulation. (4) The photosensitive core-shell NFS will promote *in vitro* wound healing.	proliferation and ASCs epidermal differentiation under light irradiation. (2) Study the mechanism of light stimulation in promoting cell proliferation. (3) Achieve faster *in vitro* wound healing on the photosensitive core-shell NFS under light stimulation	for its morphology, diameter, chemical composition, mechanical and degradable properties *etc*. (2) The comparative proliferation of HDF on these NFS with or without light stimulation was evaluated by cell proliferation assay. (3) ASCs epidermal differentiation on the photosensitive core-shell NFS were studied. (4) The *in vitro* wound healing has been done to show the capacity of the photosensitive core-shell NFS as skin grafts to promote wound healing.	

Chapter 2

Literature Review

2.1 Introduction

2.1.1 Skin composition and functions

Skin, the largest human organ, covers between 1.5 and 2 m^2 of the total surface area of human body [43]. It acts as an anatomical barrier from pathogens and damage between the internal and external environment in bodily defense and it protects the body against excessive water loss [44, 45]. The skin has two layers, the epidermis and the dermis (Fig. 2.1).

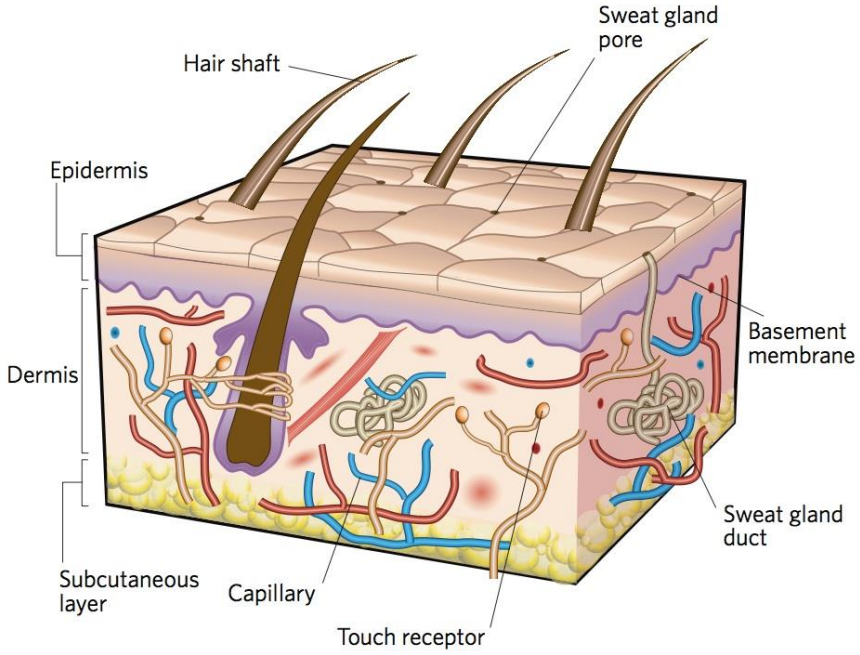

Fig. 2.1 Structure of skin [46]

The epidermis is defined as a stratified aquamous epithelium which is about 0.1 mm thick, although the thickness is greater (0.8 – 1.4 mm) on the palm and sole. The prime function

of epidermis is to act as a protective barrier. The main cell of the epidermis is the keratinocyte [47]. Keratinocytes, produced by cell division in the deepest layer of the epidermis (basal layer), are carried towards the skin surface where they are shed. The four layers of epidermis (Fig. 2.2) represent the stages of maturation of keratin by keratinocytes.

The basal cell layer (stratum basale), which is 1-3 cells thick, is comprised mostly of keratinocytes which are either dividing or nondividing. Melanocytes make up 5-10% of the basal cell population. Melanocytes contain cytoplasmic organelles called melanosomes, in which melanin pigment is synthesized from tyrosine. The melanosomes migrate along the dendrites of the melanocytes, and are transferred to the keratinocytes in the prickle cell layer. The main stimulus to melanin production is ultraviolet (UV) radiation. Melanin protects the cell nuclei in the epidermis from the harmful effects of UV radiation. Skin neoplasia is extremely uncommon in dark-skinned races because their skin is protected from UV damage by the large amounts of melanin it contains [48]. Above the basal layer is the prickle cell layer (stratum spinosum). Scattered throughout the prickle cell layer are Langerhans. Langerhans cells are dendritic cells and primarily located in stratum spinosum. Upon infection, these cells will take up and process microbial antigens to become fully-functional antigen-presenting cells [49]. Above the prickle cell layer is the granulaer layer (stratum granulosum). Cells become flattened and lose their nuclei in the granular cell layer. The flattened cells contain the darkly staining keratohyalin granules. These lamellar granules contain lipids and enzymes, and they discharge their contents into the intercellular spaces between the cells of the granular layer and stratum corneum-providing the equivalent of ‘mortar’ between the cellular ‘bricks’, and contributing to the barrier function of the epidermis [48]. The end results of keratinocyte maturation can be found in the horny layer (stratum corneum), which is comprised of sheets of overlapping polyhedral cornfield cells with no nuclei. These adjacent cells form a very effective barrier. The thickness of the stratum corneum is different and it is consistent with the region of the body [47, 48].

The main cellular elements of the dermis are fibroblasts, mast cells and macrophages. Fibroblasts synthesize the connective tissue matrix of the dermis, and are usually found in close proximity to collagen and elastin fibres. Mast cells are specialized secretory cells present thought out the derims, but they are more numerous around blood vessels and appendages. They contain granules whose contents include mediators such as histamine and prostaglandins etc. Macrophages are phagocytic cells that originate in the bone marrow, and they act as scavengers of cell debris and extracellular material [48].

2.1.1.1 Keratinocyte maturation

Keratinocyte is the principal cell type of epidermis and it is produced by cell division in the deepest layer of the epidermis (basal layer). As interfollicular epidermal stem cells in this basal layer expand due to division, some of these stem cells detach from the basement membrane and begin to migrate towards the epidermal surface, changing shape until they enter the outermost cell layer of stratum corneum as flattened cornified cells (see Fig. 2.2) [50]. As keratinocytes pass towards the skin surface, they undergo a complex series of morphological and biochemical changes known as terminal differentiation (keratinization) to produce the surface layer of tightly packed dead cells (stratum corneum or horny layer). The intermediate filaments (IF), present in the cytoplasm of epithelial cells, are a major component of the cytoskeleton. They contain a group of fibrous proteins knowns as keratins. Pairs of keratins are characteristic of certain cell types and tissues, and K5/K14 are characteristic of stratified aquamous epithelia. Epidermal basal cells express K5 and K14, but K10 is also expressed during differentiation in the suprebasal layers. After production of all materials is completed, the cells cease transcriptional and metabolic activity and undergo a programmed cell death. The inner cells keep moving outwards to continually replace the cell remnants [51]. Many proteins including keratins and non-keratins are expressed specifically during the process of epidermal differentiation and stratification according to the type of the epithelium, the stage of differentiation and the location of the keratinocytes within the epidermis. Table 2.1 is an overview of the common protein markers used for characterization of different epithelial types and disease detection [52]. The underlined

groups are used for the immunological analysis in this research to characterize the stage of skin development.

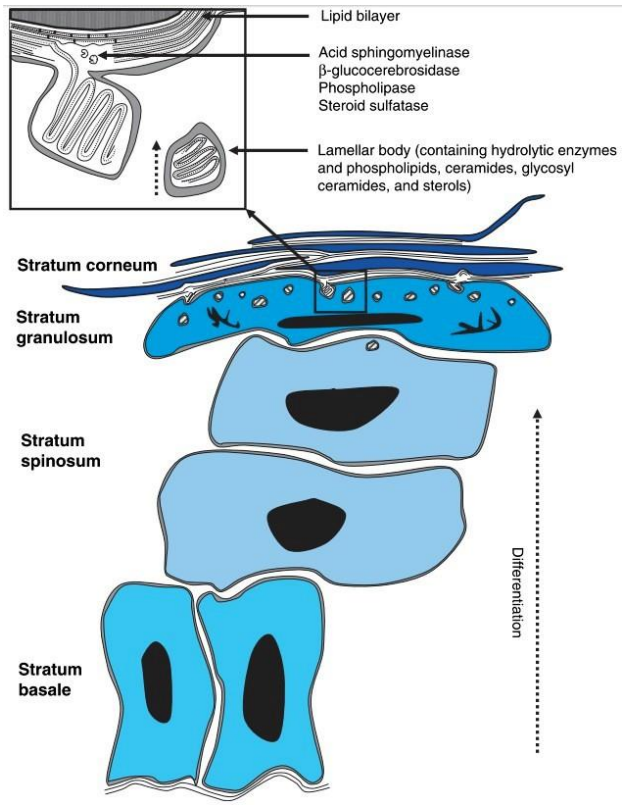

Fig. 2.2 The structures of stratified epidermis [53].

2.1.1.2 Keratins

Cytokeratins (CKs) are intermediate filament keratins found in the intracytoplasmic cytoskeleton of epithelial tissue. There are two types of CKs: the low weight (40-65 kDa), acidic (pI 4.5-6.0) type I CKs and the high weight (50-70kDa), basic or neutral (pI 6.5-8.5) type II CKs. CKs are usually found in pairs comprising a type I CK and a type II CK. The type II CKs comprise subtypes CK1-CK8. The type I CKs comprise subtypes CK 9-CK20. Table 2.1 is a list for different types of CKs [52].

Table 2.1 Keratin markers expressed in different human epithelial types (summarized from [52]).

Keratins	**Type**	**Location**	**Disease associated with gene mutation**
Keratin 1	Type II	Spinous and granular layers paired with keratin 10, a marker for early epidermal differentiation	Bullous congenital ichthyosiform erythroderma in which the palms and soles of the feet are affected.
Keratin 2	Type II	Upper spinous layer	Bullous congenital ichthyosiform erythroderma.
Keratin 3	Type II	Corneal epithelium paired with keratin 12	Meesmanns Corneal Dystrophy
Keratin 4	Type II	Differentiated layers of the mucosal and esophageal epithelia paired with keratin 13	White Sponge Nevus, characterized by oral, anal and esophageal leukoplakia
Keratin 5	Type II	Basal layer as a heterotetramer with two keratin 14 molecules	Epidermolysis bullosa Simplex
Keratin 6	Type II	Paired with keratin 16 and/or keratin 17 in the filiform papillae of the tongue, the stratified epithelial lining of oral mucosa and esophagus, the outer root sheath of hair follicles and the glandular epithelia	Pachyonychia congenita
Keratin 7	Type II	Most glandular and transitional epithelia (ovary, lung, and breast epithelia)	Carcinomas in glandular and transitional epithelia
Keratin 8	Type II	Single layer epithelial tissues paired with keratin 18	Cryptogenic cirrhosis

Keratin 9	Type I	Terminally differentiated epidermis of palms and soles	Epidermolytic palmoplantar keratoderma
Keratin 10	Type I	Suprabasal layers (Spinous and granular layers) of the epidermis paired with keratin 1, a marker for early epidermal differentiation	Variants of epidermolytic hyperkeratosis in which the palms and soles of the feet are unaffected.
Keratin 12	Type I	Corneal epithelia paired with keratin 3	Meesmann corneal Dystrophy
Keratin 13	Type I	Suprabasal layers of non-cornified stratified epithelia paired with keratin 4	Autosomal dominant disorder White Sponge Nevus
Keratin 14	Type I	Basal layer and appendages as a heterotetramer with two keratin 5 molecules	Epidermolysis bullosa simplex
Keratin 15	Type I	Some progenitor basal cells within complex epithelia, in the bulge and the bulb of follicle	Undefined
Keratin 16	Type I	Paired with keratin 6 in hyperproliferative (including tissue culture), traumatized and wound-healing epidermis; Buccal stratified squamous epithelia	Type I pachyonychia congenita, nonepidermolytic palmoplantar keratoderma and unilateral palmoplantar verrucous nevus
Keratin 17	Type I	Nail beds, hair follicles, sebaceous glands and other epidermal appendages	Jackson-Lawler type pachyonychia congenita and

			steatocystoma multiplex
Keratin 18	Type I	Single layer epithelial tissues paired with keratin 8	Cryptogenic cirrhosis
Keratin 19	Type I	Periderm, the transiently superficial layer that envelopes the developing epidermis; follicle bulge stem cell marker for epidermal stem cells in outer root sheet, basal epidermis and deep rete ridges	Undefined
Keratin 20	Type I	Mature enterocytes and goblet cells in the gastric and intestinal mucosa	Gastrointestinal, urothelial, and Merkel cell carcinomas

2.1.1.3 Non-keratins

Involucrin is a component of the keratinocyte cornified envelope and found in the cytoplasm and crosslinked to membrane proteins by transglutaminase. It is a marker of keratinocyte terminal differentiation and is expressed only in the granular and cornified layers of stratified squamous epithelium [54]. Filaggrin is a basic histidine-rich protein in epithelia and it is widely believed to promote the lateral aggregation of keratin filaments. It is one of the markers for intermediate keratinocyte differentiation [55]. Collagen IV and VII are expressed by the basal keratinocytes and form the basal layer of the stratum basale. β-integrin is highly expressed in outer root sheath of epidermal stem cells, follicle bulge and basal epidermis. α6-integrin is expressed in outer root sheath, follicle bulge and basal epidermis. Integrin β1 and α6 are epidermal stem cell marker (non-specific) due to their high expression within epidermal stem cells [56].

2.1.2 Wound healing *in vivo*

Wound healing consists four precisely programmed phases, which are continuous and overlapping. In healthy adults, wound healing contains six events: rapid hemostasis;

inflammation; differentiation, proliferation, and migration of mesenchymal cells to the wound site; re-epithelialization; and remolding [57, 58]. Hemostasis, the first stage of wound repair, occurs instantly after tissue damage. It involves vascular constriction and fibrin clot formation. Inflammatory phase involve the migration of inflammatory cells into the wound; more specifically the sequential infiltration of neutrophiles, macrophages, and lymphocytes [58-60]. Neutrophiles can clean up the initial rush of contaminating bacteria, and serve as a source of pro-inflammatory cytokines, which may provide signals to active local fibroblasts and keratinocytes [61]. The next phase is the new tissue formation phase, which is characterized re-epithelialization, the epithelial proliferation and migration over the provisional matrix within the wound. Keratinocytes will migrate over injured dermis. Following the migration of keratinocytes, granulation tissue formation characterized with capillary proliferation is in progress and the newly formed granulation tissue acts as a new substrate for keratinocyte migration. In the late part of this stage, under the stimulation of macrophages, some of the fibroblasts either from the wound edge or from bone marrow are differentiated into myofibroblasts [62]. Myofibroblasts are contractile cells that can gradually bring the edges of a wound together. Remodeling is the final stage of wound repair, which begins 2-3 weeks after the injury and lasts for usually one year or more.

In summary, the normal healing process starts with an well-organized process of hemostasis and fibrin deposition, which results result in formation of an inflammatory cell cascade, characterized by neutrophils, macrophages and lymphocytes [63]. The subsequent processes include attraction and proliferation of fibroblasts, collagen deposition, and finally the remodeling by collagen cross-linking and scar maturation. If any of part of the healing cascade is altered, the pathologic responses may lead to fibrosis or chronic ulcers [64].

2.2 Full-thickness skin wounds

Rapid, extensive, deep wounds could be caused by burns and scalds and they can lead to death due to the difficulty in treatments with common techniques [65]. 6.5 million patients are affected by chronic wounds in the United States and the treatment of chronic

wounds will cost more than US$25 billion annually. The market share of the wound care products will reach $15.3 billion by 2010 [66]. In Singapore, average annual burn admission from 1997 to 2003 was 288 with a range from 188 to 348. This represents a incidence rate of 0.07 per 1000 population (on average) for burn injury in the city of Singapore [8]. On a worldwide scale, 27 million burns that occur require professional treatment and of these, 7 million suffer large and deep burns that require hospitalization [15]. Acute large full-thickness skin wounds not only cause an immediate loss of wound coverage, but also initiate physiological instability and give rise to various complications. Without a protective barrier from injured skin, patients are easily susceptible to infections, especially the nosocomial infections from *Pseudomonas*. [67]. Therefore, normal process of natural repair is lost and the wounds are locked into a state of chronic inflammation characterized by abundant neutrophil infiltration with associated reactive oxygen species and destructive enzymes. The chronic inflammation is mainly caused by the over-abundant neutrophil. A large number of enzymes such as collagenase, which can destroy the connective tissue matrix, are released by the neutrophils. [68, 69]. In addition, elastase, an enzyme released bythe neutrophils, can destroy healing factors such as PDGF and TGF-ß [70]. Current high tech materials and topical cytokines such as PDGF will not cure these wounds, unless the wound bed is received proper care from specialists [71, 72]. However, due to the loss of epidermal and dermal tissue to their full depth in full-thickness skin wounds, the epidermal stem cells in hair follicles for epidermal renewal, the basement membrane for cell migration and the blood vessels in dermis are all destroyed, which creates great difficulties for skin regeneration. Scar tissue is preferable to no healing. However, they are not fully functional, cross-linked with only 80% of the tensile strength of the tissue it replaces and aesthetically disfiguring. Therefore, there is a great need for the development of synthetic skin, which can facilitate skin regeneration and minimize scar formation.

2.2.1 Current treatments for full-thickness skin wounds

Based on the depth of the injury, wounds can be indetified into epidermal, superficial partial-thickness, deep partial-thickness and full-thickness wounds [73]. Specific surgical treatment is not required for epidermal injuries which are characterized by erythema and

minor pain [65]. The epidermis and superficial parts of the dermis are injured in the superficial partial-thickness wounds with characterizations of epidermal blistering and severe pain accompanying. In deep partial-thickness injuries, most of the dermis is lost with only fewer skin appendages remaining and therefore they take longer to heal [65]. The most severe injury is the full-thickness wounds that are characterized by the complete lose of epithelial-regenerative elements. In the process of contraction, cells around the edge of the wound will migrate into the wound center to cover the injury area, leading to cosmetic and functional defects. Skin grafting is needed for all full-thickness skin wounds, which are more than 1 cm in diameter due to the lost self-healing ability. Moreover, the full-thickness skin wounds may lead to extensive scarring, resulting in limitations in joint mobility and severe cosmetic deformities [73].

2.2.1.1 Autografts, allografts and xenografts

Untill now, the autologous skin grafting is still the ‘gold standard’ in full-thickness injuries treatment [2, 4, 74]. The composite skin (epidermis with a superficial part of the dermis) is obtained from an undamaged skin donor site and applied to the full-thickness wound [65]. In the donor site, keratinocyte will migrate from hair follicles, sweat glands and edges of the wound to heal the wound. It will take around one week to cure the donor site. The healed donor site can be used for further split skin graft (SSG) re-harvesting. Usually, the thicker SSG will be more capable in promoting wound healing at the site of application with less contraction compared to the thin SSG. However, it will take longer time to heal the donor site [74].

Many factors such as the physiological condition of the patient, could affect the availability of SSG. Meanwhile, due to the issues of graft rejection and the possibility of disease transfer, allografts and xenografts can only be used as temporary wound coverage [75]. All of these faults give rise to the clinical need for the development of tissue-engineered alternatives.

2.2.1.2 Tissue-engineered skin grafts

To address the limitations of traditional therapies, tissue engineering is intensively applied to treat tissue loss or organ failure. The number of journal publications in tissue engineering keeps increasing year by year (Fig. 2.3). The limitation of split-thickness skin autografts drives the demand of efficient wound healing substitute - tissue engineered skin substitutes.

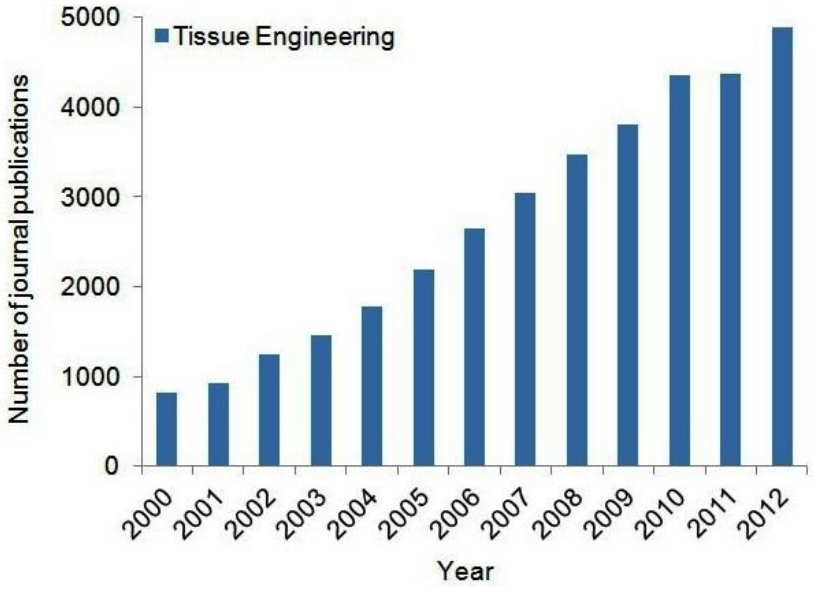

Fig. 2.3 Number of journal publications in tissue engineering

Three major requirements are needed to be satisfied for all tissue-engineered skin substitute bio-constructs. First, the tissue engineered skin substititues must be safe for the patient. Second, they should be clinically effective. Third, they are supposed to be convenient in handling and application. In general, such biomaterials must avoid toxicity, immune rejection and should not cause excessive inflammation and transmissible disease risk.

The prime approach of tissue engineering is utilizing scaffolds to support the proliferation and differentiation of specific autologous cells to form an artificial tissue. Then the cultured tissue will be transplanted into the defective site of patients to promote tissue regeneration. Obviously, scaffold, cells and their interactions will be the three key factors to affect the performance of the tissue-engineered grafts. Among them, cells play a

dominant role for the success of tissue-engineered scaffolds. The cell types applied in skin tissue engineering are fibroblasts, keratinocytes and hair follicle cells etc. Progenitor cells which are from hair follicles, interfollicular epidermis and sebaceous glands, are also used in skin tissue engineering [76]. Moreover, stem cells from the peripheral blood or bone marrow system are also studied in skin tissue engineering due to their ability of multipotential differentiation and growth factors secretion.

2.2.1.2.1 Commercialized tissue-engineered skin grafts

Tissue-engineered skin grafts have been intensively developed and the currently available products are summarized in Table 2.2 and organized according to anatomical structure classification (dermal, epidermal and composite).

2.2.1.2.1.1 Dermo-Epidermal (Composite) skin substitutes

In order to mimic the structure of normal skin, composite skin substitutes have both epidermal and dermal layers. Compared with epidermal and dermal substitutes, composite skin substitutes are the most advanced and sophisticated products. However, they are also the most expensive tissue-engineered biological constructs for tissue repair [4]. Apligraf® is one of the composite skin substitutes and it was approved by FDA in 1998 for the treatment of venous leg ulcers [77]. The matrix of Apligraf® is made of bovine type I collagen cultured with allogeneic fibroblasts and keratinocytes to mimic the normal structure of human skin. Although without immune rejection, the short survive time (one to two months) for the allogeneic cells, limits its performance as a skin graft [78, 79]. It is now believed that Apligraf® works by delivering growth factors and ECM to the wound bed [80]. The drawbacks of this graft include short time shelf life (only 5 days), difficulty in handling and risk of disease transfer from its allogeneic cells. In a large multicenter trial, it showed signs of wound infection in 29% of patients receiving Apligraf® versus 14% of patients receiving standard medical care [81]. Orcel® is another composite skin graft and it includes allogeneic keratinocytes and fibroblasts. An array of bioacters such as FGF-1, KGF-1, PDGF, VEGF and TGF-α are producted in this bilayered product and these bioactors are all favourable for host cell migration and

wound healing. However, due to the presence of allogeneic cells, Orcel® can only act as a temporary coverage and it will be resorbed within 7-14 days [65].

Several other composite skin substitutes combining dermal and epidermal elements have been developed. One of them is PolyActive, which is a Polyactive matrix cultured with autologous keratinocytes and fibroblasts. A soft polyethylene oxide terephthalate is the main component of the porous Polyactive matrix and a hard polybutylene terephthalate is further applied to prevent contraction of this polymer [82, 83]. Autologous cells are cultured in this matrix and therefore cross-contamination by infective agents or immune rejections are greatly reduced. However, it will take longer time for autologous cells expension and this may limit its immediate availability and increase its costs compared with competitive allogeneic-based products. Moreover, the non-biodegradable synthetic dermal component makes this tissue engineered graft only as a temporary skin substitute [65].

2.2.1.2.1.2 Dermal skin substitutes

Integra®, which consists of porous bovine type I collagen matrix and a silicone pseudo-epidermis to prevent contraction, is a representative dermal skin substitute [84]. After being applied onto the wounded site, the type I collagen sponge recruited host dermal fibroblasts and degraded during cell invasion and the pseudo-epidermal component protects wounds from bacterial contamination and vapour loss. Integra® has received the approval of the US Food and Drug Administration (FDA) in 1996 for the treatment of deep-dermal and full-thickness wounds [77]. The product is widely adopted because of its great performances in handling, storage, with less immune rejection and disease transmission, good cosmetic outcomes with reduced rates of contraction and scarring [85]. However, meticulous surgical preparation, long time for vascularization (10-14 days) and requirement of a second operative procedure to replace the silicone layer consist the disadvantages of Integra®. TransCyte consists of a pseudo-epidermal semipermeable silicon film bonded to nylon fabric with incorporated porcine collagen and neonatal allogeneic fibroblasts are cultured in this scaffold. This bioengineered construct provides growth factors, matrix proteins and cytokines necessary for wound

healing improvement; it is effective for pain relief and vapour loss control. However, the silicon film is non-degradable and it has to be removed after 7-14 days. Extra treatments (applying an extra temporary wound cover etc.) are need after removing silicon film. The biomaterial applied in Dermagraft is polyglactin mesh; further fibroblasts are seeded in the scaffold. The cultured fibroblast can proiduce growth factors and ECM components to mediate wound healing. The will degrade by hydrolysis in 20-30 [86]. However, no significant difference is found in clinical trials comparing the application of meshed skin graft to the application of meshed skin graft combined with Dermagraft [87], and its performances were found to be similar to allograft [88]. Multiple applications, higher cost and safety issues are the main limitations of this skin bio-construct [86].

2.2.1.2.1.3 Epidermal skin substitutes

Isolation of keratinocytes and its ex vivo expension are the key challenges in the designing and production of epidermal substitutes. Epicel® is an epidermal skin substitute and it is produced using an autologous keratinocyte sheet cultured for 15 days. The unavoidable drawbacks of this approach are long culture time; difficulties in handling and application. Furthermore, the poor long-term results, poor mechanical properties, high cost and a short (24 h) shelf-time limit its application [89]. MySkin®, which uses a specially surface coated silicone to support autologous keratinocytes, greatly improve the difficult handling issue of Epicel® and decrease the time for culture [90].

2.2.1.2.2 Drawbacks of current commercialized skin grafts

Although increased healing rates of burn and/or chronic wounds can be observed with current engineered constructs, several intrinsic shortcomings limit their use [91]: (a) epidermal grafts are fragile and therefore difficult to handle; (b) cell-populated matrices used in ‘skin substitutes’ are not readily scalable for manufacturing and are difficult to store and transport; (c) use of autologous skin cells require creation of fresh wounds; (d) it takes about 2 to 3 weeks for autologous skin cells to expand *in vitro* before reaching sufficient numbers for grafting. This time interval cannot satisfy patients with urgent clinical requirements [76]; (e) use of allogeneic keratinocytes or fibroblasts may induce

immune rejection; (f) allogeneic or xenogeneic skin substitutes may carry infectious agents including prions [92]. Moreover, disadvantages include cost, short shelf life limit the applications of tissue engnineered skin grafts. It has been recommended that informed consent must be obtained from all patients before the implantation of such biological material [93]. Further improvements are needed to address these limitations and the ideal tissue-engineered skin grafts should be cost-effective, user-friendly and safe to use (minimal risk of infection).

Table 2.2 Examples of current commercialized tissue-engineered skin substitutes with associated advantages and disadvantages

	Product Name	**Component**	**Advantages**	**Disadvantages**
Composite Substitutes	Karoskin	Human cadaver skin	Provide temporary cover and pain relief during the first few weeks	Immune rejection after 3 to 4 weeks post-grafting
	Apligraft	Allogeneic neonatal keratinocyte layer overlying a type I bovine collagen matrix with embedded allogeneic neonatal foreskin fibroblasts	Improves granulation tissue deposition and have good healing results for venous leg ulcer and diabetic foot ulcer	Graft rejection and disease transfer from allogeneic cells; repeated application required
	Orcel	Allogeneic neonatal keratinocyte layer overlying a bovine collagen sponge with embedded	Provides a cell-friendly environment for host cell proliferation, migration and provides cytokines	Can not be used as a permanent skin replacement; risk of rejection and disease transfer from allogeneic

		neonatal foreskin fibroblasts	and growth factors secreted by cells.	cells
	PolyActive	Autologous cultured keratinocytes and fibroblasts seeded into a polyethylene oxide terephthalate and polybutylene terephthalate matrix	Because of using autologous cells, no cross-contamination or immune rejection	Limited 'off the shelf' availability and high cost
Dermal Substitutes	Hyalograft 3D	Hyaluronic acid derivates with cultured autologous fibroublast and growth factors	Enhanced keratinocyte take, and reduced hypertrophy. Successful treatment of severe scleroderma cutaneous ulcers	Long time for cell expansion. Did not show effective results in plantar diabetic feet ulcer treatment.
	Alloderm	Processed cadaver allograft	Success in resurfacing full-thickness burns	Graft rejection and disease transfer
	Dermagraft	Allogeneic neonatal fibroblasts on a 3D polyglactin bioabsorbable scaffold	Neonatal fibroblasts rapidly proliferate to produce GAGs, collagen and growth factors to aid wound healing	Graft rejection and disease transfer; currently off the market
	Integra	Synthetic polysiloxane polymer on a	Encourages cell ingrowth and wound healing in	Bovine collagen presents antigenicity and

		scaffold composed of bovine type I collagen and GAGs	deep-dermal and full-thickness wounds	disease risk; polyxiloxane layer needs to be replaced with an epidermal autograft after 14 to 21 days
	Transcyte	A thin silicone layer on a collagen-coated nylon mesh with embedded ECM secreted by neonatal allogeneic fibroblasts	Success in treating second- and third-degree burns. fibroblasts secrete collagen, GAGs and growth factors to aid wound healing	Graft rejection and disease transfer; nylon mesh not biodegradable; currently off the market
	Permacol	Porcine-derived acellular dermal matrix	Non-immunogenic; supports host fibroblast infiltration and revascularization	Revascularization sometimes insufficient to support overlying epidermal graft
Epidermal Substitutes	Epicel	Cultured epidermal autograft	Large area of permanent wound coverage with little risk of rejection	3 weeks for cell expansion; fragile cell sheet; susceptible to blistering post-grafting
	Cellspray	Autologous keratinocytes (nultured or non-cultured)	Reduced cell culture time	It is limited to partial-thickness and graft donor site wounds.
	Laserskin	Cultured autologous	A less fragile system for keratinocytes;	3 weeks for cell expansion

		keratinocytes in a perforated HA membrane	HA/cell interaction properties improve mechanical stability	
	EpiDex	Cultured autologous outer root sheath hair follicle cells	Increased cell proliferation capacity; success in chronic ulcer treatment	6 weeks for cell expansion; fragile cell sheet
	Myskin	PCV polymer coated scaffold cultured with autologous keratinocytes	Improvement in cell attachment and proliferation; a more stable cell delivery system; cells can be thawed for repeated application	Long time (2 weeks) for cell expansion; repeated application required for good clinical outcome

2.2.2 Potential of photocurrent therapy for wound healing and skin regeneration

2.2.2.1 Phototherapy

Phototherapy (low intensity radiation from a laser or LED) is reported to have beneficial results in many clinical situations, from pain remission to wound healing. Phototherapy is gaining recognition for the immediate relief of acute and chronic pain, for treating inflammatory conditions, and for the promotion of wound healing. At the inflammatory phase, a cellular modulation occurs with a decrease in cell inflammation [25] and an increase in the release of growth factors [26], initiating the proliferative phase. In the second phase, neovascularization is enhanced by photo-stimulation of endothelial cells [27]; increased proliferation of fibroblasts and collagen deposit [28, 29] also contribute towards granulated tissue formation and the ensuing closing of the wound. In the last phase, tissue remodeling occurs where low level laser therapy (LLLT) has induced intense neovascularization and collagen deposit with elevated collagen orientation and

maturation [29, 94]. Several studies have reported enhanced healing following LLLT [25, 95-99]. LLLT affects the cellular components of wound healing by modulating the proliferation of macrophages [100], lymphocytes [101], fibroblasts [102], and keratinocytes [103]. It also influences microcirculation [104], cellular respiration and ATP synthesis [105, 106], the release of granulocyte-monocyte colony-stimulating factor and other cytokines [107], transformation of fibroblasts into myofibroblasts, and collagen synthesis [108, 109]. These studies indicate that LLLT speeds up healing by modulating the inflammatory response, fibroblast proliferation, angiogenesis, collagen deposition, and re-epithelialization. In the aspect of growth stimulation, the same wavelength lights generated from laser or lamp show similar performance, no significant difference was found [110] and the main light sources of phototherapy for wound healing are LED and lasers. Continuous diode laser was used by Damante et al. to irradiate human gingival fibroblasts twice (6 h interval) to study the relation of laser phototherapy on the release of growth factors by fibroblasts [111]. They found that basic fibroblast growth factor (bFGF) was 1.49 times greater in groups treated with infra-red laser than groups without laser phototherapy and bFGF accelerated granulation tissue formation and induced re-epithelialization [112]. Sousa and colleagues evaluated the effect of light stimulation on fibroblast proliferation *in vivo*. Red (700 ± 20 nm), green (530 ± 20 nm) and blue (460 ± 20 nm) LEDs are applied and the output power for these LEDs is 10J/cm^2. They found that red LED and green LED showed a significant increase in fibroblast numbers ($p < 0.01$) when compared with the control group (without light irradiation) [113]. Table 2.3 summarizes the applications of phototherapy in wound healing.

Table 2.3 Phototherapy applied in the field of wound healing.

Light type	Source (wavelength)[a]	Energy	Result	Refs.
Red	LED (670 nm)	8 J/cm^2	LED produced *in vitro* increases of cell growth of 140–200% over untreated controls in mouse-derived fibroblasts	[26]
Red	LED (627 nm)	4 J/cm^2	Right circularly polarized light and linearly polarized light promoted the process of wound	[114]

			healing by increasing the proliferation of fibroblasts	
Red	LED (670 nm)	3.6 J/cm^2	Mice exposed to 670-nm red light showed significantly faster healing than control mice	[115]
Blue	LED (470 nm)	50 mW/cm^2	Keratin-10 mRNA level elevated in light treated group compared to control group in rat model	[116]
Green	LED (570 nm)	10–0.2 mW/cm^2	Green LED yielded a significantly higher number of cells, than red ($p < 0.001$) and infrared LED light ($p < 0.001$) and than the cultures irradiated with the LLLT ($p < 0.001$)	[117]
Green and Red	LED (700 and 530 nm	10J/cm^2	Red LED and green LED showed a significant increase in fibroblast.	[113]
Cluster of LED	LED (510-670, 867 nm)	5J/cm^2	The effect of LED therapy in oval full-thickness wound-healing in the diabetic model with the use of 5 J/cm ^{2} is promising.	[118]

2.2.2.2 Electrotherapy

The generation of endogenous electric fields around the wound sites is confirmed by many studies and these generated electric fields are important in wound healing [119, 120]. Electric fields couple to directed cell migration through phosphatidylinositol-3-OH kinase-g (PI(3)Kg) and phosphatase and tensin homolog (PTEN) signaling [121]. This study gives us a promising and novel perspective to cure skin wound by electrical stimulation (ES) via manipulation of the endogenous electric fields generated by skin lesion. [122]. The effects of noninvasive electro-magnetic field (EMF) on keratinocytes and fibroblasts proliferation were assessed by Huo and colleagues in an incisional wound model. The cDNA microarray and RT-PCR were applied to study the gene expression in the EMF treated keratinocytes. They found that EMFS can accelerate keratinocyte migration. cDNA micro-array and RT-PCR performed revealed increased expression of CDC2-related protein kinase 7 and Homeobox C8 genes in treated keratinocytes. HOXC8

has been shown to be involved in gene regulation and CRK7 which has been implicated in promoting cell migration [122].

Chronic wounds such as diabetic and venous ulcer remain a serious healthcare problem into the 21st century. Unlike conventional foot ulcers, the chronic foot ulcer is unique in that, owing to poor circulation and damage to sensory nerve endings, many chronic ulcers remain unable to heal [123]. ES has been intensively studied in curing chronic ulcers. The ability of electrical stimulation in enhancing chronic wound healing was proved by both preclinical [124, 125] and clinical [126-128] studies [129]. Morris and colleagues developed the Ahn/Mustoe lapine wound model for systematic investigation of the effects of ES on ischemic wound therapy [130]. In their study, transcutaneous blood gas levels, histology, total RNA content were measured and a2 (I) collagen (COL-I), type IV collagen (COL-IV), a1 (V) collagen (COL-V), and vascular endothelial growth factor (VEGF) expressions were measured. All markers for stimulated wounds showed increased activity relative to nonstimulated control wounds. Both COL-I and COL-V showed significantly increased activity between day 7 and day 14 for longer duration of electrical pulse treatment, potentially indicating a continued effect on matrix remodeling. In a more recently study, Goudarzi and colleagues used extremely low frequency pulsed EMFs to treat skin wounds in diabetic rats. They found that low frequency pulsed EMFs significantly promote wound healing compared with the control group (without EMF stimulation) [131]. These results were supported by a clinical study performed by Young and colleagues, who evaluated the effect of low-intensity pulsed current on chronic wound healing for a period of 10 days. The reduction of oedema levels in chronic wounds was achieved by applying the pulsed current stimulation [180]. Meanwhile, Baker and colleagues found that square-wave pulse electrical stimulation could enhance the healing of diabetes ulcers of patients by nearly 60% over the control rate of healing [132].

The skin is the outer covering of the body. In human, it is the largest organ of the integumentary system, made up of multiple layers of ectodermal tissue, and it guards the underlying muscles, bones, ligaments and internal organs. As skin gets exposed to sun-light directly, it provides opportunities to use photocurrent in skin regeneration. The

mechanism of photocurrent therapy is probably the combination of electrotherapy and phototherapy.

2.2.2.3 Photocurrent therapy

Bart Vanhaesebroeck evaluated Zhao and colleagues' work as "Charging the batteries to heal wounds" [133] and we believed that photocurrent therapy will play a promising role in wound healing. Photocurrent is the current that flows through a photosensitive device such as a photodiode, after exposure to radiant power. When visible light irradiates matter (metals and non-metallic solids, liquids or gases), electrons are emitted from the matter as a consequence of their absorption of energy from visible light. As electrotherapy and phototherapy have shown positive results in wound healing, the combination of these two therapies could be more helpful in skin regeneration. When light irradiate on photosensitive fibers, electrons are generated in the photosensitive polymer molecules and when the electrons flow in the same direction, an electrical current is formed. Mean while, an electromagnetic field gets created and when the cells in the electromagnetic field get stimulated, Ca^{2+} ion translocates through the cell-membrane voltage-gated calcium channels. Ca^{2+} ion translocates through voltage-gated calcium channels leading to an increase in cystolic Ca^{2+} and this increase in cystolic Ca^{2+} leads to an increase in activated calmodulin. Activated calmodulin is known to promote nucleotide synthesis and cellular proliferation. Light stimulation also has a similar effect on cell proliferation. Porphyrin absorbs the energy of photons on light irradiation and becomes photo excited porphyrin (referred to as porphyrin*). The photo excited porphyrin can increase the proton-motive force (pmf) by transfering molecules of oxygen in the ground state $O_2(^3\Sigma)$ into singlet oxygen $^1O_2$,($^1\Delta_g$) which is a potent oxidizer. Thus more calcium is released into the cytoplasm from the mitochondria.

Fig. 2.4 shows the schematic illustration of photocurrent stimulation in regenerative medicine. All these reactions in the cell will lead to an increase is cell proliferation and the healing time gets decreased greatly. Based on this theory, phototherapy is described as the combination of electrotherapy and phototherapy. This conclusion corresponds to

the *in vitro* and *in vivo* studies which are described earlier in this review in skin, nerve and bone regeneration therapies.

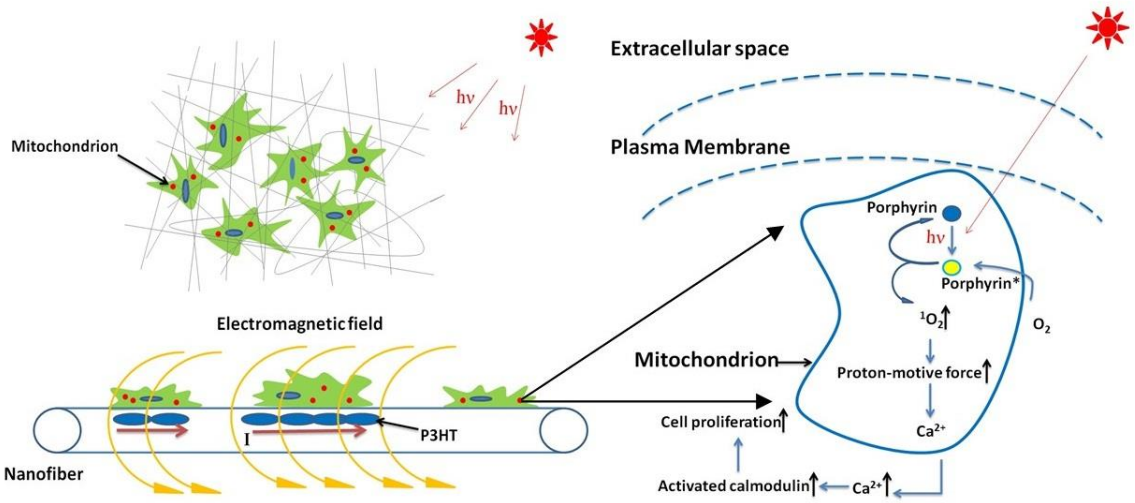

Fig. 2.4 Schematic illustration of photocurrent stimulation in regenerative medicine [134]

2.2.3 Potential of human adipose-derived stem cells (ASCs) for skin regeneration

Aiming to recovery or replace the defective or lost tissue, regenerative medicine is developing rapidly. The dominant approach in regenerative medicine is stem cell therapy. Stem cells have the ability of shelf-renew and the capacity to differentiate into specialized cell types. Therefore, stem cells play a significant role in regenerative medicine [135, 136]. Among stem cells, embryonic stem cells can differentiate into any cell types derived from all three embryonic germ layers, including skin cells [137]. However, the use of embryonic stem cells carries a great risk of tumorigenesis and provokes ethical controversy [138]. Epidermal stem cells are essential to epidermal, however, they are destroyed in full-thickness skin wounds and difficult to isolate from healthy sites. In recent years, the therapeutic application of adipose-derived stem cells (ASCs) is gaining more and more interests due to their availability in greater quantities. It was found that ASCs possesse higher stem cell proliferation rate than BM-MSCs [139]. Therefore, the application of autologous ASCs in tissue-engineered skin grafts became feasible [37].

2.2.3.1 Characteristics of human ASCs

Rodbell and colleagues are the pioneers to isolate stem cells from minced rat fat pads [140, 141]. They incubated the fat tissue together with collagenase and then centrifuged the digest. After centrifuge, the pelleted stromal vascular fraction (SVF) will be at the bottom of the centrifuge tube. However, many cells types (circulating blood cells, fibroblasts, pericytes and endothelial cells) are in the SVF [140, 141]. Therefore, they performed the final isolation to selecte the plastic adherent population within the SVF cells. Subsequently, this procedure was further developed to isolate stem cells from human adipose tissue specimens [142-145]. The surface immunophenotype of ASCs isolated from human and other species [146-149]. Direct comparisons between human ASC and MSC immunophenotypes are > 90% identical [147]. Nevertheless, differences in surface protein expression have been noted between ASCs and MSCs. For example, the glycoprotein CD34 is present on human ASCs early in passage but has not been found on MSCs [150, 151]. ASCs express various surface markers including CD9, CD29, CD44, CD49, CD54, CD71, CD105, CD166 et al. and are negative for CD11b, CD16, CD18, CD31, CD45, CD50, CD56, CD62 and CD104. A more extensive phenotypic profile of MSCs can be found in Table 2.4 [152].

Table 2.4 Immunophenotype of passaged human ASCs [152]

Antigen category	Surface-positive Antigens	Surface-negative Antigens
Adhesion molecules	CD9 (tetraspan), CD29 (β_1 integrin), CD49 days (α_4 integrin), CD54 (ICAM-1), CD105 (endoglin), CD166 (ALCAM)	CD11b (α_b integrin), CD18 (β_2 integrin), CD50 (ICAM-3), CD56 (NCAM), CD62 (E-selectin), CD104 (α_4 integrin)
Receptor molecules	CD44 (hyaluronate), CD71 (transferrin)	CD16 (Fc receptor)
Enzymes	CD10 (common acute lymphocytic leukemia antigen), CD13	

	(aminopeptidase), CD73 (5' ecto-nucleotidase), aldehyde dehydrogenase	
Extracellular matrix molecules	CD90 (Thy1); CD146 (Muc18); collagen types I and III; osteopontin; osteonectin	
Cytoskeleton	α-smoothmuscleactin, vimentin	
Hematopoietic		CD14, CD31, CD45
Complement cascade	CD55 (decay-accelerating factor), CD59 (protectin)	
Histocompatibility Antigen	HLA-ABC	HLA-DR
Stem cell	CD34, ABCG2	
Stromal	CD29, CD44, CD73, CD90, CD166	

ASCs display multipotency and they are guided to differentiate into several cell types including adipose [144], bone [153, 154], cartilage [155, 156], endothelial cells [157] and epithelial cells [158, 159] (Fig. 2.5 [160]). The multipotency of these cells makes them as an important candidate in regenerative medicine.

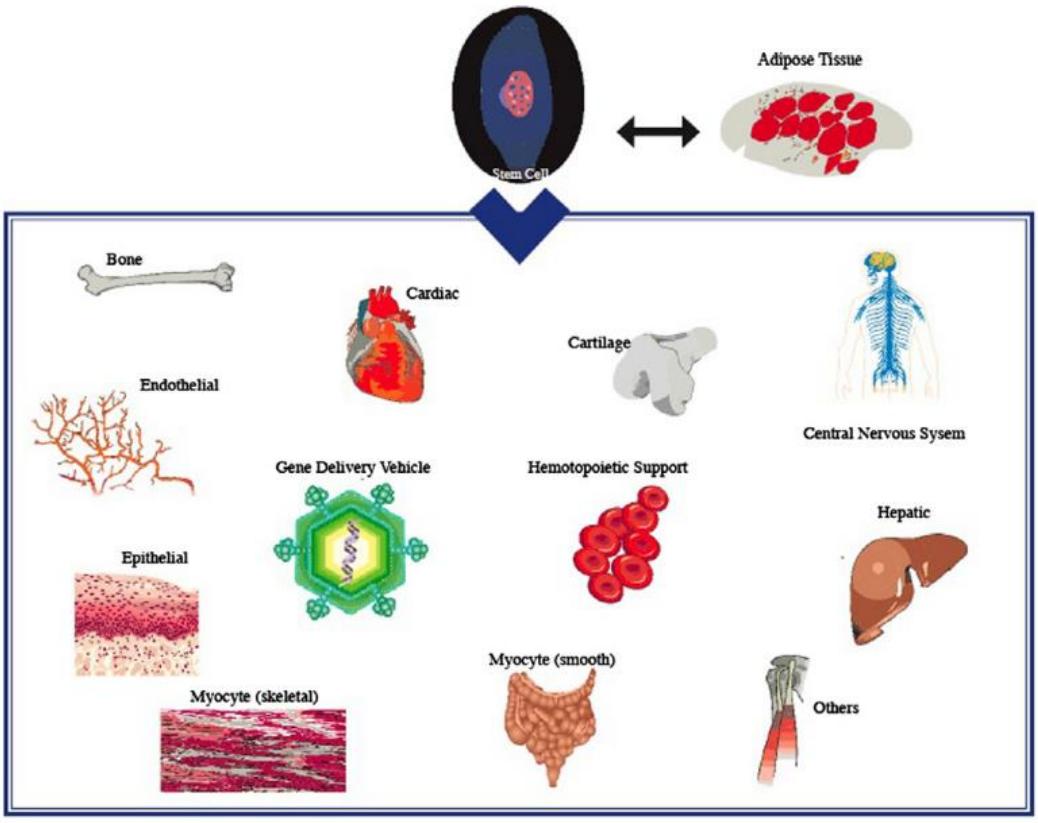

Fig. 2.5 Multilineage differentiation potential for adipose-derived stem cells [160]

2.2.3.2 Contributions of human ASCs in wound healing and skin regeneration

ASCs could promote wound healing by differentiation into various cell lineages and secretion of angiogenic growth factors. ASCs can be easily obtained from liposuction of human adipose tissue, can be cultured on a large scale [39-41]. The ability of ASCs to promote angiogenesis, to secrete growth factors and to differentiate into multiple cell types, could create a viable skin substitute. ASCs are known to significantly reduce the wound size and accelerate the re-epithelialization process via promoting the proliferation of human dermal fibroblasts (HDF), not only by cell-to-cell direct contact, but also by paracrine activation through secretory factors [42]. Ebrahimian and colleagues also demonstrated that ASCs promote wound healing, have the potential to differentiate into keratinocytes, and to produce KGF as well as vascular endothelial growth factor (VEGF) [158]. Furthermore, it was also demonstrated that ASCs can differentiate into epithelial lineage [159]. Meruane and colleagues combined adipose-derived stem cells and Integra (Integra LifeSciences, Plainsboro, N.J.) for treating full-thickness tissue injury on

Sprague-Dawley rats. Adipose-derived stem cells were isolated from the inguinal region of eight Sprague-Dawley adult rats, seeded onto a piece of dermal substitute for 48 hours, and then implanted into the same rat, followed by comparison of the evolution with a contralateral implant without adipose-derived stem cells. After 1, 2, and 3 weeks of regeneration *in vivo*, implants were removed for histologic evaluation. The histologic evaluation showed that adipose-derived stem cells significantly increased microvascular density (7.7 ± 0.6 percent versus 5.3. ± 0.5 percent, as assessed by immunohistochemical staining of factor VIII) and the synthesis of collagen type I (24 ± 3 percent versus 16 ± 2 percent, as assessed by Sirius red staining) [161]. ASCs are demonstrated to accelerate chronic wound healings. Davis et al. demonstrated that purified ASCs delivered in a trans-glutaminase gel significantly accelerated wound closure in chronically irradiated animals compared to the controls (gel alone without cells) [162]. Meanwhile, Nambu and colleagues demonstrated that scaffold cultured with autologous ASCs significantly accelerated wound healing in diabetic mice [163].

2.2.4 Potential of electrospun nanofibrous scaffolds (NFS) as tissue-engineered skin grafts

2.2.4.1 NFS as tissue-engineered scaffolds

It is agreed that cells play a significant role in tissue engineering. In addition, the design and fabrication of scaffolds also contribute an important part for the success of tissue engineering. The scaffold fabricated from synthetic and natural polymers can support the survival, proliferation, differentiation and migration of different cell types for the regeneration of tissues and organs. The design of tissue-engineering scaffold should mimic the structure and biological function of native extracellular matrix (ECM) as much as possible, both in terms of chemical composition and physical structure.

Micro- or naon- scaled collagen fibrils form a three-dimensional fiber network in native ECM of huma skin [164]. Polymeric nanofiber, which is on the same scale with fibrils in natural ECM, is among the most promising biomaterials for native ECM analogs. Phase-separation, self-assembly and electrospinning are the currently applied technologies to fabricate nanofibrous scaffolds to mimic natural ECM. The

phase-separation technique is based on thermodynamic demixing of a homogeneous polymer-solvent solution into a polymer-rich phase and a polymer-poor phase, usually by either exposure of the solution to another immiscible solvent or cooling the solution below a bimodal solubility curve. Polymeric foam will be obtained after removing solvent by freeze-drying. However, only certain polymers could be effectively processed by phase-separation and it is strictly a laboratory scale technique [165]. Self-assembly can also fabricate nanofibers and it involves the spontaneous organization of individual components into an ordered and stable structure with preprogrammed non-covalent bonds [166]. However, due to its complexity and low productivity, the application of self-assembly is limited [167].

Electrospinning is a simple and effective way to fabricate nano- and micro- scale fibers from organic polymer solutions or polymer melts. The polymers can be functionalized with chemical or biomolecular components via electrospinning to improve cell adhesion and proliferation on the electrospun scaffolds [168]. The set-up of electrospinning consists four components: a high voltage supplier, a syringe pump, a capillary tube attached with a small diameter needle, and a collector. The high voltage between the need tip and collector, provides an electrical force to extrude fibers from constantly flowed polymer solutions. The extruded fibers will become solidified before reaching collector. Uniform fibrous membrane with interconnected pores will be collected on the collector [169, 170].

Amongst all the techniques mentioned above, electrospinning is the most versatile, simple, cost-effective and scalable method to fabricate nanofibers. Electrospinning can produce scaffolds with most of the structural features (fibrous structure and porosity etc.) required for cell growth and subsequent tissue organization. It also offers many advantages over conventional scaffold methodologies. For example, it can produce ultra-fine fibers with spatial orientation and a high surface-to-volume ratio, have control over fiber diameter and also give flexibility for surface modification [171].

2.2.3.2 Fabrication of NFS by electrospinning

This technique of electrospinning was first introduced by Zelency in 1914 [172]. Now, electrospinning has attracted increasingly worldwide attention in both the academic community and industrial world [17]. The fabrication process involves an electrostatic field of the order of 5-30 kV between a collector and the spinneret (usually in the form of a needle) (Fig. 2.6). The polymer melt or solution is pumped out of the spinneret at a controlled rate. When a stretching force provided by the sufficiently high electric field overcomes the surface tension of the polymer solution, a thin jet of the liquid flies towards the collector plate. The jet is only stable near the tip of the spinneret, after which it undergoes bending instability. As the charged jet accelerates toward regions of lower potential, the entanglements of the polymer chain will prevent the jet from breaking up, while the solvent evaporates resulting in the formation of randomly oriented nanofibers that can be collected on a grounded collector [14, 16].

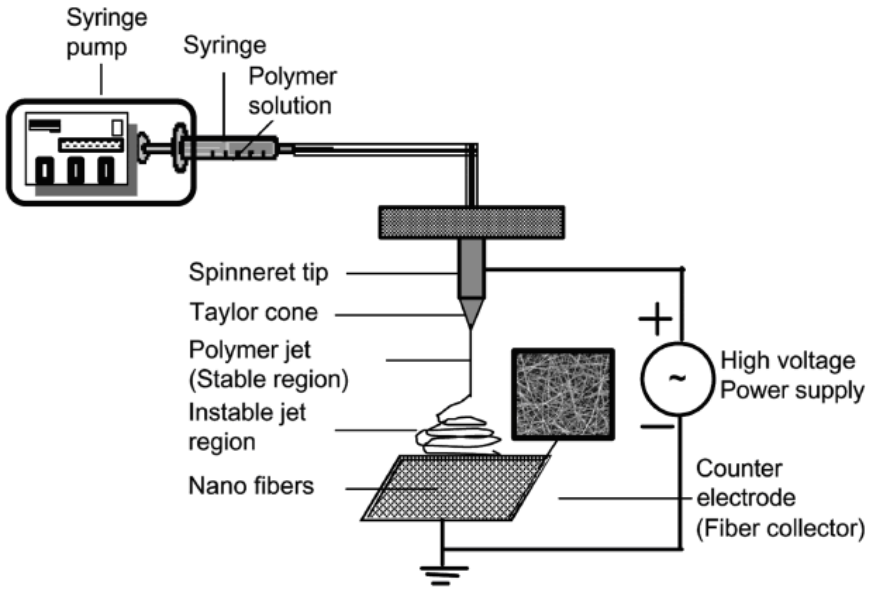

Fig. 2.6 The scheme of electrospinning system [14].

The diameters of the electrospun fibers are at least one order of magnitude smaller than those made by conventional extrusion techniques. Several parameters can affect the electrospinning process and fiber morphology (Table 2.5). We can therefore change various conditions to obtain suitable fibers for specific applications.

Table 2.5 Effect of changing electrospinning process parameters on the resultant fiber morphology [171].

Process Parameter	Effect on fiber morphology
Viscosity/concentration	▪ Low concentrations/viscosities yielded defects in the form of beads and junction; increasing concentration/viscosity reduced the defects; ▪ Fiber diameters increased with increasing concentration/viscosity.
Conductivity/solution charge density	▪ Increasing the conductivity aided in the production of uniform bead-free fibers; ▪ Higher conductivities yielded smaller fibers in general, except poly(acrylic acid) and polyamide-6.
Surface tension	▪ No conclusive link established between surface tension and fiber morphology.
Polymer molecular weight	▪ Increasing molecular weight reduced the number of beads and droplets.
Dipole moment and dielectric constant	▪ Successful spinning occurred in solvents with a high dielectric constant.
Flow rate	▪ Lower flow rates yielded fibers with smaller diameters; ▪ High flow rates produced fibers that were not dry upon reaching the collector.
Field strength/voltage	▪ At too high voltage, beading was observed; ▪ Correlation between voltage and fiber diameter was ambiguous.
Distance between tip and collector	▪ A minimum distance was required to obtain dried fibers; ▪ At distance either too close or too far, beading was observed.
Needle tip design	▪ Using a co-axial, two-capillary spinneret, hollow fibers were produced.
Collector composition	▪ Smooth fibers resulted from metal collectors; ▪ Aligned fibers were obtained using a conductive frame, rotating drum, or a wheel-like bobbin collector;

	▪ Yarns and braided fibers were also obtained.
Ambient parameters	▪ Increased temperature caused a decrease in solution viscosity, resulting in smaller fibers; ▪ Increasing humidity may result in the appearance of circular pores on the fibers.

2.2.3.3 Electrospun NFS as tissue-engineered skin grafts

Electrosupn Nanofibers, which mimic the collagen fibrils in the native skin ECM and have high porosity, suitable mechanical properties and large surface-to-volume ratio, can be an ideal substitute for wound healing and burn wound care. Natural polymers such as chitosan, gelatin, collagen, fibrinogen, silk, hemoglobin, myoglobin and synthetic polymers such as polyesters and polyphosphazenes, poly(L -lactic acid)–co-poly(3-caprolactone) (PLLCL) and poly (D,L)-lactic-co-glycolic acid (PLGA) have been electrospun to micro- and nano- fibers for their use as scaffolds for skin regeneration [173-180].

Synthetic materials including both nonbiodegradable and biodegradable polymers have also been used to manufacture NFS for promoting wound healing. Medical grade biostable polyurethane (PU) is a notable example of nonbiodegradable polymer for wound care. It has been shown that PU nanofiber dressings promoted faster healing compared with commercialized permeable PU (TegadermTM). Electrospun PU NFS was found to effectively control evaporative water loss, allow oxygen permeability and enhance drainage of wound exudates due to nanofiber porosity [181]. However, due to its long-term biostable properties, medical grade PU, either in nanofiber or commericialized form, can only be used as a temporary dressing *in vivo* and required to take off after completion of its functions. For the skin graft application, the hydrolyzates from the degraded scaffolds should not be toxic and cause any immune rejections.

Other biodegradable synthetic polymers include polyesters, polyanhydride, polyorthoester, polycarbonate, and polyfumarate [182]. Hydrolytical and enzymatically

hydrolysis are the two ways for polymeric materials degradation. Accordingly, polymers are classified into hydrolytically degradable polymers and enzymatically degradable polymers [183]. Hydrolytically degradable polymers such as such as poly(lactic acid) (PLA), polycaprolactone (PCL) and their copolymers are most commonly used for tissue engineering [184-186]. PLA undergoes hydrolytic scission to its monomeric form, lactic acid, which is eliminated from the body by incorporation into the tricarboxylic acid cycle. The principal elimination path for lactic acid is respiration, and it is primarily excreted by lungs as carbon dioxide. PCL undergoes hydrolytic degradation due to the presence of hydrolytically labile aliphatic ester linkages [187]. FDA has approved the use of above mentioned polymers for certain human clinical use, such as surgical sutures and some implantable devices. All of these biodegradable polymers have been used to construct NFS for tissue-engineered scaffolds because of their favorable mechanical and biodegradation properties to promote the ingrowth of new tissue [182]. PLLCL is a synthetic, biodegradable and non-toxic co-polymer of poly-L-lactic acid (PLLA) and PCL, investigated as a biomaterial for surgery and drug delivery systems. Unlike PLA or PCL, the biodegradation rate of PLLCL can be adjusted by changing the molar ratio of lactic acid and caprolactone in the co-polymer [188, 189]. Thus, PLLCL is more capable to meet the requirement of different degradation rates in biomedical applications, compared to PLA and PCL.

However, the major disadvantage of synthetic materials is the lack of cell-recognition signals. Therefore, manufacturing process of electrospun NFS which incorporates both biodegradable synthetic and natural materials was explored, such as electrospun PCL/Collagen NFS [190], PCL/gelatin NFS [191], poly(L-lactide-co-ε-caprolactone)/gelatin NFS [192] for wound healing and skin reconstitution.

Collagen type I is a particular good candidate for constructing NFS skin grafts because it is the most abundant ECM substance in human skin tissue [193]. Rho and colleagues produced a cross-linked nanofibrous matrix of type I collagen via electrospinning to develop biodegradable and biomimetic scaffolds. They also examined the effect of

collagen nanofibers on open wound healing in rats. They found that collagen nanofibrous matrices promoted cell adhesion and they were very effective as wound-healing accelerators in early-stage wound healing [194]. However, the application of collagen is limited due to its high price and poor mechanical properties. Gelatin, which is a natural biopolymer derived from collagen has many advantages (biological origin, biodegradability, biocompatibility) and most importantly, it can be available at relatively low cost. These merits credit the wide applications of gelatin in the pharmaceutical and medical fields [195]. Chong and colleagues developed a cost-effective composite consisting of a nanofibrous scaffold directly electrospun PCL/gelatin nanofiber onto a polyurethane dressing (Tegaderm^{TM}, 3M Medical) for dermal wound healing. Their results suggest that PCL/gelatin nanofibrous scaffold achieved significant cell adhesion, growth and proliferation [191]. Kim and colleague choosed polyurethane instead of PCL to electrospin gelatin/polyurethane nanofibers for wound healing applications. They found that as the total amount of gelatin increased, the cell proliferation increased with the same amount of culture time [196]. Other natural polymers such as chitosan and silk are also electrospun into nanofibers for wound healing. Kang and colleagues studied the wound healing ability of chitosan coated poly(vinyl alcohol) (PVA) nanofiber *in vivo*. They found that The chitosan coated PVA nanofibrous matrices showed faster wound healing than the control without coating [197]. Meanwihle, Schneider and colleagues fabricated silk nanofibrous scaffold for wound healing via electrospinning. They tested the scaffold on top of a wounded human skin-equivalent in order to measure the wound healing rate in tissues that accurately mimic the human wound response. The use of EGF-charged silk mats increased the rate of wound closure by more than 3.5-fold when compared to the silk dressing without EGF [198].

The nano or micro size fibrils in native skin ECM maintain the integrity of skin tissue and guide tissue remodeling. In addition, these fibrils also act as reservoirs to store bioactive factors for the regulation of cell migration, proliferation, and differentiation [12]. Core-shell incorporated with bioactive factors of ECM could be a promising scaffold for wound healing. The controlled release of bioactive factors can be realized via core-shell nanofibers, meanwhile, it can also protect the biological agents from the harsh

environments [24]. Choi and colleagues used amine-functionalized block copolymers composed of PCL and PEG to electrospin coaxial nanofibrous scaffolds which encapsulate bFGF in the core. Then EGF was further conjugated onto the surface of the nanofibrous meshes. The wound healing capability of the two growth factors loaded nanofibrous scaffolds were evaluated *in vivo*. Accumulation of collagen and keratin was found for cells cultured on the core-shell nanofibrous meshes and then they conclude that this nanofibrous matrix could play an promising role in wound healing rates while reducing scar [199]. Unlike these researchers, Zhao and his colleagues studied wound healing in a different way where they used electrical signals to regulate wound re-epithelialization. They found that with percolation of an electric field with a polarity that along the default healing direction, the cells will move following the direction of the electric signal and the wound got closed [121]. Meanwhile, Tada and colleague confirmed that LED irradiation promoted the process of wound healing by increasing the proliferation of fibroblasts. All the facts make us believe that it is time to "Charge the batteries to heal wounds". Poly(3-hexylthiophene) would be one of the most promising photosensitive materials for regenerative medicine and wound healing due to its low thermal conductivity, non-toxicity and low cost properties [200] .

Poly(3-hexylthiophene) or P3HT, has been the focus of great interest in organic solar cells [201] because of its optical and conductive properties. It has been used as an electron donating polymer in bulk heterojunction (BHJ) solar cells [202]. P3HT can be synthesized by the chemical polymerization of 3-hexylthiophene monomer by using iron(III) chloride as a catalyst [203] and it is known for its high mobility, good solubility and good film forming properties [204]. When light irradiates on P3HT, it will absorb the energy of photons with a certain wave length and if the energy of photons is greater than the electron binding energy of P3HT polymer, P3HT molecules will release electrons and this is the general mechanism of photosensitivity of P3HT. The biocompatibility of PCL/P3HT nanofibers was studied in our group and results showed that cells can attach on containing P3HT molecules on its surface. Being biocompatible together with its photosensitive properties, Electrospun core-shell nanofiber incorporating with P3HT and

bioactive factors could be a suitable substrate for cell attachment and could be utilized for enhanced skin tissue regeneration.

2.3 Summary

To promote wound healing, current research focuses mainly on the creation and development of an ideal skin graft that will most probably encompass several strategies such as the use of functional cellular components, different biodegradable materials and scaffolds with analogous ECM structures and components, which have been described in this chapter. Electric signal was found to contribute in wound healing via promoting cell migration towards the wound area. Meanwhile, LED irradiation promoted the process of wound healing by increasing the proliferation of fibroblasts. In the present study, a biomimetic and photosensitive nanofibrous skin graft will be designed and developed by combining the functionality and flexibility of electrospun NFS with the promising photosensitive property of P3HT. Biodegradable PLLCL and Gelatin will be blended for fabrication of the electrospun core-shell NFS encapsulating EGF and P3HT. The feasibility of resultant biomimetic and photosensitive NFS/ASCs composites as skin grafts will be evaluated under light stimulation. The strategy aims to provide a new aspect to heal acute full-thickness skin wounds.

Chapter 3

Fabrication and optimization of cost-effective nanofibrous scaffolds for *in vivo* wound healing

3.1 Introduction

Wound injuries could be caused by acute trauma, genetic disorders, surgical interventions and disease leading to skin necrosis. One of the most common causes for major skin injury is thermal trauma [1]. According to WHO, 6 million patients worldwide suffer from burns every year and 300,000 deaths are annually attributed to burn injuries [3]. Moreover, in patients with extensive burns, limited availability of autografts complicate wound closure and the delayed wound healing can compromise recovery, increase the risk of invasive wound infection and mortality [9]. The need for permanent wound closure in burn patients has driven the development of tissue engineered skin replacements [10]. In tissue engineering, scaffold plays an important role, since it can maintain and promote the growth of the cells or tissue [205]. Electrospun nanofibrous matrices show morphological similarities to the natural ECM, characterized by ultrafine continuous fibers, high surface-to-volume ratio, high porosity and variable pore-size distribution similar to the dimensions of basement membranes. Due to the interconnected highly porous structures, electrospun nanofibrous matrices could be applied as tissue engineered scaffolds to facilitate cellular migration and transport of nutrients, and metabolic wastes to allow the formation of new tissue [206]. Furthermore, natural proteins such as collagen, gelatin, fibronectin and chitosan were incorporated into electrospun nanofibers to improve its biocompatibility [19, 178, 195, 207]. Because of their abundance in skin and their recognition by cell surface receptors, these natural materials display low toxicity and low chronic inflammatory response [208]. Electrospun collagen based nanofibrous scaffolds were observed to induce fast wound healing and tissue regeneration both *in vitro* and *in vivo* [209-211]. Collagen makes up approximately

70% of the dry weight of skin [212] and in order to provide an environment as similar as the native ECM of human skin, previously we fabricated collagen/poly(L -lactic acid)–co-poly(ε-caprolactone) (Coll/PLLCL) nanofibrous scaffolds with a collagen:PLLCL ratio of 70:30 (wt.%) by electrospinning and studied the epidermal differentiation of bone marrow derived mesenchymal stem cells (BM-MSC) on this scaffold. We found that the stem cells on Coll/PLLCL nanofibers had higher percentage of differentiated cells (66.2%) than those on PLLCL nanofibers (33.3%) without regional differentiation [176]. However, the poor mechanical properties and high cost limit the application of collagen in wound healing. Compared with collagen, gelatin, which is derived from collagen by controlled hydrolysis, is cheaper and does not show antigenicity under physiological conditions [21, 22]. Moreover, gelatin is biodegradable, biocompatible and displays many integrin binding sites for cell adhesion, migration, proliferation and differentiation due to the abundant Arg–Gly–Asp (RGD) sequences in its amino acid chain [16, 23]. Chong and colleagues electrospun poly(ε-caprolactone)/gelatin (PCL/gelatin) nanofibers from a gelatin and PCL blended solution at a ratio of 50:50 (v:v) to developed a cost-effective composite for dermal wound healing. Their results suggest that PCL/gelatin nanofibers achieved significant cell adhesion, growth and proliferation [191]. Lately, Heo and colleagues found that the electrospun gelatin/polyurethane nanofibers could promote the regeneration of burn-wounds [213]. For clinical applications, a proper scaffolding system must be inexpensive and retain structural integrity and stability during implantation *in vivo*, and after surgery, must provide sufficient mechanical support during the process of tissue regeneration [214, 215]. Jeong et al. electrospun naonfibers from blends of gelatin and PLLCL (blending ratio: 0, 30, 70 and 100 wt% gelatin to PLLCL) solutions to prepare non-woven fibers for the development of mechanically functional engineered skin grafts. They found that pure gelatin and 70% gelatin containing naonfibers are the ideal scaffolds for cell attachment and proliferation. Meantime, PLLCL and 30% gelatin containing nanofibers had better mechanical properties and they are stable for long-term mechanical stimulation [192]. However, they failed to find out the optimized amount of gelatin containing nanofiber which has suitable mechanical properties meanwhile favors cell proliferation. In order to find a cost-effective and the optimized electrospun NFS for

wound healing, we blended gelatin with PLLCL and electrospun to obtain composite gelatin/PLLCL nanofibers with four different weight ratios of gelatin:PLLCL (w/w) of 80:20 [Gelatin/PLLCL(80)], 70:30 [Gelatin/PLLCL(70)], 60:40 [Gelatin/PLLCL(60)] and 50:50 [Gelatin/PLLCL(50)]. The mechanical properties of the scaffolds were evaluated in both dry and wet conditions. The comparative proliferation of human dermal fibroblasts (HDF) on these electrospun nanofibers was studied by cell proliferation assay. Based on our results, we confirmed that Gel/PLLCL(60) is the optimized skin graft and its capability in wound healing was further confirmed *in vivo* in a mouse model.

3.2 Materials and methods

3.2.1 Materials

Human dermal fibroblasts (HDFs) were purchased from American Type Culture Collection, USA. Dulbecco's modified Eagle's medium/nutrient mixture F12 (DMEM/F12), fetal bovine serum (FBS), penicillin-streptomycinsolution, 4,6-diamidino-2-phenylindole, dihydrochloride (DAPI), were all purchased from Invitrogen (Carlsbad, CA). Hematoxylin and eosin (H&E), gelatin, and 1,1,1,3,3,3-hexafluor-2-propanol (HFP) were all purchased from Sigma-Aldrich (Singapore). Actin Cytoskeleton/Focal Adhesion Staining Kit was purchased from Merck Millipore. Poly(L-lactic acid)-co-poly-(ε-caprolactone) (PLLCL) (70:30,molecular weight 150 kDa) was purchased from Boehringer Ingelheim Pharma GmbH (Ingelheim, Germany).

Male Kunming white mice (weight, 30-40 g) were obtained from center for animal resources and housed in the animal holding unit of Second Affiliated Hospital of Harbin Medical, China. Mice consumed both sterile water and standard mouse chow ad libitum.

3.2.2 Electrospinning of nanofibers

PLLCL was dissolved in HFP to obtain an 8% (w/v) solution. Gelatin and PLLCL were dissolved in HFP at a ratio of 80:20, 70:30, 60:40 and 50:50 (wt.%), respectively, to obtain 10% (w/v) solution and stirred overnight. A 3 ml standard syringe attached with a

27G blunted stainless steel needle was used to contain the polymer solutions separately and the solutions were pumped by pump a syringe pump (KDS 100, KD Scientific, Holliston, MA) at a flow rate of 1.0 ml h^{-1}. 15 kV high was applied when the polymer solution was drawn into fibers and collected on an aluminum foil wrapped collector at a distance of 12 cm from the needle tip. Nanofibers collected on 15 mm coverslips and the aluminum foil were dried overnight under vacuum and used for the characterization and cell culture experiments.

3.2.3 Morphology and characterization of electrospun nanofibers

Field Emission Scanning Electron Microscope (FESEM) (FEI-QUANTA 200F, Netherlands) was used to study the morphology of the electrospun nanofibers at an accelerating voltage of 10 kV, after sputter coating with gold (JEOL JFC-1200 fine coater, Japan). The obtained SEM images were applied to obtain the diameters of the electrospun fibers using image analysis software (Image J, National Institutes of Health, USA). VCA Optima Surface Analysis system (AST products, Billerica, MA) was applied to measure the hydrophilic/hydrophobic properties of the electrospun nanofibrous scaffolds. A CFP-1200-A capillary flow porometer (PMI, New York, NY) was used in this study to measure the pore size. Calwick with a defined surface tension of 15.9 dynes/cm (PMI, New York, NY) was used as the wetting agent for porometry measurements. Nanofibers were cut into 3 cm × 3 cm squares for porometry measurement. Nanofibers with similar thickness were obtained and each sample was tested individually. Functional groups of the electrospun nanofibrous scaffolds were evaluated by attenuated total reflectance fourier transform infrared (ATR-FTIR) spectroscopic analysis in a Nicolet Avatar 380 spectrometer (Thermo Nicolet, Waltham, MA) over the range 600-3800 cm^{-1} at a resolution of 4 cm^{-1}. A tabletop tensile tester (Instron x345, Canton, MA) was applied to determine the tensile properties of the electrospun nanofibrous scaffolds at a load cell capacity of 10 N. The mechanical properties of the electrospun NFS were examined under both dry (D) and wet (W) conditions. The dry specimens were cut into approximately 20 mm × 10 mm (length × width) in order to be loaded into the uniaxial testing machine. Specimens were measured with a 10 N load cell under a cross-head speed of 10 mm min^{-1} (n = 5). For the measurement of the NFS in the wet condition, specimens were immersed

in distilled water at room temperature for 24 h. The measurement method was the same as that in the dry condition. The tensile stress strain values obtained from the instrument were plotted using an Excel sheet.

3.2.4 Culture of HDFs

HDFs were cultured in DMEM supplemented with 10% FBS and 1% antibiotic and antimycotic solutions (termed as normal growth media) in a 75 cm^2 cell culture flask. Cells were incubated at 37 °C in a humidified atmosphere containing 5% CO_2 and the culture media was changed once in every 3 days. The 15-mm cover slips with electrospun nanofibers were placed in 24-well plate and pressed with a stainless steel ring to ensure complete contact of the scaffolds with the wells. The specimens were sterilized under UV light, washed thrice with phosphate buffered saline (PBS) and subsequently incubated in DMEM overnight before cell seeding. HDFs were grown to confluency, detached by trypsin, counted by trypan blue assay using a hemocytometer and seeded on the scaffolds at a density of 10,000 cells/well.

3.2.5 Cell proliferation

The comparative proliferation of HDFs on electrospun NFS was determined using the colorimetric MTS assay (CellTiter 96 AQueous One solution, Promega, Madison, WI). After culturing the cells for a period of 3, 6 and 9 days, cells were rinsed with PBS to remove any unattached cells and incubated with 20% MTS reagent in serum free medium for a period of 3 hrs at 37 °C. Absorbance of the obtained dye was measured at 490 nm using a spectrophotometric plate reader (FLUOstar OPTIMA, BMG lab Technologies). The amount of formazan crystals formed is directly proportional to the number of live cells, which was also directly proportional to the absorbance values obtained.

3.2.6 F-actin staining

F-actin staining was performed to study cell morphology on different substrates after 9 days culture. 5 % paraformaldehyde was added to fix the cells at room temperature for 15 min, and then the cell substrate composites were washed with PBS and further incubated with 2 % BSA to block any unspecific binding. After that, phalloidin was used to stain the

cytoskeleton (F-actin) for 2 h at room temperature. Further, DAPI (1:5000) was added to staing the nuclear of cells for 30 min at room temperature. Final washing of the constructs was done with PBS before mounting on a glass slide and visualized under laser scanning confocal microscopy (LSCM).

3.2.7 Expression of collagen

The presence of collagen in the cell matrix was studied by Sirius Red staining. Sirius Red is a strong anionic dye whose sulfonic acid groups interact with the basic groups of collagen producing red stains. The intensity of red stains was used to determine the secretion of the collagen-containing ECM by fibroblasts. Sirius red stain consisting of 0.1% Sirius red F3B in a saturated aqueous solution of picric acid was used to stain the cell substrate composites which were first fixed with 2.5% formaldehyde for 1 h. Then, mild acidified water was used to wash the composites, followed by 100% ethanol and viewed under a Leica BM IRB microscope. Collagen is stained red on a yellow background in the nanofibrous scaffolds.

3.2.8 Surgical procedures

Twenty four male Kunming white mice were anesthetized by isoflurane inhalation, and their back were shaved and swabbed with povidine–iodine followed by 70% ethanol for three times. Then a sterile template measuring 8 × 8 mm was placed on the skin and the outline was traced using a sterile fine felt-tipped pen. Full thickness skin wound (FTSW) of 8 × 8 mm were made by excising the skin within the confines of the square down to the level of subcutaneous panniculus carnosus. FTSW (n = 12 for each group) were then subjected to two different kinds of treatments: (1) receiving no nanofibers (control); (2) receiving Gel/PLLCL(60) nanofibers. After the surgery, each animal was placed in one cage. Postsurgery care included analgesic and antibiotic injections. Checking of any postsurgery pain, distress, or complications was done 24 h after surgery and daily afterward. Then, on postoperative days 5 and 10, four mice in each group were euthanized and the reconstituted skin was harvested for the following evaluations. The left four mice in each group were not euthanized until complete wound closure.

3.2.9 Histological and immunological analyses

The reconstituted skin was cut to the control depth determined as the layer of panniculus carnosus, and fixed in 4% paraformaldehyde, dehydrated, and then paraffin-embedded. Serial 10 mm paraffin sections were cut with a rotating microtome (MICROM) and stained with H&E according to routine histology protocol.

3.2.10 Statistical analysis

All the data presented are expressed as mean ± standard deviation (SD) of the mean. Each experiment was repeated three times. Statistical differences were determined by Student's two-sample t test. Differences were considered statistically significant at $p \leq 0.05$.

3.3 Results and discussions

Collagen is the dominant protein in the native ECM of human skin and around 70% of the dry weight of the ECM from skin is represented by collagen [212]. It has been incorporated to tissue engineered skin grafts to modulate cell behavior and augment the *in vivo* performance [177]. However, due to the high cost and poor mechanical properties of collagen, the application of collagen in tissue engineered scaffolds is limited. On the contrary, gelatin derived from the hydrolysis of collagen has been widely utilized in the pharmaceutical and medical fields in a variety of applications, including tissue engineering, wound dressing, drug delivery and gene therapy for its biocompatibility, biodegradability and most important cost efficiency [216]. For these reasons, gelatin could be an ideal candidate for fabricating cost-effective tissue engineered skin grafts. Besides mimicking the component of native ECM, the physical structure, mechanical properties and biocompatibility of the scaffold are also important for the success of tissue engineered scaffold. In the current study, we electrospun nanofibers from the solutions with different content of gelatin in blend (80, 70, 60 and 50 wt%) and examine the mechanical properties of these nanofibers in both dry and wet conditions. Cell proliferation assay was applied to study the biocompatible properties of these gelatin containing nanofibers. Finally, the optimized NFS was further evaluated *in vivo* in a mouse model.

3.3.1 Morphology and characterization

Nanofibers of Gel/PLLCL(80), Gel/PLLCL(70), Gel/PLLCL(60), Gel/PLLCL(50) and PLLCL were fabricated by electrospinning and the fiber morphology was examined under scanning electron microscope (SEM). SEM micrographs of electrospun NFS revealed uniform beadless fibrous structures under the optimized spinning conditions utilized during this study (Fig. 3.1a). Uniform nanofibers of Gel/PLLCL(80), Gel/PLLCL(70), Gel/PLLCL(60), Gel/PLLCL(50) and PLLCL with fiber diameters of 537.5 ± 121.9, 487.4 ± 152.8, 354.8 ± 70.1, 970.6 ± 81.8 and 613.3 ± 92.4 nm, respectively, were obtained. Applied with low pressure, capillary flow porometry provides a simple and non-destructive technique for rapid and accurate measurement of pore size [217]. Therefore, capillary flow porometry can provide reproducible pore size measurements with ignorable distortion errors [218]. The pore size as determined by capillary flow porometer, for the Gel/PLLCL(80), Gel/PLLCL(70), Gel/PLLCL(60), Gel/PLLCL(50) and PLLCL was 1.48, 1.31, 1.01, 1.74 and 1.53 µm, respectively. The mean pore sizes obtained for the nanofibers were found inversely proportional to the diameter of the fibers and our results were also in agreement with the results reported by Li et al [218]. For use as a wound dressing, scaffolds need to have an ideal structure that gives high porosity and small pore size yet serves as a good barrier. Among the electrospun NFS, Gel/PLLCL(60) has the smallest fiber diameter and pore size and this makes Gel/PLLCL(60) a more suitable skin graft than other electrospun NFS.

PLLCL was found to be highly hydrophobic with a contact angle of 131 ± 2 °C (Fig. 3.1b). However, with the incorporation of gelatin, the Gel/PLLCL(80), Gel/PLLCL(70), Gel/PLLCL(60) and Gel/PLLCL(50) nanofibers became more hydrophilic, with a contact angle of 39 ± 7^0, 44 ± 8^0, 30 ± 1^0 and 45 ± 6^0, respectively. Fig. 3.1c shows the ATR-FTIR spectra of electrospun nanofibers. The characteristic ester absorption peak of PLLCL was observed at 1760 cm^{-1}, and C-O-C stretching vibrations were observed at 1097, 1133 and 1187 cm^{-1}. The Gel/PLLCL(80), Gel/PLLCL(70), Gel/PLLCL(60) and Gel/PLLCL(50) showed the characteristic amide I and amide II peaks of gelatin at 1650 cm^{-1} and 1550 cm^{-1} in addition to the characteristic peaks of PLLCL.

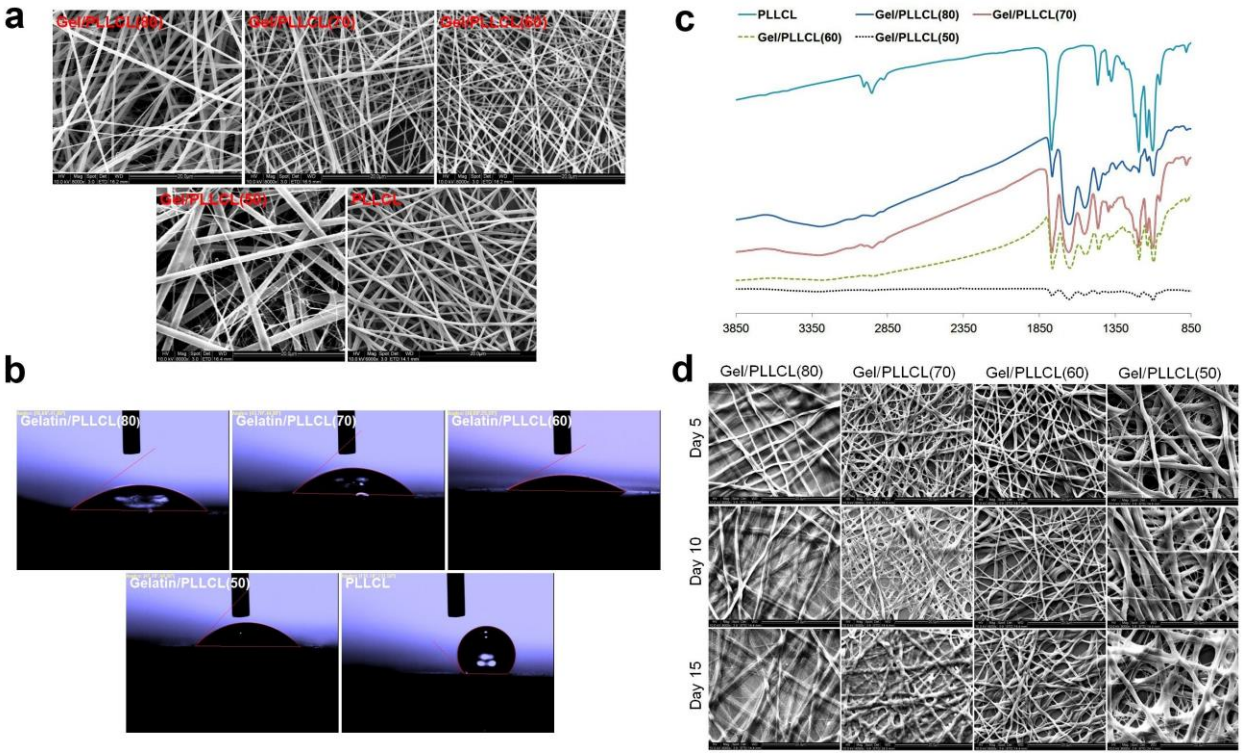

Fig. 3.1 **Characterizations of electrospun nanofibers**. **a**. SEM morphology of Gel/PLLCL/(80), Gel/PLLCL/(70), Gel/PLLCL/(60), Gel/PLLCL/(50) and PLLCL nanofibers. **b**. Water contact angle for electrospun nanofibers. **c**. FTIR spectra of Gel/PLLCL/(80), Gel/PLLCL/(70), Gel/PLLCL/(60), Gel/PLLCL/(50) and PLLCL nanofibers. **d**. Morphological changes of Gel/PLLCL/(80), Gel/PLLCL/(70), Gel/PLLCL/(60) and Gel/PLLCL/(50) nanofibers after degradation in PBS for 5, 10 and 15 days.

Fig. 3.1d exhibits the morphological changes in electrospun NFS during *in vitro* degradation at three different time points (day 5, 10 and 15). After 5 days of degradation, the gelatin containing nanofibers appeared to have swollen and lost their initial surface smoothness (Fig. 3.1d). Moreover, Gel/PLLCL(80) had significant morphological changes duo to the massive loss of gelatin in the surface layers. After 10 days of degradation in PBS, Gel/PLLCL(70) had apparently swelled (Fig. 3.1d). This can be explained by the dissolution of gelatin in the buffer. However, the fiber structure still can be found in Gel/PLLCL(60) and Gel/PLLCL(50). No further morphological changes were observed after 15 days of degradation.

In addition to physically integrating into the skin wound, scaffold materials must be able to withstand the load of the tissue and provide mechanical strength [219]. The ideal tissue

engineered scaffold should be easily handled and retain certain mechanical strength after implantation to provides it with good resilience and compliance to movement as a skin graft. The mechanical behavior in the wet state is extremely important in predicting the mechanical properties of the membrane *in vivo*. Therefore, it is necessary to examine the mechanical properties of the electrospun NFS in both dry and wet conditions. Fig. 3.2 shows the stress-strain curves of different electrospun nanofibers under tensile loading.

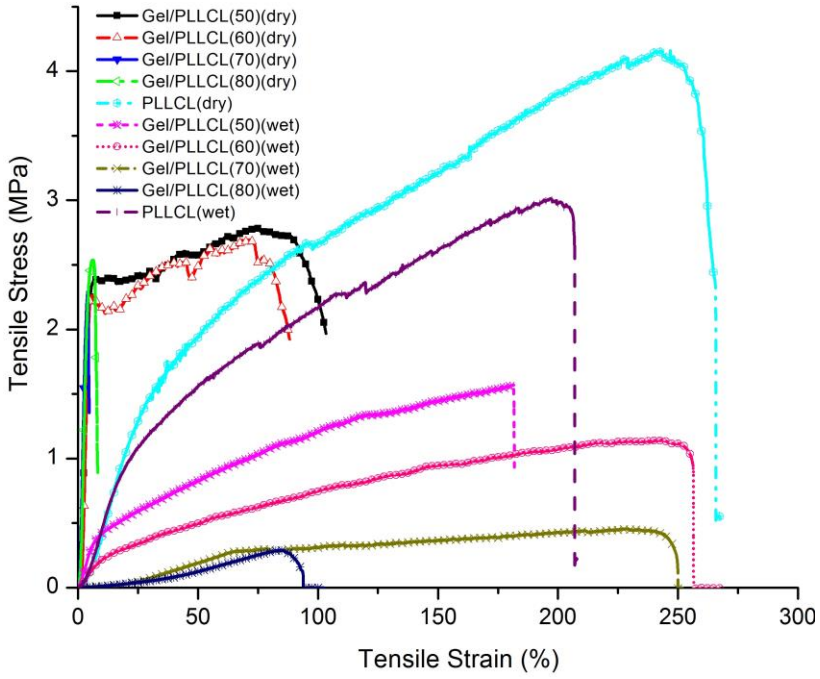

Fig. 3.2 Typical stress-strain curves of random Gel/PLLCL/(80), Gel/PLLCL/(70), Gel/PLLCL/(60), Gel/PLLCL/(50) and PLLCL nanofibrous scaffolds in dry and wet conditions.

Comparing the stress-strain curves of gelatin containing NFS with those of the stress-strain curve of PLLCL in the dry condition, we found that the incorporation of higher amounts of gelatin to PLLCL led to a significant increase in elastic modulus and decrease in ultimate strain of the electrospun composite scaffolds ($p \leq 0.05$). Mechanical evaluations of the Gel/PLLCL(80) and Gel/PLLCL(70) naonfibers in dry conditions show a linear segment up to the proportionality limit, followed by a brittle fracture. Gelatin was found mainly contributes to the crystallinity of the electrospun membrane [220] and 80% or 70% gelatin makes Gel/PLLCL(80) and Gel/PLLCL(70) become extremely crystalline. The crystalline morphology of electrospun nanofibrous scaffold

can strongly influence its mechanical properties [221, 222]. Lim and colleagues found that the fibers with smaller diameter have higher degree of crystallinity and molecular orientation in the form of oriented fibrillar structure. The fibrillar structure would result in higher resistance to axial tensile force due to the higher degree of molecular orientation in the direction of applied stress [222]. Thus, Gel/PLLCL(80) and Gel/PLLCL(70) with higher crystallinity have higher elastic modulus with low or non ductility. Instead of showing a brittle fracture after liner segment, Gel/PLLCL(60), Gel/PLLCL(50) and PLLCL show a non-linear curve, which was characterized by considerable elongation without a corresponding increase in loading stress. This feature is mainly attributed to fiber arrangement in the mat. The fiber arrangement in the mat is expected to change during the stress–strain measurement. It was demonstrated that fibers tend to align in the direction of applied force before getting thinner and finally the breaking occurs [186, 223]. However, in the wet condition, only Gel/PLLCL(60), Gel/PLLCL(50) and PLLCL showed the similar tensile behaviors as in the dry condition. The hydrated Gel/PLLCL(80) and Gel/PLLCL(70) nanofibers are barely retain their mechanical properties. The tensile properties of nanofibrous substrates are summarized in Table 3.1.

Table 3.1 Tensile properties of the electrospun nanofibers in both dry and wet conditions

Property	Tensile Modulus (MPa)		Tensile Stress (MPa)		Strain at break (%)	
	Dry	Wet	Dry	Wet	Dry	Wet
Gel/PLLCL/(80)	82.44 ± 1.72	0.16 ± 0.04	2.52 ± 0.03	0.28 ± 0.03	6.29 ± 0.98	86.05 ± 3.02
Gel/PLLCL/(70)	87.42 ± 1.01	0.17 ± 0.03	2.29 ± 0.03	0.44 ± 0.01	3.64 ± 1.04	237.25 ± 5.90
Gel/PLLCL/(60)	74.92 ± 6.19	3.05 ± 0.24	2.68 ± 0.02	1.16 ± 0.03	79.65 ± 4.46	246.13 ± 5.44
Gel/PLLCL/(50)	73.43 ± 4.45	5.93 ± 0.40	2.76 ± 0.03	1.55 ± 0.15	93.25 ± 6.73	179.43 ± 2.13
PLLCL	7.72 ± 0.51	6.33 ± 0.23	4.10 ± 0.06	2.95 ± 0.16	252.78 ± 9.82	198.11 ± 6.49

The Young's modulus of Gel/PLLCL(80), Gel/PLLCL(70), Gel/PLLCL(60), Gel/PLLCL(50) and PLLCL nanofibers in dry condition was 82.44 ± 1.72, 87.42 ± 1.01, 74.92 ± 6.19, 73.43 ± 4.45 and 7.72 ± 0.51 MPa, respectively. In the wet condition, the Young's modulus and tensile strength at break of gelatin containing nanofibers decreased significantly. However, the Young's modulus of Gel/PLLCL(60), Gel/PLLCL(50) and

PLLCL nanofibers still can be calculated as was 3.05 ± 0.24, 5.93 ± 0.40 and 6.33 ± 0.23 MPa, respectively. The decrease in elastic modulus for the gelatin containing nanofibers can be attributed to hydration of considerable amounts of uncrosslinked hydrophilic gelatin in the surface layers [224]. The hydrated gelatin without enough crystallinity leads to the decrease of mechanical properties for gelatin containing nanofibers. Compared to Gel/PLLCL(80) and Gel/PLLCL(70) in the wet condition, the hydrated Gel/PLLCL(60) and Gel/PLLCL(50) still maintain the mechanical integrity of the membrane.

3.3.2 HDF proliferation on electrospun nanofibers

The capacity for NFS to support HDFs proliferation was evaluated using cell proliferation assay as shown in Fig. 3.3.

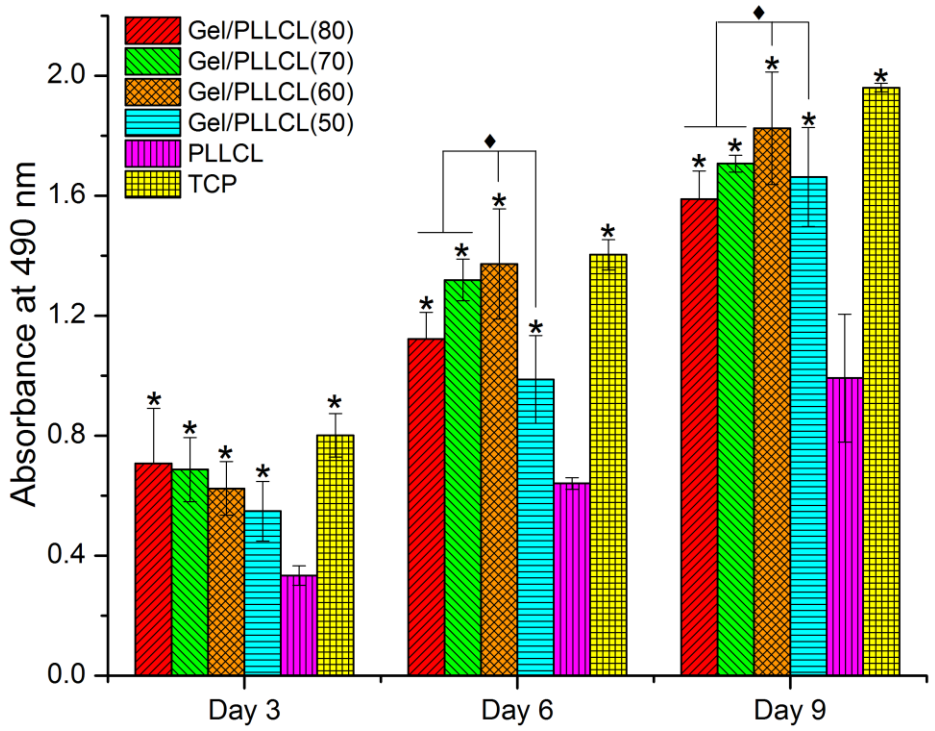

Fig. 3.3 HDFs proliferation on electrospun Gel/PLLCL/(80), Gel/PLLCL/(70), Gel/PLLCL/(60), Gel/PLLCL/(50) and PLLCL nanofibers. *Significant against cell proliferation on PLLCL at $p \leq 0.05$; ♦Significant against cell proliferation on Gel/PLLCL/(80), Gel/PLLCL/(70) and Gel/PLLCL/(50) nanofibers.

It was observed that the optical density of HDFs on all the electrospun substrates increased during the 9 days of cell culture. In the first three days, the attachment of HDFs

on naonfibrous scaffolds was proportional to the amount of gelatin included in the nanofibers. The reason is that gelatin displays many integrin binding sites for cell adhesion, migration, proliferation and differentiation due to the abundant Arg–Gly–Asp (RGD) sequences in its amino acid [16]. The more amount of gelatin presented in the nanofibers, the more integrin binding sites which lead to more cell attachments. However, after 6 days, the rate of proliferation on Gel/PLLCL(60) scaffold was significantly higher ($p \leq 0.05$) than on Gel/PLLCL(80) and Gel/PLLCL(70) nanofibers. This is due to the degradation and morphology changes of Gel/PLLCL(80) and Gel/PLLCL(70) nanofibers in wet condition. Both Gel/PLLCL(80) and Gel/PLLCL(70) nanofibers loss their nanofibrous morphology faster than Gel/PLLCL(60) and they almost loss their nanofibrous structure after 10 days degradation as shown in Fig. 3.1d. The cell proliferation on Gel/PLLCL(60) scaffold was significantly higher than cells on Gel/PLLCL(50). The effect of fiber diameter on cell proliferation has been explored, with the conclusion that smaller fibers seem to encourage better cell proliferation and signaling [225, 226]. Moreover, the large diameter (970 nm) of Gel/PLLCL(50) will restrain its high surface-to-volume ratio and binding sites, then lead to less cell proliferation on Gel/PLLCL(50) nanofibers.

After 9 days of cell culture, the cell proliferation on Gel/PLLCL(60) nanofibers was the highest among all the electrospun NFS. We observed 15%, 7%, 10% and 84% higher cell proliferation on Gel/PLLCL(60) compared to cell proliferation on Gel/PLLCL(80), Gel/PLLCL(70), Gel/PLLCL(50) and PLLCL nanofibers, respectively. The percentage increase in the rate of proliferation from day 3 to day 9 on Gel/PLLCL(80), Gel/PLLCL(70), Gel/PLLCL(60), Gel/PLLCL(50) and PLLCL nanofibrous scaffolds was found to be 124%, 151%, 195%, 202% and 200% respectively. Results of cell proliferation assay suggested that HDFs cultured on the electrospun Gel/PLLCL(60) nanofibers had better cell proliferation compared to other electrospun NFS. In addition, Gel/PLLCL(60) showed proper mechanical properties in both dry and wet conditions. On the basis of the results above, the electrospun Gel/PLLCL(60) nanofibers could be an ideal scaffold for skin tissue engineering and the capability of Gel/PLLCL(60) as a skin graft was further evaluated both *in vitro* and *in vivo*.

3.3.3 Cell morphology on nanofibers

The cell morphology on Gel/PLLCL(60), PLLCL and TCP were studied by SEM on day 9 and the results are shown in Fig. 3.4. Fibroblasts attached on the scaffolds and stretched across the nanofibrous substrates upon proliferation. Much more fibroblasts attached on Gel/PLLCL(60) (Fig. 3.4A) nanofibers compared to the cells attached on PLLCL nanofibers (Fig. 3.4B). The morphology of fibroblasts attached on Gel/PLLCL(60) nanofibers was a characteristic spindle shape and comparable to the cells attached on TCP, while the fibroblasts attached on PLLCL nanofiber showed irregular morphology (Fig. 3.4B).

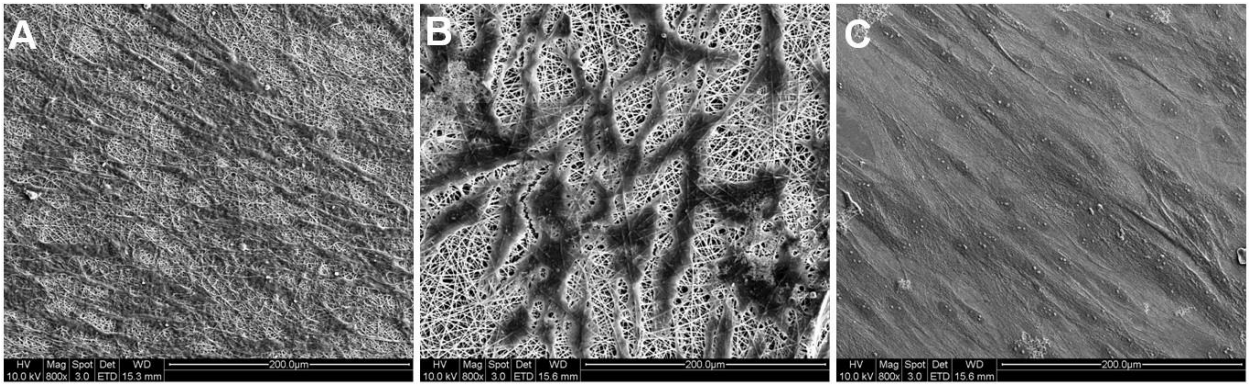

Fig. 3.4 SEM images of HDFs on Gel/PLLCL/(60), PLLCL and TCP.

To understand the interaction of fibroblasts with Gel/PLLCL(60) scaffolds, phalloidin and vinculin staining were carried out after 9 days of cell culture and the F-actin stains showed a cytoplasmic filamentous distribution under LSCM (Fig. 3.5). Vinculin is a widely distributed protein associated with the cytoplasmic surface of the plasma membrane where it is believed to link actin filaments to adhesion plaque structures [227]. HDFs attached on Gel/PLLCL(60) showed sufficient cell-to-cell communication. The number of vinculin-expressed HDFs on Gel/PLLCL(60) (Fig. 3.5) was higher compared to the number of cells on TCP and much better than the cells on PLLCL. The results confirmed that the biocompatibility of Gel/PLLCL(60) and it could be a promising scaffold for skin tissue engineering.

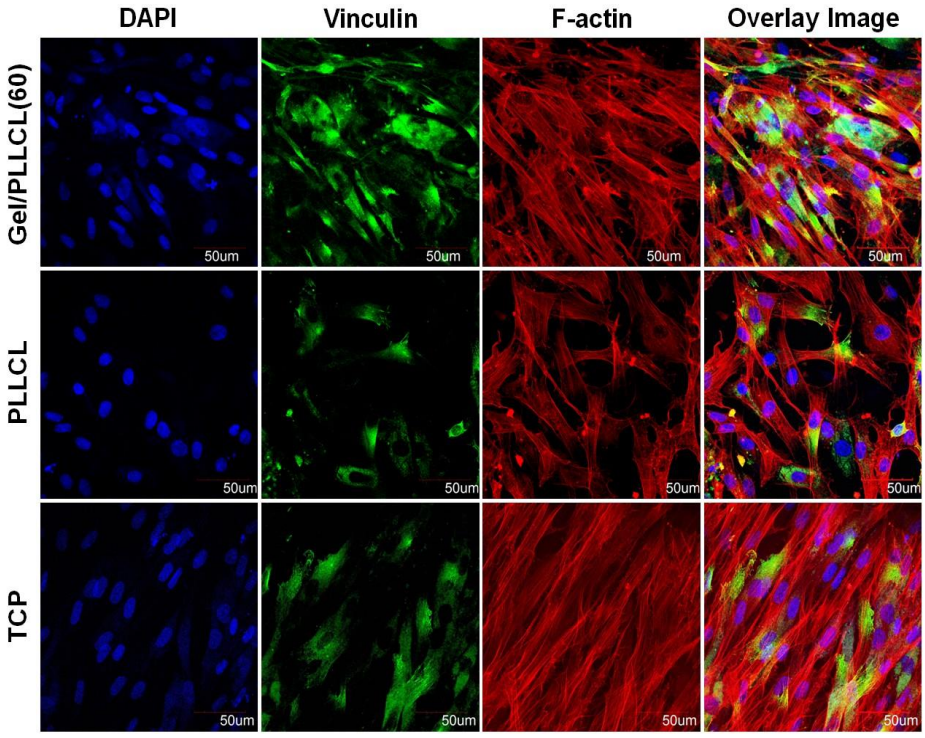

Fig. 3.5 Dual immunocytochemical analysis for the expression of F-actin, vinculin and the merged images showing the dual expression of both F-actin and vinculin on electrospun Gel/PLLCL/(60), PLLCL nanofibers and TCP.

3.3.4 Collagen expression

The wound healing process is characterized predominantly by ECM synthesis and remodeling into a highly organized architecture [228]. During wound healing, fibroblasts produce collagen-based ECM that ultimately replace the provisional fibrin-based matrix and help reapproximate wound edges through their contractile properties [42]. Collagen staining with Picro-sirius red confirmed the secretion of ECM by the cells in culture. Fig. 3.6 shows the secretion of collagen by fibroblasts grown on different electrospun scaffolds after 9 days of cell culture. The dark red dots indicate collagen produced by HDFs. The secretion of collagen was more predominant on Gel/PLLCL(60) scaffold (Fig. 3.6A) compared to the other materials as characterized by the Sirius-red staining. In our study we found that the higher cell proliferation on Gel/PLLCL(60) contributed to increased collagen stains on this scaffold. This abundant secretion of ECM by the cells proves that Gel/PLLCL(60) scaffolds are suitable material for wound healing through its regenerative potential.

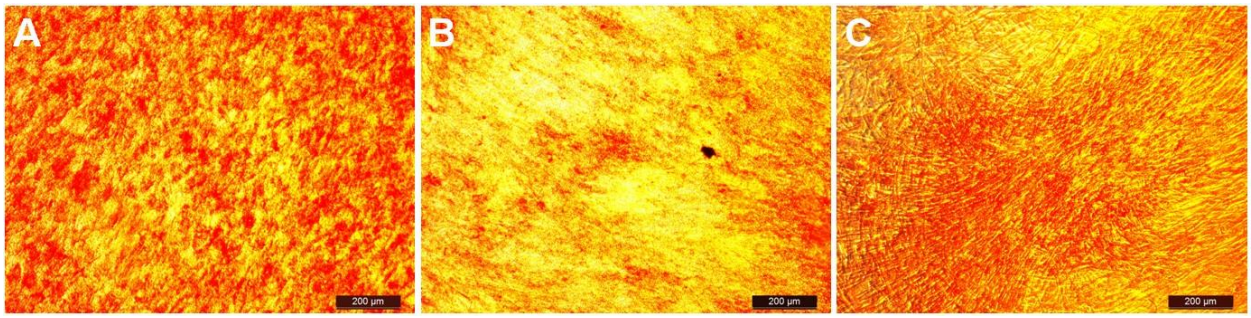

Fig. 3.6 Collagen staining on nanofibrous scaffolds: (A) Gel/PLLCL(60), (B) PLLCL and (C) TCP.

3.3.5 Wound size measurements

Materials for wound dressing made from the electrospinning product have been increasingly investigated [229]. The electrospun nanofiber is appropriate for use as a wound dressing material due to its useful properties, including oxygen-permeable high porosity, variable pore-size distribution, high surface-to-volume ratio, and most importantly, morphological similarity to the natural ECM in the skin, all of which promote cell adhesion, migration and proliferation [230, 231]. The *in vivo* evaluation of Gel/PLLCL(60) as a skin graft has been carried out in a mouse model. The wounds in NFS-treated group have completely closed after 14 days (Fig. 3.7I). However, around 21% of wounds are still can be found in the control group. Fig. 3.7I also shows that Gel/PLLCL(60) can promote wound healing form day 2 to day 14. The initial FTSW of 8 × 8 mm wounds were shown in Fig. 3.7II in both groups on day 0. After 5 days, the wounds in NFS-treated group are apparently smaller than the wounds in control group. On day 10, the wounds in NFS-treated groups were almost closed, however, the largest un-epithelialized wounds were still can be found in the control group. It takes 18 days for the closure of wounds in control group.

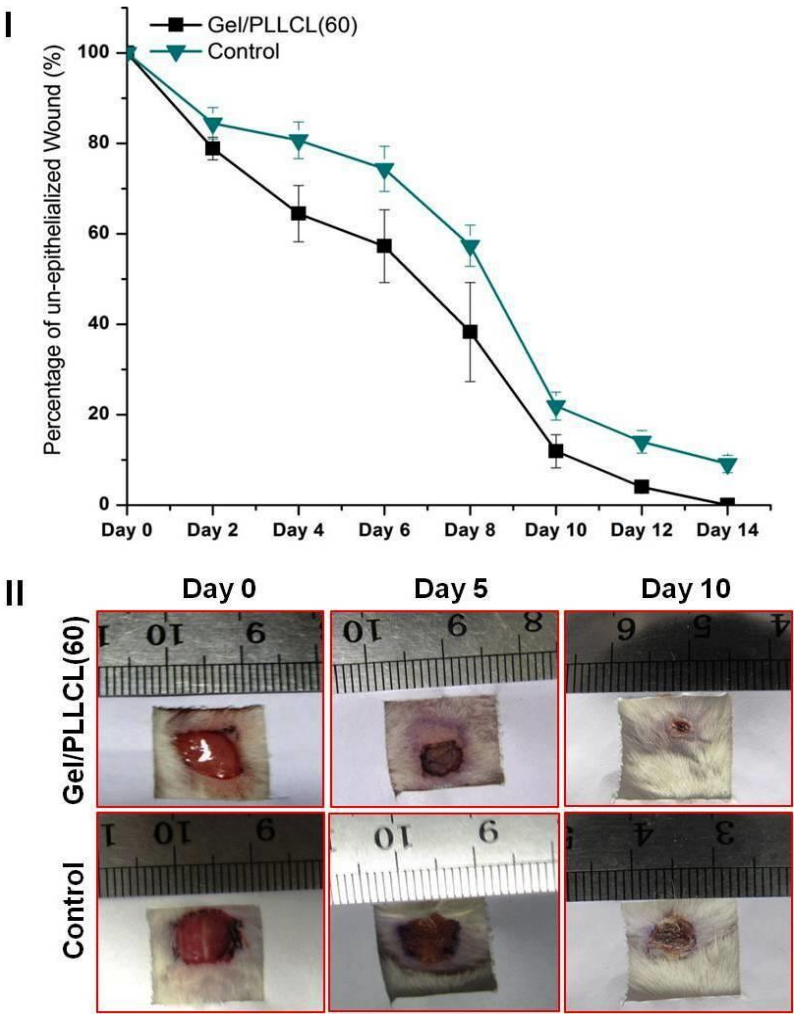

Fig. 3.7 Wound size measurements and appearances at different time points. (I) Percentages of unepithelialized wound area in different groups from day 1 to 14. (II) Appearances of wounds in different groups on days 0, 5 and 10.

3.3.6 Histological analysis

The histological structures (obtained by H&E staining) of wounds in different groups are shown in Fig. 3.8. Compared to normal healthy skin, full-thickness wounds displayed hyperplasia of epidermis, granulation tissue formation and the presence of inflammatory cells (Fig. 3.8). After 5 days wound healing, inflammatory cells and fibroblasts densely infiltrated the wounds from control groups. However, the newly formed capillary (red dots) can be found in the NFS-treated wounds. On day 10, the wounds from control group were still thickly filled with inflammatory cells and fibroblast. Moreover, the

capillary hyperproliferation was found in the control group. All these observations indicated that wounds in control group still remained in inflammatory phase. In contrast, wounds in NFS-treated group demonstrated epithelialization without capillary hyperplasia. Moreover, the skin appendage sebaceous glands could be found in the NFS-treated groups.

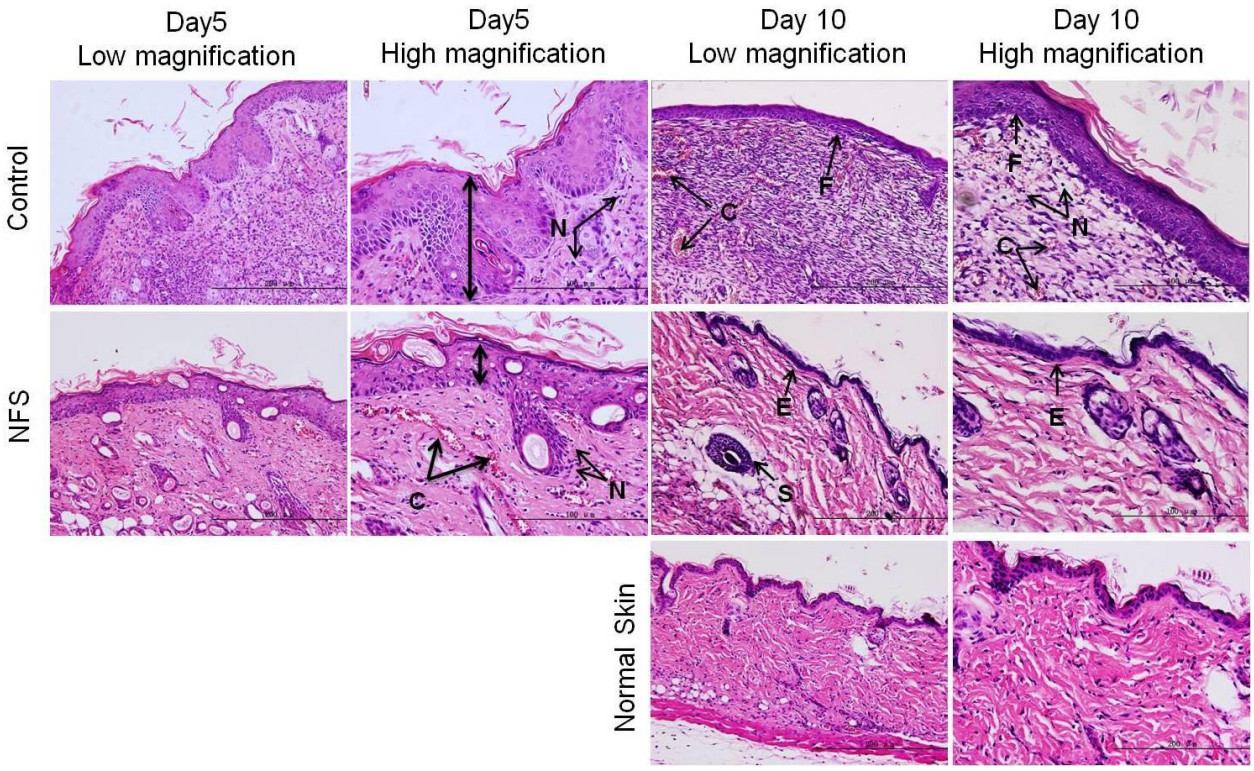

Fig. 3.8 Hematoxylin and eosin staining in different groups on days 5 and 10. Scale bars: 200 mm (low magnification), 100 mm (high magnification). F, fibrinous debris; N, neutrophils; C, capillary; S, sebaceous gland; E, epithelialization.

Our results demonstrated that the optimized Gel/PLLCL(60) can accelerate wound closure by 4 days compared with the control groups. Moreover, Gel/PLLCL(60) was found to promote wound reepithelialization and the newly formed epidermis is comparable to the epidermis of normal skin. Our animal studies further confirmed the promising application of the cost-effective nanofibers in skin tissue engineering.

3.4 Conclusion

In the present study, different amount of gelatin containing NFS were fabricated by

electrospinning. The mechanical properties of these electrospun nanofibers were evaluated in both dry and wet conditions. Moreover, the comparative cell proliferation on these NFS was studied by cell proliferation assay. Our results demonstrated that Gel/PLLCL(60) which had sufficient mechanical properties in both dry and wet conditions, along with the highest cell proliferation was the optimized NFS for skin tissue engineering. The capability of Gel/PLLCL(60) in promoting wound healing was further evaluated in a mouse model. *In vivo* results showed that wounds in NFS-treated group completed closure 4 days earlier than the control group and realized epithelialization. Our study demonstrated that the cost-effective Gel/PLLCL(60) NFS was suitable applied in wound healing and skin tissue engineering. Further improvements such as encapsulating bioactive factors etc. could be made based on this scaffold.

Chapter 4

Stem cell epidermal differentiation on multiple epidermal induction factors encapsulated core-shell nanofibers

4.1 Introduction

Globally, over 6 million patients suffer from severe burns each year among which more than 300 000 persons die annually [232, 233]. Even today, acute burn care, rehabilitation and reconstruction remain a major problem worldwide [234]. Unlike disruptive or incisional wounds, burn injury damages blood vessels in the immediate area of the wound to cause restriction or cessation of blood flow at the site of injury and modifications to blood flow occur in the surrounding area [235]. Thus, the management and treatment of burn injuries involving damaged blood vessels is a challenge among the clinicians and investigators. Different strategies have been explored by various researchers to improve the wound healing process from hemostasis to reepithelialization. Hemostasis begins immediately after injury and fibrin pad was demonstrated to prevent bleeding. These researchers found that fibrin pad was as effective as a conventional therapy for the primary management of severe bleeding with minimal time requirement for surgery [236]. Moreover, chitin was found to accelerate macrophage migration and its degradation products, and is able to stimulate macrophages and positively influence collagen deposition, thus accelerating the wound healing process [230]. Hydrogels with spatially specific cues are also known to promote wound remodeling and re-epithelialization [237, 238]. A variety of mediators have been identified as involved in wound healing process and these mediators act via multiple (specific) receptors facilitating wound closure [239]. Epidermal growth factor (EGF) plays an important role in the wound healing process, especially in stimulation of proliferation and migration of keratinocytes [240] and EGF has also been shown to accelerate wound healing *in vivo* [241]. Similarly, it was demonstrated that high doses of insulin can be safely administered to massively burned

patients to improve wound matrix formation [242]. Other bio-reagents such as hydrocortisone and retinoic acid (RA) has the capacity to promote keratinocyte growth [243] and are applied as agents to guide epithelial differentiation of stem cells [244]. Incorporation of such growth factors and bioreagents in biocompatible and biodegradable nanofibers might be a potential alternative to regulate cell proliferation, migration and differentiation, thus enhancing skin tissue regeneration by providing adequate signaling and concentration of growth factors. However, optimizing the release profiles of these mediators for wound healing for a desired period of time remains a huge challenge. This is mainly because, protein based growth factors (EGF, insulin, etc.) are easily being attacked by the hydrolytic enzymes present at the wound sites. Moreover, the dilution of the released growth factors by body fluids such as blood and lymphatic fluids reduce the therapeutic efficacy of these growth factors at the wound sites [199]. Electrospun naonfibers were used to encapsulate and control the release rates of therapeutic proteins and drugs [245, 246]. However, low delivery efficiency and burst release are some of the problems with electrospun nanofibers fabricated from polymer solutions blended with growth factors. Gandhi et al. examined the release of two model protein compounds, bovine serum albumin (BSA) and an anti-integrin antibody (AI), from electrospun polycaprolactone (PCL) nanofibers, where the proteins were directly blended with the polymeric solution of PCL. Up to 87% and 55% burst release of BSA and AI, respectively was observed [247]. Recently, Jiang et al. utilized a scaffold-based approach to direct the neuronal differentiation of stem cells. For this, 3 mg ml^{-1} of retinoic acid (RA) solution was added to a mixture of PCL and gelatin solution and electrospun to obtain RA-encapsulated fibers. Results of their studies showed enhanced expression of neuronal specific markers such as Tuj-1 and MAP2, but a 35% burst release was observed within the first day from the RA-encapsulated fibers [248]. Such burst release may discredit the stem cell differentiation effect and similar shortcoming was also observed by other researchers [249, 250]. In order to overcome the problem of burst release to a certain extent, core-shell structured nanofibers have been developed. With application of core-shell nanofibers, the unstable biological agents can be protected from harsh environments, deliver the bioactive molecules or drugs in a sustained way, and functionalize the surface of the nanostructures without affecting the core material [24].

Besides the positive effects of mediators in wound healing, selection of a suitable cell source is also important for tissue engineering. Adipose-derived stem cells (ASCs) are known to significantly reduce the wound size and accelerate the re-epithelialization process [159]. In addition, ASCs promote the proliferation of human dermal fibroblasts (HDF), not only by cell-to-cell direct contact, but also by paracrine activation through secretory factors [42]. Meanwhile, Davis et al. demonstrated that purified ASCs delivered in a trans-glutaminase gel significantly accelerated wound closure in chronically irradiated animals compared to the controls (gel alone without cells) [251]. Furthermore, it was also demonstrated that ASCs could accelerate wound healing through epithelial differentiation and might represent a novel therapeutic approach in cutaneous wounds [159].

Aiming to protect the wound healing mediators from the attack by hydrolytic enzymes at the wound sites and to achieve sustained release of the mediators; we fabricated EIF encapsulated core-shell nanofibers by co-axial electrospinning. Parallely, we prepared EIF blended nanofibers by electrospinning a blend solution of EIF with gelatin and PLLCL. The release profile of EGF from both kinds of nanofibers was evaluated by performing epidermal differentiation of ASCs on the EIF-containing nanofibrous scaffolds and differentiation effect was evaluated.

4.2 Materials and Methods

4.2.1 Materials

Human adipose-derived stem cells (ASCs) were obtained from Lonza (Portsmouth, NH). DMEM/F12, FBS, penicillin-streptomycinsolution, DAPI, Alexa Fluor 488 and Alexa Fluor 594 were all purchased from Invitrogen (Carlsbad, CA). Epidermal growth factor (EGF), hydrocortisone, insulin, retinoic acid (RA), bovine serum albumin, gelatin and HFP were all purchased from Sigma-Aldrich (Singapore) and CD 105 was purchased from Abcam (USA). Mouse anti-human keratin 10 (Ker 10) and filaggrin antibodies were obtained from Thermo Fisher Scientific (Singapore). PLLCL co-plomer was purchased

from Boehringer Ingelheim Pharma GmbH (Ingelheim, Germany).

4.2.2 Electrospinning of nanofibers

8% (w/v) of PLLCL solution was prepared by dissolving block copolymer in HFP. Gelatin and PLLCL were dissolved in HFP at a ratio of 60:40 (wt.%) to obtain 10% (w/v) solution and stirred overnight. The solutions were individually placed in a 3 ml standard syringe attached with blunted steel needles with 27 G inner diameters. Then, the solution loaded syringe was located in a syringe pump (KDS 100, KD Scientific, Holliston, MA) at a flow rate of 1.0 ml h^{-1}. Nanofibers were fabricated via electrospinning at 15 kV (Gamma High Voltage Research, Ormond Beach, FL) and collected on an aluminum foil wrapped flat grounded steel plate at a distance of 12 cm from the needle tip. A vacuum desiccator was used to evaporate residual solution of the nanofibers collected on 15 mm coverslips.

To fabricate EIF encapsulated electrospun nanofibers, the loading level of each growth factor in epidermal induction medium was calculated based on the study by Jiang et al [248]. The concentrated epidermal induction medium (CEIM) includes 17 µl of 0.1 mg ml^{-1} EGF, 68 µl of 12.5 mg ml^{-1} insulin, 340 µl of 200 µg ml^{-1} hydrocortisone and 85 µl of 10 mM RA. To fabricate EIF blended nanofibers, CEIM was added into gelatin-PLLCL solution for electrospinning. The resulting drug-loaded polymeric solution was further charged at 15 kV and fed at a flow rate of 1 ml h^{-1}. All fibers were finally collected on an aluminum foil wrapped collector at a distance of 12 cm from the needle tip. The electrospinning process was also protected from light to minimize the degradation of EIF.

To fabricate EIF encapsulated core-shell nanofibers, gelatin and PLLCL were dissolved in HFP at a ratio of 60:40 (wt.%) to obtain a 10% (w/v) shell solution. The CEIM was diluted into 1 ml solution with 5% bovine serum albumin (BSA) and it was used as the core solution. A two-fluid coaxial spinneret was designed for electrospinning (Scheme 4.1). The inner needle has an inner diameter of 0.8 mm and an outer diameter of 1 mm; the outer needle has an inner diameter of 1.8 mm. The spinneret was designed such that

the fluids were immiscible before exiting the nozzle. Two syringe pumps (KD Scientific, Inc.) were provided to pump a constant-volume flow rate of 0.3 mL/h for the core solution and 1.0 mL/h for the shell solution. A high-voltage electric field (DC high-voltage power supply from Gamma High Voltage Research) was applied at the tip of the spinneret of 15 kV. A Taylor cone was formed at the coaxial tip with an outer droplet surrounding the inner one. The outer droplet was then transformed into a jet, because of the surface charges created whereas no surface charges were created for the inner droplet owing to the rapid evaporation of the solvent, which reduces the solvent mixing during this process, thereby producing core-shell fibers. A collector plate was placed at a distance of 12 cm from the tip of the spinneret to collect the core-shell fibers. Hereafter, in this manuscript EIF encapsulated core-shell nanofibers and EIF blended nanofibers will be represented as Gel/PLLCL/EIF(cs) and Gel/PLLCL/EIF(b), respectively.

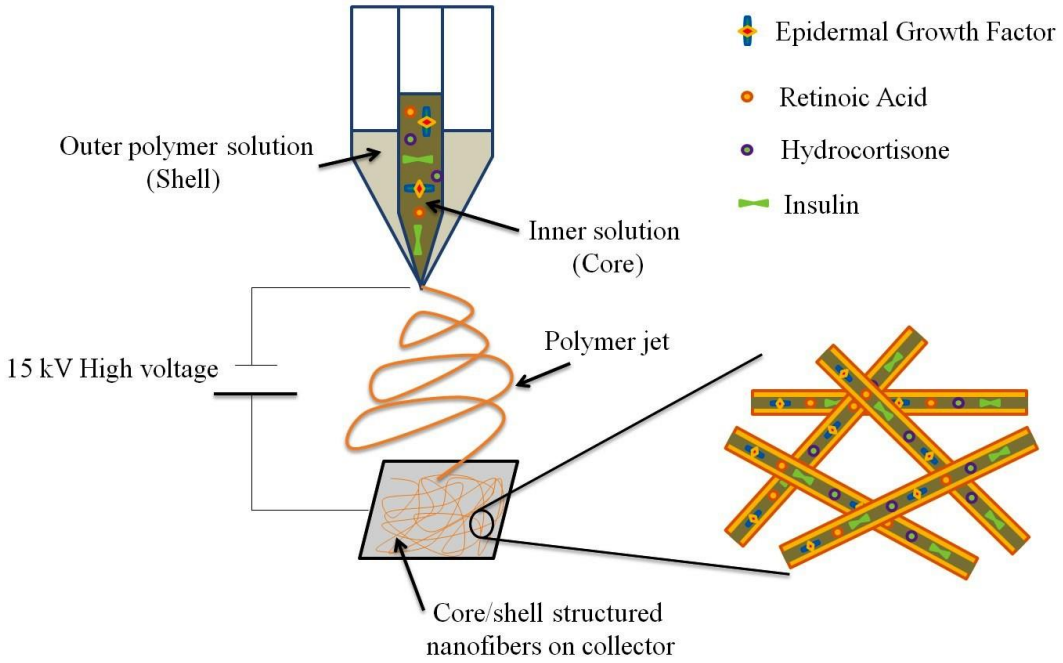

Scheme 4.1 Basic set-up for coaxial electrospinning and EIF encapsulated core-shell nanofibers.

4.2.3 Morphology and characterization of electrospun nanofibers

FESEM (FEI-QUANTA 200F, Netherlands) was used to study the morphology of the

electrospun nanofibers at an accelerating voltage of 10 kV, after sputter coating with gold (JEOL JFC-1200 fine coater, Japan). The obtained SEM images were applied to obtain the diameters of the electrospun fibers using image analysis software (Image J, National Institutes of Health, USA). The core-shell structure of Gel/PLLCL/EIF(cs) was examined using a JEOL JEM-2010F transmission electron microscopy (TEM). To determine the distribution of EIF within the core-shell nanofibers, the electrospun Gel/PLLCL/EIF(cs) and Gel/PLLCL/EIF(b) with FITC-dextran were also observed under the laser scanning confocal microscopy (Olympus FLUOVIEW FV1000, Japan). CFP-1200-A capillary flow porometer (PMI, New York, NY) was used in this study to measure the pore size. Calwick with a defined surface tension of 15.9 dynes/cm (PMI, New York, NY) was used as the wetting agent for porometry measurements. Nanofibers were cut into 3 cm × 3 cm squares for porometry measurement. Nanofibers with similar thickness were obtained and each sample was tested individually. Functional groups of the electrospun nanofibrous scaffolds were evaluated by ATR-FTIR spectroscopic analysis in a Nicolet Avatar 380 spectrometer (Thermo Nicolet, Waltham, MA) over the range 600-3800 cm^{-1} at a resolution of 4 cm^{-1}. A tabletop tensile tester (Instron x345, Canton, MA) was applied to determine the tensile properties of the electrospun nanofibrous scaffolds at a load cell capacity of 10 N. The specimens were cut into approximately 20 mm × 10 mm (length × width) in order to be loaded into the uniaxial testing machine. Specimens were measured with a 10 N load cell under a cross-head speed of 10 mm min^{-1} (n = 5). The tensile stress strain values obtained from the instrument were plotted using an Excel sheet.

4.2.4 Culture of ASCs on the scaffolds

The method of ASCs culture and scaffolds sterilization is the same to that mentioned in section 3.2.4. The density of ASCs seeded on the scaffolds 5,000 cells/well.

4.2.5 Drug release study

To evaluate the drug delivery behavior, individual scaffolds of Gel/PLLCL/EIF(cs) and Gel/PLLCL/EIF(b) (average weighing 50mg, n = 3) was soaked in a 15-mL centrifuge tube with 10 mL of phosphate-buffered saline (PBS). To account for possible dissolution of gelatin from the nanofibers, Gelatin/PLLCL nanofibers (average weight 50 mg, n = 1)

were used as the control. The fibrous mats were protected from light and incubated at 37 °C in a continuous horizontal shaker. At predetermined time points (1, 3, 6, 9, 12 and 15 day), 1 ml of supernatant was retrieved and replenished with 1 ml of fresh PBS. Quantikine human EGF kit was used to determine the quantity of EGF released at different time intervals following the instructions of the manufacturer. The Quantikine Human EGF Immunoassay kit is a 4.5 hour solid phase ELISA designed to measure EGF level and employs the quantitative sandwich enzyme immunoassay technique, whereby the minimum detectable dose of EGF was typically less than 3.9 pg/mL. The optical density for each sample was determined by microplate reader (Genios, Tecan, Basel, Switzerland), and the results were expressed by cumulative release as a function of release time:

Cumulative amount of release (%) = $M_t/M_x \times 100\%$

where M_t is the weight of EGF released at time t and M_x is the total amount of EGF in the nanofibers theoretically. All experiments were tested in triplicate.

4.2.6 Cell proliferation assay

The comparative proliferation of ASCs on electrospun NFS was determined using the colorimetric MTS assay (CellTiter 96 AQueous One solution, Promega, Madison, WI). After culturing the cells for a period of 5, 10 and 15 days, cells were rinsed with PBS to remove any unattached cells and incubated with 20% MTS reagent in serum free medium for a period of 3 hrs at 37 °C. Absorbance of the obtained dye was measured at 490 nm using a spectrophotometric plate reader (FLUOstar OPTIMA, BMG lab Technologies). The amount of formazan crystals formed is directly proportional to the number of live cells, which was also directly proportional to the absorbance values obtained.

4.2.7 Induction of ASCs towards the epidermal lineage

For induction of ASCs to epidermal lineage, ASCs were seeded at a concentration of 5000 cells on the scaffolds per well in 24-well plates using basic epidermal induction medium (BEIM) comprising of Ham's F12 medium (3:1) including 10% FBS, 100 IU ml^{-1} penicillin and 100 μg ml^{-1} streptomycin without supplements. All samples were incubated for 15 days under standard culture conditions (37 °C with 5% CO_2) and the

culture medium was changed every 3 days.

4.2.8 Immunostaining analysis of differentiated ASCs

ASCs grown on Gel/PLLCL/EIF(cs), Gel/PLLCL/EIF(b) and Gelatin/PLLCL, PLLCL and TCP using BEIM for 15 days were processed for immunocytochemistry. The cell scaffold composites were fixed by 2.5% paraformaldehyde at room temperature for 15 min. Then PBS was used to wash the composites and incubated with 2% BSA to block any non-specific binding. The cells were further stained with primary antibody Ker 10 for 2 h at room temperature. Subsequently, the cell-scaffold composites were revealed with Alexa Fluor 594 (red) secondary antibody for 60 min at room temperature. After that, the samples were washed three times with PBS and treated with diluted filaggrin (1:100) for 2 h at room temperature. Then, the secondary antibody Alexa Fluor 488 (green) was added for 60 min at room temperature. Finally, the samples were treated with DAPI after washing thrice with PBS and incubated for 30 min at room temperature. The stained samples were mounted on a glass slide and examined by LSCM.

To confirm the differentiation of ASCs along the epidermal lineage, double immunostaining was performed. After 15 days, the cell-scaffold composites were washed with PBS, fixed with 2.5% paraformaldehyde. The ASCs on Gel/PLLCL/EIF(cs), Gel/PLLCL/EIF(b), Gelatin/PLLCL, PLLCL nanofibers and TCP for 15 days were blocked for nonspecific staining using 2% BSA then immunostained with ASC-specific marker CD 105 for 2 h at room temperature. Subsequently, the cell-scaffold composites were revealed with Alexa Fluor 488 (green) secondary antibody for 60 min at room temperature. After that, the samples were washed three times with PBS and treated with diluted Ker 10 (1:100) for 2 h at room temperature. Then, the secondary antibody Alexa Fluor 594 (red) was added for 60 min at room temperature. Finally, the samples were treated with DAPI after washing thrice with PBS and incubated for 30 min at room temperature. The stained samples were mounted on a glass slide and examined by LSCM.

4.2.9 Morphology of differentiated ASCs

Morphological evaluation of ASCs grown on electrospun Gel/PLLCL/EIF(cs),

Gel/PLLCL/EIF(b), Gelatin/PLLCL, PLLCL nanofibers and TCP using BEIM was performed after 15 days of cell culture by SEM. The cell-scaffold constructs were rinsed twice with PBS and fixed in 3% glutaraldehyde for 3 h. The scaffolds were further rinsed in deionized water and dehydrated with increasing concentrations of ethanol (50%, 70% 90%, and 100%) for 10 min each. Finally, the cell-scaffold constructs were treated with hexamethyldisilazane and air dried in a fume hood overnight.

4.2.10 Statistical analysis

All the data presented are expressed as mean ± standard deviation (SD) of the mean. Each experiment was repeated three times. Statistical differences were determined by Student's two-sample t test. Differences were considered statistically significant at $p \leq 0.05$.

4.3 Results and discussion

Electrospun nanofibers, with high porosity and large surface-to-volume ratio, can provide more structural space for accommodating the migrating and proliferating cells, enable sufficient nutrient delivery, gas exchange and waste excretion and at the same time, the small pore size of nanofibers can protect the wound from bacterial penetrations [15]. To improve the biofunctionality of electrospun naonfibers, core-shell nanofibers were fabricated by incorporating therapeutic growth factors as the core into the Gelatin/PLLCL shell, thereby protecting the growth factors from harsh chemical environment faced during the normal electrospinning of a polymer-solvent mixture. An enormous number of studies have shown the potential benefits of the topical treatment of wound using growth factor, such as EGF [252], basic fibroblast growth factor [253], etc. which enhanced the wound-healing ability in primate models and in clinical trials. In this study, we dissolved gelatin and PLLCL in HFP and electrospun core-shell naonfibers to deliver EIF in a sustained manner, and we aimed to retain the bioactivity of EIF within the core of the nanofibers, while avoiding direct contact of EIF with HFP. It is know from literature that HFP is effective in solubilizing a wide range of polymers and is widely used for the preparation of solutions for electrospinning. It has been suggested that collagen dissolved in HFP may result in structures composed merely of gelatin fibers

[254]. However, literature also revealed minor differences between the structures of electrospun collagen dissolved in HFP, in PBS, or in PBS/ethanol binary mixtures, indicating that the structural properties of collagens are retained even with the use of HFP [255]. Accordingly, unlike the structure of collagen, gelatin with its fibrillar structure and lack of internal structure will most likely retain its bioactivity within HFP compared to collagen. Moreover, in this study, we used a synthetic polymer PLLCL along with gelatin to fabricate a 'composite' scaffold of Gelatin/PLLCL, thereby increasing the mechanical stability while maintaining its bioactivity.

4.3.1 Morphology, chemical and mechanical characterization of electrospun nanofibers

Nanofibers of Gel/PLLCL/EIF(cs), Gel/PLLCL/EIF(b), Gelatin/PLLCL and PLLCL were fabricated by electrospinning and the fiber morphology was examined under scanning electron microscope (SEM). SEM micrographs of electrospun nanofibrous scaffolds revealed porous, beadless, nano-scaled fibrous structures under the optimized spinning conditions utilized during this study (Fig. 4.1A-D). Uniform nanofibers of Gel/PLLCL/EIF(cs), Gel/PLLCL/EIF(b), Gelatin/PLLCL and PLLCL with fiber diameters of 366 ± 125, 299 ± 46, 382 ± 100 and 456 ± 62 nm, respectively, were obtained. Applied with low pressure, capillary flow porometry provides a simple and non-destructive technique for rapid and accurate measurement of pore size [256, 257]. Therefore, capillary flow porometry can provide reproducible pore size measurements with ignorable distortion errors [218]. However, the fiber diameter and fiber mass plays a dominant role in controlling the pore diameter of the networks [218, 258]. The pore size as determined by capillary flow porometer, for the Gel/PLLCL/EIF(cs), Gel/PLLCL/EIF(b), Gelatin/PLLCL and PLLCL was 0.72, 0.51, 0.88 and 1.48 µm, respectively. In our study, the thickness of Gel/PLLCL/EIF(cs), Gel/PLLCL/EIF(b), Gelatin/PLLCL and PLLCL was kept identical at approximately 35 µm. The mean pore sizes obtained for the nanofibers were found inversely proportional to the diameter of the fibers and our results were also in agreement with the results reported by Li et al [218]. They found that at a given network mass per unit area and porosity, an increasing fiber diameter results in an increase in mean pore sizes [218].

PLLCL nanofibrous scaffolds were found to be highly hydrophobic with a contact angle of 136 ± 2 °C. However, with the incorporation of gelatin, the Gel/PLLCL/EIF(cs), Gel/PLLCL/EIF(b) and Gelatin/PLLCL nanofibers became more hydrophilic, with a contact angle of 25 ± 6 ^{0}, 35 ± 9 ^{0} and 38 ± 2 ^{0}, respectively. The TEM images (Fig. 4.1E, 4.1F) and laser scanning confocal microscopic (LSCM) images (Fig. 4.1G, 4.1H) of Gel/PLLCL/EIF(cs) and Gel/PLLCL/EIF(b) were respectively obtained.

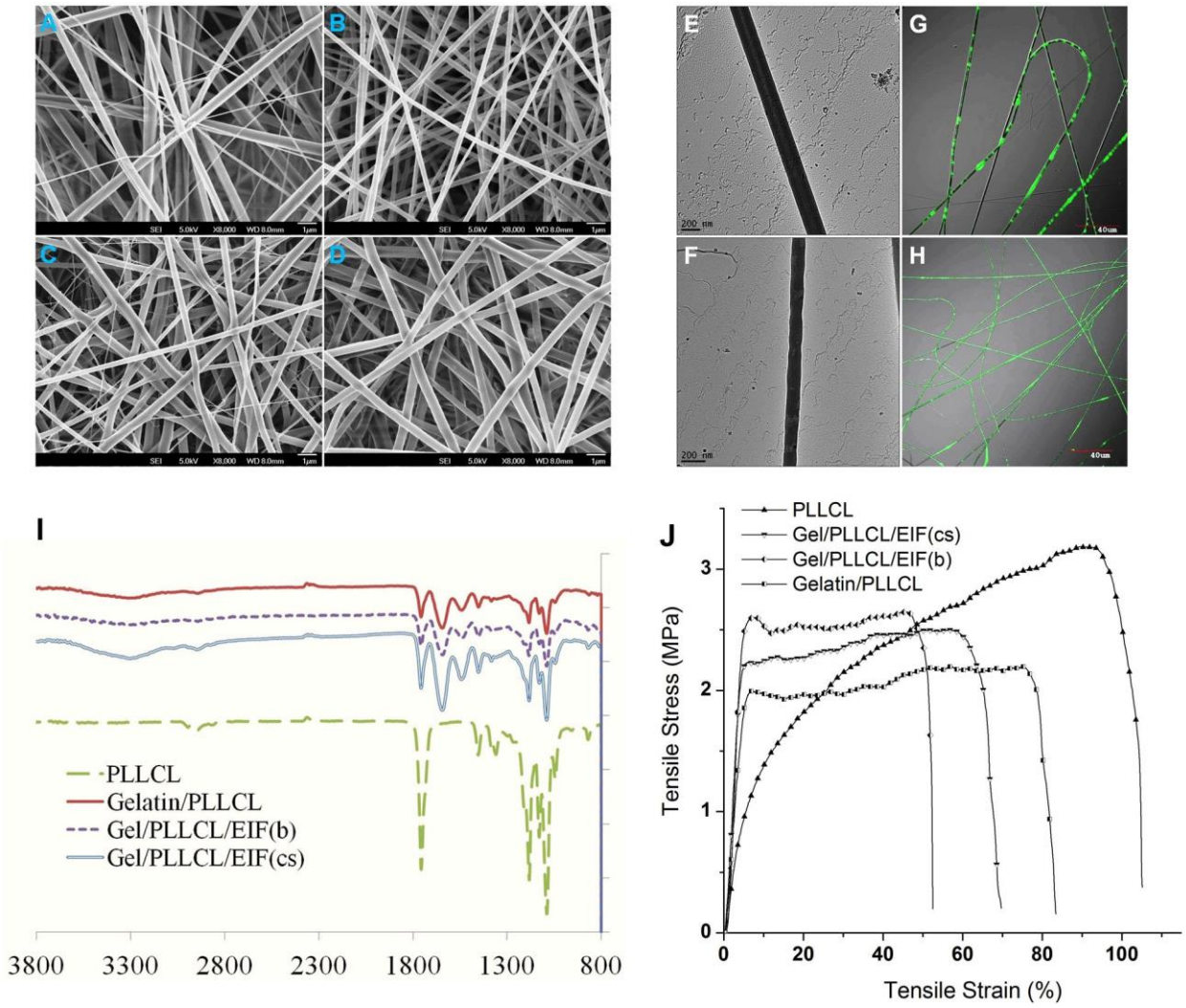

Fig. 4.1 **Characterizations of electrospun nanofibers**. SEM morphology of (A) Gel/PLLCL/EIF(cs), (B) Gel/PLLCL/EIF(b), (C) Gelatin/PLLCL and (D) PLLCL nanofibers. TEM micrographs of (E) Gel/PLLCL/EIF(cs), (F) Gel/PLLCL/EIF(b) and fluorescence microscopic images of (G) Gel/PLLCL/EIF(cs) with FITC-dextran in the core, (H) Gel/PLLCL/EIF(b) with FITC-dextran stained all over the fibers. (I) FTIR spectra of Gel/PLLCL/EIF(cs), Gel/PLLCL/EIF(b), Gelatin/PLLCL and PLLCL nanofibers. (J) Stress-strain curve of the electrospun nanofibers.

The core-shell structure of the Gel/PLLCL/EIF(cs) was clearly demonstrated in Fig. 4.1E and it was even more clearly disclosed by the application of FITC-dextran through LSCM. Fig. 4.1G shows that the electrospun nanofibers consisted of green core and a dark outer layer, and the boundary between the two produced a sharp distinction. Fig. 4.1G suggested that EIF were encapsulated in the core area of the Gel/PLLCL/EIF(cs) and Fig. 4.1H suggested that EIF were uniformly distributed throughout the whole single fiber. Fig. 4.1I shows the ATR-FTIR spectra of electrospun Gel/PLLCL/EIF(cs), Gel/PLLCL/EIF(b), Gelatin/PLLCL and PLLCL nanofibers. The characteristic ester absorption peak of PLLCL was observed at 1760 cm^{-1}, and C-O-C stretching vibrations were observed at 1097, 1133 and 1187 cm^{-1}. The Gel/PLLCL/EIF(cs), Gel/PLLCL/EIF(b) and Gelatin/PLLCL nanofibrous scaffolds showed the characteristic amide I and amide II peaks of gelatin at 1650 cm^{-1} and 1550 cm^{-1} in addition to the characteristic peaks of PLLCL. The mechanical properties of electrospun nanofibrous scaffolds were studied and Fig. 4.1J shows the stress-strain curves of different electrospun nanofibers under tensile loading. Mechanical evaluations of all scaffolds in Fig. 4.1J show a linear segment up to the proportionality limit, followed by a non-linear curve, which was characterized by considerable elongation without a corresponding increase in loading stress. This feature is mainly attributed to fiber arrangement in the mat. The fiber arrangement in the mat is expected to change during the stress–strain measurement. It was demonstrated that fibers tend to align in the direction of applied force before getting thinner and finally the breaking occurs [186, 223]. The Young's modulus of Gel/PLLCL/EIF(cs), Gel/PLLCL/EIF(b), Gelatin/PLLCL and PLLCL nanofibers was 58.44 ± 6.35, 55.77 ± 18.92, 36.29 ± 7.24 and 24.66 ± 4.99 MPa, respectively. Comparing the stress-strain curves of gelatin containing nanofibrous scaffolds with those of the stress-strain curve of PLLCL in Fig. 4.1J, we found that the incorporation of higher amounts of gelatin to PLLCL led to a significant decrease in ultimate strain of the electrospun composite scaffolds ($p \leq 0.05$). In our study, among the gelatin containing scaffolds, Gel/PLLCL/EIF(b) showed the highest ultimate tensile stress (followed by Gel/PLLCL/EIF(cs)). Wong et al. studied the effect of fiber diameter towards the tensile properties of electrospun fibers. They found that the effect of fiber diameter on tensile

strength became more predominant for fibers with diameters less than ~700 nm [259][40]. It was found that the crystalline morphology of electrospun nanofibers strongly influenced the mechanical properties of polymers [221, 222] and gelatin mainly contributes to the crystallinity of the electrospun membrane [220]. Lim and colleagues confirmed that the fibers with smaller diameter have higher degree of crystallinity and molecular orientation in the form of oriented fibrillar structure. The fibrillar structure would result in higher resistance to axial tensile force due to the higher degree of molecular orientation in the direction of applied stress [222]. This could be the reason for the higher strength of Gel/PLLCL/EIF(b) nanofibers compared to the other gelatin containing fibers. However, compared to pure PLLCL nanofibers, the gelatin containing nanofibers had a higher degree of molecular orientation and crystallinity, and thus higher elastic modulus with low ductility. The tensile properties of nanofibrous substrates are summarized in Table 4.1.

Table 4.1 Tensile properties of the electrospun nanofibers

Property	Gel/PLLCL/GF(cs)	Gel/PLLCL/GF(b)	Gel/PLLCL	PLLCL
Tensile Modulus (MPa)	58.44 ± 6.35	55.77 ± 18.92	36.29 ± 7.24	24.66 ± 4.99
Tensile Stress (MPa)	2.50 ± 0.01	2.65 ± 0.07	2.16 ± 0.02	3.18 ± 0.13
Strain at break (%)	62.61 ± 3.84	49.80 ± 2.53	77.63 ± 2.40	98.00 ± 3.93

The tensile modulus of Gel/PLLCL/EIF(cs) (58.44 ± 6.35) was the highest among the different nanofibrous scaffolds of this study and the value lies well within the range of the tensile modulus of human skin (15-150 MPa) [260]. The tensile modules of Gel/PLLCL/EIF(cs) provides the scaffold with good resilience and compliance to movement as a skin graft. To further evaluate the potential of electrospun nanofibers as skin graft, the degradations of electrospun nanofibers were studied. Fig. 4.2A shows the morphological changes of different electrospun nanofibers after degradation in PBS at three different time points (day 5, 10 and 15). After 5 days of degradation, the gelatin containing nanofibers appeared to have swollen and lost their initial surface smoothness

compared to pure PLLCL fibers (Fig. 4.1D). After 10 days of degradation in PBS, the gelatin containing nanofibers had apparently swelled (Fig. 4.2A). This can be explained by the dissolution of gelatin in the buffer. However, after 15 days of degradation there were no further morphological changes observed on the fiber surfaces. Being a synthetic polymer, we did not observe any changes in the morphology of electrospun PLLCL nanofibers.

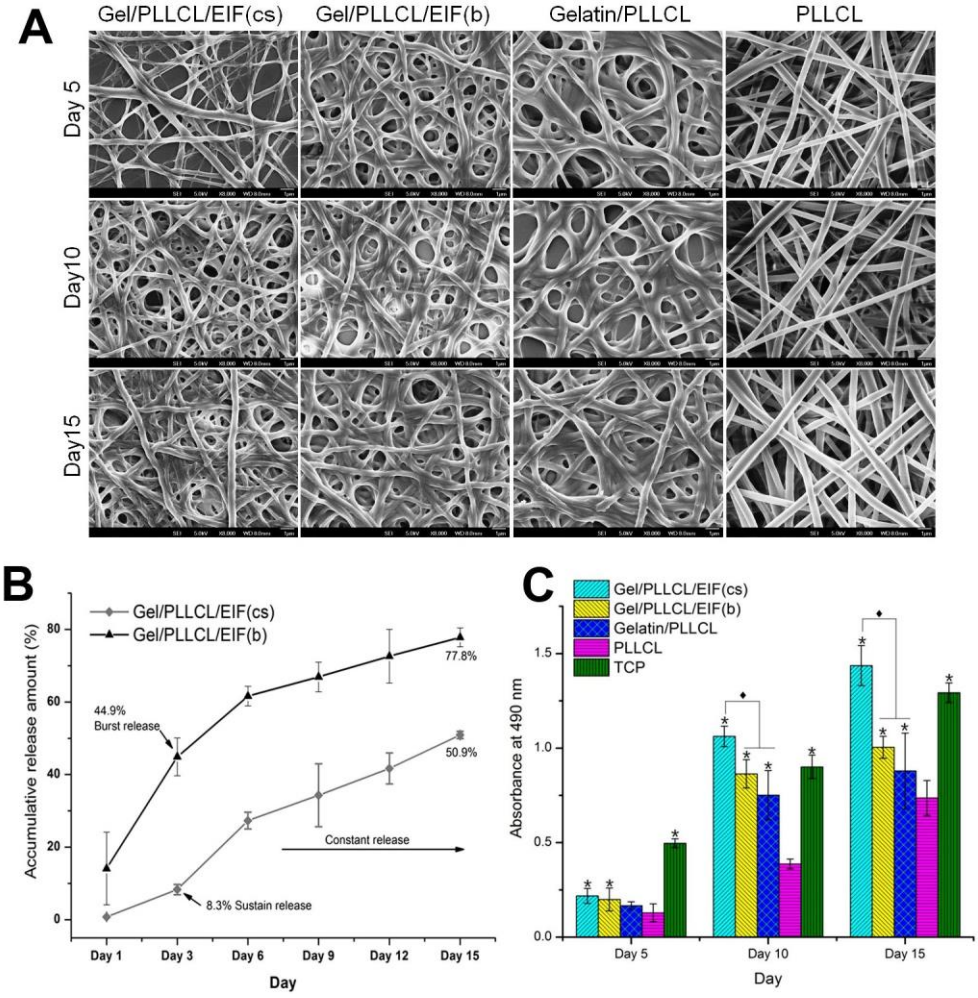

Fig. 4.2 **Release profiles of electrospun nanofibers and their effect on proliferation of ASCs**. **(A)** Morphological changes of Gel/PLLCL/EIF(cs), Gel/PLLCL/EIF(b), Gelatin/PLLCL and PLLCL nanofibers after degradation in PBS for 5, 10 and 15 days. **(B)** Release profiles of EGF from Gel/PLLCL/EIF(cs) and Gel/PLLCL/EIF(b). **(C)** ASCs proliferation on electrospun Gel/PLLCL/EIF(cs), Gel/PLLCL/EIF(b), Gelatin/PLLCL and PLLCL nanofibers. *Significant against cell proliferation on PLLCL at $p \leq 0.05$; ♦Significant against cell proliferation on Gel/PLLCL/EIF(b) and Gelatin/PLLCL nanofibers

4.3.2 Drug release study

It is believed that EGF stimulates the growth of keratinocytes *in vivo* and promotes the epidermal differentiation of stem cells *in vitro*, and it plays an important role in the process of wound healing [176, 260]. Coaxial electrospinning would provide an alternative and simple means to encapsulate drugs. With coaxial electrospinning, two components can be coaxially and simultaneously electrospun through different feeding the capillary channels to generate composite nanofibers in the form of core-shell structure. The controlled release of EGF from composite fibrous mats were studied and their release profiles from electrospun nanofibrous mats at a temperature of 37 °C and pH 7.4 are shown in Fig. 4.2B. The experiments were performed in triplicate and the error bars indicate the standard deviation. The release profile of EGF was studied at three stages: an initial burst release (stage I), further a decreased release (stage II), followed by constant release (stage III).

As shown in Fig. 4.2B, an initial burst release of EGF was observed within the first three days (stage I) from the Gel/PLLCL/EIF(b) scaffolds. From day 3 to day 6 (stage II) the release curves exhibited a decreasing release rate of EIFs. By day 15, the amount of EGF released from Gel/PLLCL/EIF(b) scaffolds reached 77.8%. For the Gel/PLLCL/EIF(b) fibers, which was prepared by blend spinning, the initial burst release can be attributed to the EGF that was located near the surface of the nanofibers. Fig. 4.2B also shows the cumulative release profiles of EGF from Gel/PLLCL/EIF(cs) and no burst release was observed within the first 3 days (stage I), and at the same time the release of EGF was stable and sustained. The amount of released EGF reached 50.9% after 15 days from Gel/PLLCL/EIF(cs) scaffolds. The initial burst release was apparently alleviated and the sustainability of nanofiber-based releasing devices was improved for Gel/PLLCL/EIF(cs) nanofibers. This conclusion is in agreement with the results obtained from other similar core-shell structured fibers [261]. The release of the proteins can be varied by altering the method of electrospinning, whether it is blending or coaxial electrospinning. Furthermore, the diffusion rate is affected by the method of protein loading. When the protein is encapsulated in the core of the fibers, the release profile follow a slow and steadily

increasing profile, however, when the drug or protein is within the blended nanofiber, an initial burst release occurs at the beginning of the release process.

4.3.3 ASCs proliferation on electrospun nanofibers

The proliferation capacity of ASCs on electrospun Gel/PLLCL/EIF(cs), Gel/PLLCL/EIF(b), Gelatin/PLLCL and PLLCL nanofibrous scaffolds in BEIM after 5, 10 and 15 days was determined by MTS assay (Fig. 4.2C). The presence of a natural ECM protein (gelatin) in Gelatin/PLCL nanofibers caused an increase in proliferation of ASCs on Gelatin/PLLCL nanofibrous scaffolds compared to those on PLLCL scaffolds. A still higher cell proliferation was obtained for both the EIF loaded scaffolds (Gel/PLLCL/EIF(cs) and Gel/PLLCL/EIF(b)); than the cell proliferation on Gelatin/PLLCL and PLLCL nanofibers. This can be attributed to the presence of EIF and its release from both the EIF loaded scaffolds, thus enhancing cell proliferation on them compared to the EIF-deprived scaffolds. After 15 days, the proliferation of ASCs on Gel/PLLCL/EIF(cs) was 43.6 % higher than the cell proliferation on Gel/PLLCL/EIF(b) and this is because of the different release profiles between Gel/PLLCL/EIF(cs) and Gel/PLLCL/EIF(b). BEIM was changed every 3 days to mimic the dynamic environment induced by body fluids. After 3 days, 44.9% EIF released from Gel/PLLCL/EIF(b) were removed during medium renewal (Fig. 4.2B). However, only 8.3% of EIF released from Gel/PLLCL/EIF(cs) were removed during medium renewal after 3 days. The initial loss of EIF in Gel/PLLCL/EIF(b) led to a lower cell proliferation on Gel/PLLCL/EIF(b) compared to the cell proliferation on Gel/PLLCL/EIF(cs) scaffolds. The results of the day 15 MTS assay also showed that the cell proliferation on Gel/PLLCL/EIF(cs) was 63.4% and 95.0% higher ($P \leq 0.05$) than the cell growth on Gelatin/PLLCL and PLLCL scaffolds, respectively. The percentage increase in the rate of cell proliferation on Gel/PLLCL/EIF(cs) and Gel/PLLCL/EIF(b) nanofibrous scaffolds from day 5 to day 15 was found to be 560% and 404%, respectively.

4.3.4 Induced epidermal morphology

The epidermal differentiation capacity of ASCs was performed on all the electrospun nanofibrous scaffolds for a period of 15 days. Adipose tissue as a stem cell source is

ubiquitously available and has several advantages compared to other sources. It is easily accessible in large quantities with a minimal invasive harvesting procedure, and the isolation of ASCs yields a high amount of stem cells, which is essential for most of the stem cell-based therapies and accompanied tissue regeneration [262]. Moreover, ASCs have several advantages like (i) they are abundant, (ii) more accessible and (iii) have lower donor morbidity, especially from a clinical perspective where large cell numbers are required for regeneration, and it appears that ASCs are the most useful cell type than even the bone marrow derived mesenchymal stem cells. Here we studied the plasticity of ASCs towards epithelial cells on electrospun nanofibers. ASCs seeded with normal growth medium on TCP attached and remained undifferentiated with a fibroblastic phenotype (Fig. 4.3A).

The epidermal differentiation capacity of ASCs on EIF incorporated 'core-shell' and 'blend' fibers were studied in BEIM after 15 days and analyzed by immunostaining studies. The predominant EIF of skin tissue regeneration such as the EGF, insulin, hydrocortisone and RA were incorporated in Gel/PLLCL/EIF(cs) and Gel/PLLCL/EIF(b) scaffolds. Two types of antibodies were used to detect the expression of proteins specific to epidermal differentiation at two different stages: early (Ker 10) and intermediate (filaggrin). Expression of Ker 10 (Fig. 4.3B) and filaggrin (Fig. 4.3B) were observed after 15 days of cell culture on Gel/PLLCL/EIF(cs) and Gel/PLLCL/EIF(b) scaffolds. Direct observation of the cells under LSCM for Ker 10 (red) showed a filamentous cytoplasmic distribution. The same pattern of filaggrin distribution was observed after staining a green color (Fig. 4.3B). The distinguishable phenotypical features of keratinocyte-like cells were observed on Gel/PLLCL/EIF(cs) in BEIM. However, only a few cells showed polygonal and round morphologies on the Gel/PLLCL/EIF(b) in BEIM. This could also be due to the differences in the release profiles of the EIF occurring from core-shell and blended fibers. Briefly, the initial loss of EIF in Gel/PLLCL/EIF(b) led to insufficient cell differentiation on Gel/PLLCL/EIF(b) compared to the cell differentiation on Gel/PLLCL/EIF(cs) scaffolds. And hence, more keratinocyte-like cells were observed on Gel/PLLCL/EIF(cs) scaffolds. The 3D expression of Ker 10 and filaggrin (Fig. 4.3C) were obtained after 15 days cell culture on Gel/PLLCL/EIF(cs).

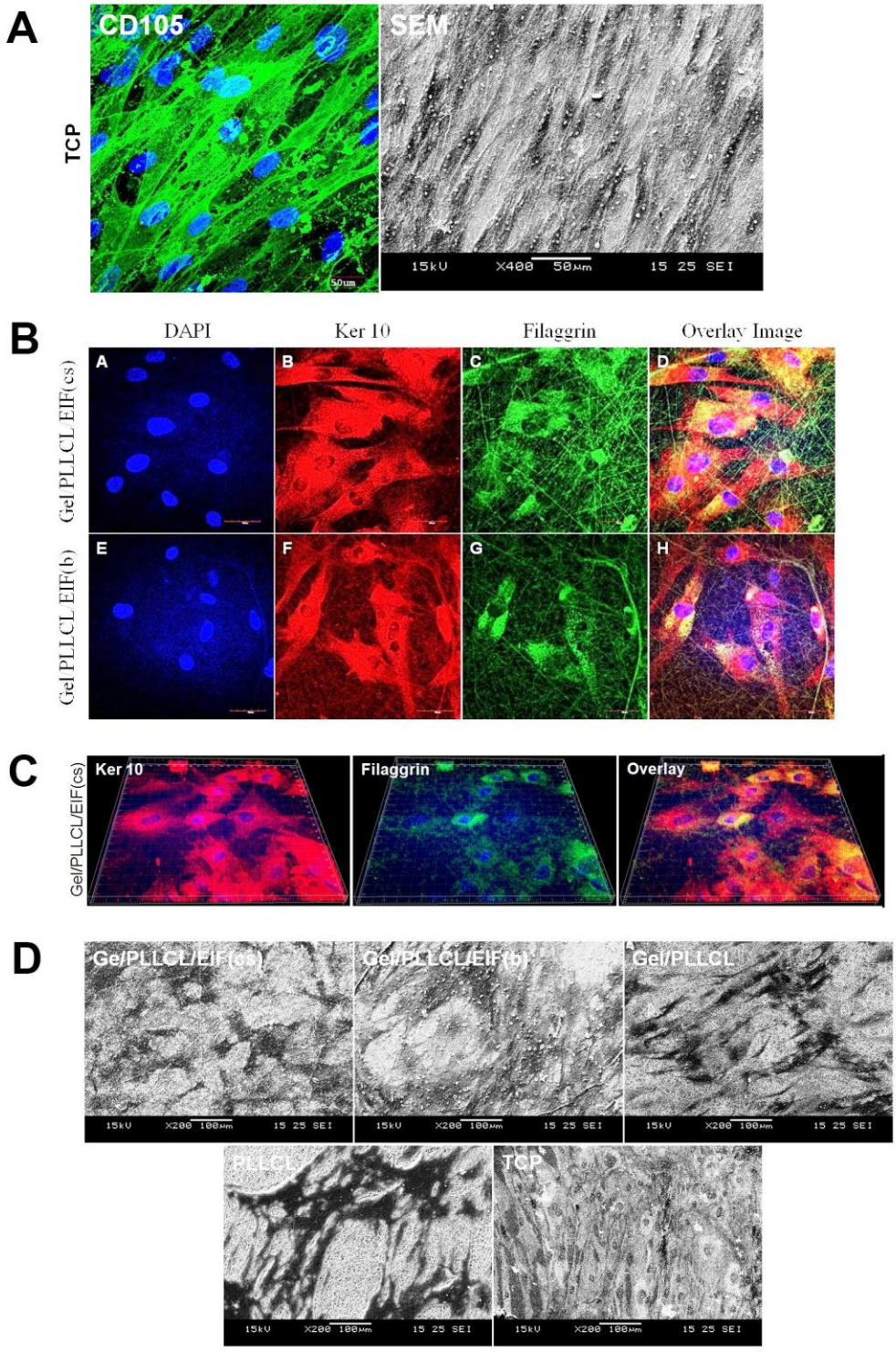

Fig. 4.3 **Protein expression and cell morphology studies. (A)** Laser scanning confocal microscope (LSCM) image of undifferentiated ASCs stained with CD 105 on TCP and SEM image showing the cell morphology, observed on day 15. **(B)** Two dimensional immunostaining images show the expression of Ker 10, filaggrin and the merged image on electrospun Gel/PLLCL/EIF(cs), Gel/PLLCL/EIF(b) at 60 x magnification. **(C)** Three dimensional immunostaining images show a filamentous cytoplasmic distribution of Ker

10 (red) and filaggrin (green). **(D)** SEM images of epidermally differentiated ASCs on Gel/PLLCL/EIF(cs) and Gel/PLLCL/EIF(b); undifferentiated ASCs on Gelatin/PLLCL, PLLCL and TCP.

Fig. 4.3D shows the comparative SEM images of ASCs on Gel/PLLCL/EIF(cs) and Gel/PLLCL/EIF(b) after 15 days of differentiation time. There were more ASCs on Gel/PLLCL/EIF(cs) and they acquired polygonal and round morphologies compared to the cells on Gel/PLLCL/EIF(b). However, ASCs on Gelatin/PLLCL, PLLCL and TCP remained undifferentiated with a fibroblastic phenotype. Fig. 4.4 shows the results of dual immunocytochemical analysis of ASCs on all the different electrospun scaffolds and TCP. The total cell number was obtained by counting the total number of cell nuclei (blue). Cells were stained for ASC-specific marker CD 105, while epidermally differentiated cells were counted based on the expression of Ker 10 (red stain). The percentage of differentiated epidermal cells on the Gel/PLLCL/EIF(cs) and Gel/PLLCL/EIF(b) were calculated, which gave figures of 62.2% and 43.0%, respectively. Due to the absence of EIF, very little expression of Ker 10 was observed for ASCs on Gelatin/PLLCL, PLLCL nanofibrous scaffolds and TCP in BEIM. ASCs on Gel/PLLCL/EIF(cs) showed less CD 105 expression compared with ASCs on Gel/PLLCL/EIF(b) (Fig. 4.4C and 4.4G). This also demonstrated that a higher percentage of ASCs on Gel/PLLCL/EIF(cs) differentiated to keratinized epithelial cells, compared with those on Gel/PLLCL/EIF(b). The results of our immunocytochemical studies proved that the electrospun Gel/PLLCL/EIF(cs) can act as a suitable substrate for epidermal differentiation of ASCs. Our findings also indicate that the differentiated ASCs were in the early and intermediate stages of epidermal differentiation. The studies open up new opportunities for transplantation of wound healing mediators containing nanofibrous scaffolds as skin graft for skin tissue engineering.

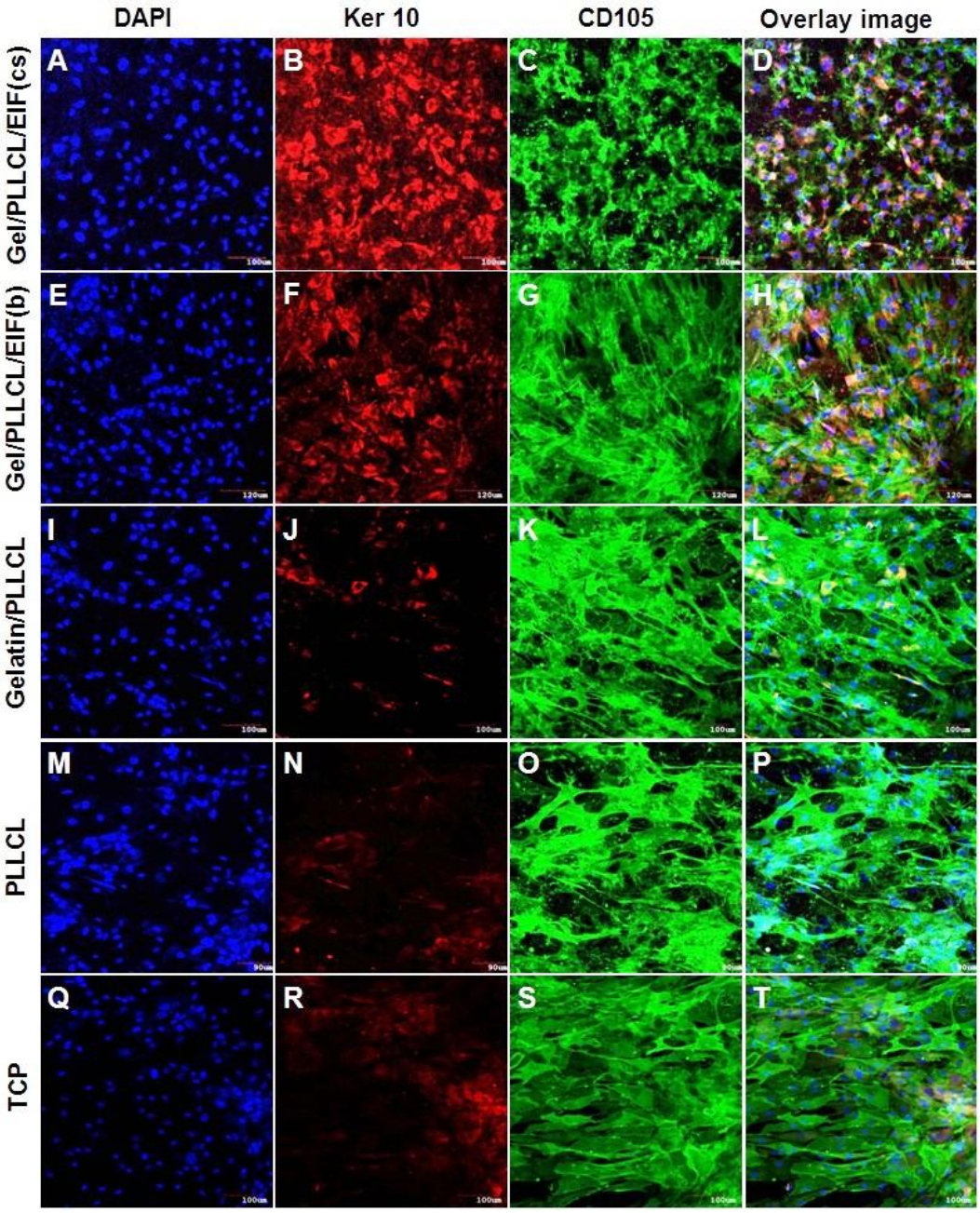

Fig. 4.4 Dual immunocytochemical analysis for the expression of Ker 10, CD 105 and merged image showing the dual expression of both CD 105 and Ker 10 on (A-D) Gel/PLLCL/EIF(cs); (E-H) Gel/PLLCL/EIF(b); (I-L) Gelatin/PLLCL; (M-P) PLLCL and (Q-T) TCP at 20 × magnification.

4.4 Conclusion

In the present study, a few major epidermal induction factors were incorporated into

polymeric gelatin-PLLCL solutions to obtain core-shell and blended nanofibers and the results of the release studies demonstrated that the core-shell nanofibers achieved sustained release without burst release. The expression of early and intermediate epidermal differentiation markers was observed by performing the differentiation of ASCs to epidermal lineages on both Gel/PLLCL/EIF(b) and Gel/PLLCL/EIF(cs). With sustained release of EIF from Gel/PLLCL/EIF(cs), the percentage of epidermally differentiated ASCs on core-shell nanofibers was significantly higher than that on Gel/PLLCL/EIF(b). Our study not only provides insight into the design of a site-specific niche-like microenvironment for ASCs epidermal differentiation, but also sheds light on the design of an ideal EIF delivery vehicle for wound healing and skin reconstitution.

Chapter 5

Electrospun photosensitive nanofibers for photocurrent therapy in skin regeneration

5.1 Introduction

Human skin acts as an anatomical barrier from pathogens and damage between the internal and external environment in bodily defense and it plays a key role in protecting the body against excessive water loss [44, 53]. However, skin wounds such as burn injuries cause millions of patients to remain disabled and it also requires hospitalization [233, 263]. Several bioengineered grafts including the autografts and xenografts have been employed to cure skin wound, and autografts have been regarded as the golden standard for treating full-thickness wounds. However, problems associated with limited donor sites restrict the application of autografts [264]. Skin tissue-engineering (TE) involves the use of scaffolds that support cell attachment and proliferation, together with the formation of skin tissue-like structure to substitute the skin [265]. Photocurrent therapy with participation of light and electrical stimulations could be an innovative and promising approach in skin regenerative medicine [266]. The effects of electrical and photic signals on cell behaviors have been studied for a long time and the main signals used for electrical stimulation (ES) are DC electrical signal, pulsed cathodal electrical signal and electromagnetic field. DC electrical signal was found to be a directional cue which can significantly affect the spatial organization of the vascular structure [267]. Feedar et al found that a pulsed cathodal ES has a beneficial effect on healing chronic dermal ulcer [268]. Three types of electromagnetic fields (inductive coupling, capacitive coupling, and combined electromagnetic fields) were applied by Brighton et al. to stimulate bone cells. A significant increase in DNA content was achieved by stimulation of these electromagnetic fields compared to the controls without stimulation [269]. Concurrently, phototherapy is the therapy in the presence of light irradiation and clinical

application of phototherapy or the therapeutic applications of light has been increased over the recent years. Accelerated repair of chronic skin wounds was realized by the stimulation from near-infrared (600-700 nm) and infrared (700-1200 nm) light delivered through light-emitting diodes or lasers [270]. Phototherapy can reduce inflammatory reactions; increase the production of basic fibroblast growth factor; enhance cell proliferation and accelerate cutaneous wound healing [271]. With electrotherapy and phototherapy having positive effects on regenerative medicine, it is also thought that photocurrent (the current generated under light stimulation) could be a promising method which can be applied in regenerative medicine.

Aiming to prepare a suitable scaffold for photocurrent therapy in skin TE, we fabricated photosensitive nanofibrous scaffolds by electrospinning. Electrospinning is capable of producing continuous fibers with diameters down to nanometers to mimic the fiber size and orientation of *in vivo* extracellular matrix (ECM) [168]. Poly (3-hexylthiophene) (P3HT) is one of the most promising photovoltaic polymers and it shows great promise for a range of applications, including organic LEDs and photocurrent therapy [272]. It is used in polymer-based photovoltaic cells mainly because P3HT possess a high absorption coefficient close to the maximum photon flux in the solar spectrum and high charge-carrier mobility [273]. However, electrospinning of pure P3HT (though attempted), is not possible mainly due to the absence of chain entanglement [272, 274]. Polycaprolactone (PCL) is a bio-resorbable and biocompatible polymer, and it has been studied as a wound dressing material since 1970s. Extensive research has been conducted on its biocompatibility and efficacy, both *in vitro* and *in vivo*, resulting in FDA approval of a number of medical and drug delivery devices composed of PCL [191]. Polymer blending is one of the most effective methods for preparing desirable biocomposite scaffolds for particular applications [275] and during this study we blended PCL with P3HT to fabricate PCL/P3HT nanofibers via electrospinning. The chemical, mechanical and photovoltaic characteristics of the electrospun nanofibers, together with its cell biocompatibility evaluations were carried out. Our study results demonstrated that the PCL/P3HT(10) could be a promising scaffold for tissue engineering, especially in photocurrent induced skin tissue regeneration.

5.2 Materials and Methods

5.2.1 Materials

PCL (M_w 80,000), P3HT (M_w 45,000-65,000, Aldrich 99.995 %), chloroform, methanol, dimethyl sulfoxide (DMSO) and phalloidin (Fluorescein Isothiocyanate Labeled) were all obtained from Sigma-Aldrich Pte Ltd., Singapore and used as received. Dulbecco's Modified Eagle's Medium (DMEM), fetal bovine serum (FBS), penicillin-streptomycin solution and 4,6-diamidino-2-phenylindole, dihydrochloride (DAPI) were purchased from Invitrogen Corporation, USA.

5.2.2 Electrospinning of PCL/P3HT nanofibers

PCL and P3HT with three different weight ratios (150:2, 150:10 and 150:20) were dissolved in chloroform/methanol/DMSO (75/20/5 v/v) to obtain 9 % (w/v) solution, each. The solutions were individually placed in a 3 ml standard syringe attached with blunted steel needles with 27 G inner diameters. Then, the solution loaded syringe was located in a syringe pump (KDS 100, KD Scientific, Holliston, MA) at a flow rate of 1.0 ml h^{-1}. Nanofibers were fabricated via electrospinning at 15 kV (Gamma High Voltage Research, Ormond Beach, FL) and collected on an aluminum foil wrapped flat grounded steel plate at a distance of 12 cm from the needle tip. A vacuum desiccator was used to evaporate residual solution of the nanofibers collected on 15 mm coverslips.
Hereafter, in this manuscript P3HT containing PCL nanofibers with three different weight ratios 150:2, 150:10 and 150:20 will be represented as PCL/P3HT(2), PCL/P3HT(10) and PCL/P3HT(20), respectively.

5.2.3 Characterization

UV-Vis spectra of the polymer solutions were measured using Shimadzu UV-3600 UV-Vis-NIR spectrophotometer after dispersing the materials in chloroform and methanol (75/25 v/v). FESEM (FEI-QUANTA 200F, Netherlands) was used to study the morphology of the electrospun nanofibers at an accelerating voltage of 15 kV, after sputter coating with gold (JEOL JFC-1200 fine coater, Japan). The obtained SEM images

were applied to obtain the diameters of the electrospun fibers using image analysis software (Image J, National Institutes of Health, USA). The pore size and distribution of each electrospun nanofibers was evaluated by a CFP-1200-A capillary flow porometer (PMI, New York, NY). The wetting agent used for porometry measurements is Calwick with a defined surface tension of 15.9 dynes/cm (PMI, New York, NY). Nanofibers with similar size (3 cm × 3 cm) and thickness were obtained and each sample was tested individually. The J-V characteristics of and the different PCL/P3HT composite nanofibers were recorded under inert atmosphere and at room temperature using a calibrated San-Ei XES-151 S (Japan) class A solar simulator under standard conditions (1 Sun, 1.5 G). Before test, The FTO plate having the photosensitive nanofiber was pressed against an aluminium (Al) sputtered FTO using binder clips and connected to stimulator with wires. Photoluminescence (PL) spectra were recorded using the photonic multichannel spectral analyzer (Hamamatsu Photonics K.K., PMA 11) and the wavelength of the excitation beam was set between 380 and 420 nm.

5.2.4 Human dermal fibroblast culture

This method is the same to that mentioned in section 3.2.4.

5.2.5 Light stimulation

To study the effects of different amount of P3HT incorporated in PCL nanofibrous scaffolds on fibroblast proliferation under light stimulation, illumination of human dermal fibroblasts on PCL, PCL/P3HT(2), PCL/P3HT(10) and PCL/P3HT(20) was performed using white color light emitting diodes (LEDs) (DIODER Lighting strip, IKEA, Singapore). The calibration of LEDs was performed with a USB 2000 spectrometer (Ocean optics, FL, USA). The wavelength of white LED is 421 to 670 nm, within the range of visible light (390 – 750 nm). Fig. 5.1 shows the schematic explanation of light stimulation.

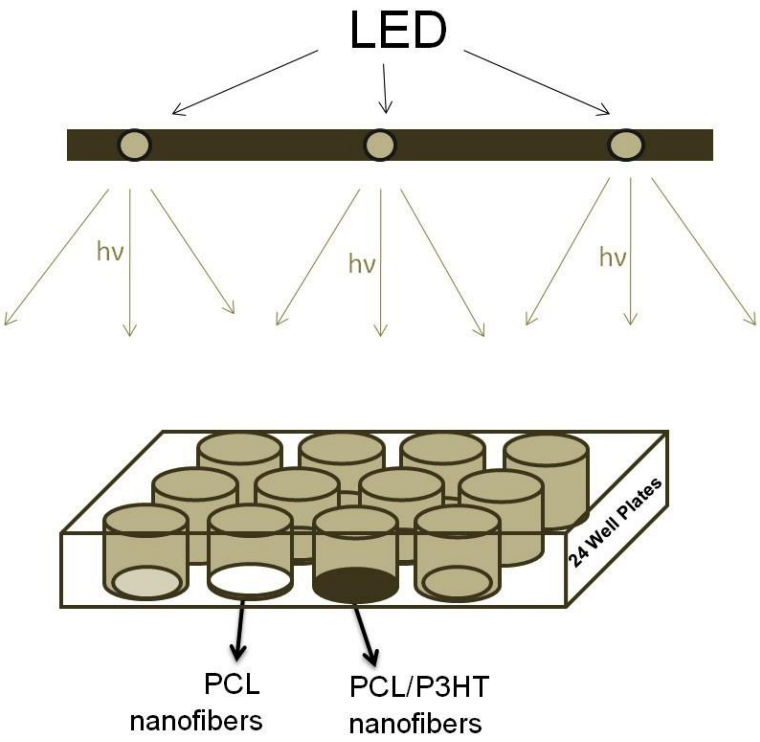

Fig. 5.1 Schematic explanation of the method used for light irradiation on cell-scaffold constructs. PCL (white) and P3HT containing nanofibrous scaffolds (purple) were put in 24 well plates and directly located under LED.

After seeding cells, the 24 well plates containing cell-scaffold composites were directly located under LEDs. Light stimulation study was carried out for 6 days and fibroblasts on PCL, PCL/P3HT(2), PCL/P3HT(10) and PCL/P3HT(20) were irradiated for 1 hour once every 24 hours. After culturing the cells for a period of 6 days, cell proliferation was evaluated after light stimulation by colorimetric MTS assay (CellTiter 96 AQueous One solution, Promega, Madison, WI). After culturing the cells for a period of 2, 4 and 6 days, cells were rinsed with PBS to remove unattached cells and incubated with 20 % MTS reagent in serum free medium for a period of 3 hrs at 37 °C. Absorbance of the obtained dye was measured at 490 nm using a spectrophotometric plate reader (FLUOstar OPTIMA, BMG lab Technologies). The absorbance of the formazan dye is measured at 490 nm and the amount of formazan crystals formed is directly proportional to the number of live cells. As a control, cells were also cultured on the scaffolds under non-stimulative conditions to understand the specific effect of light stimulation towards cell proliferation after seeding cells on the same scaffolds.

5.2.6 F-actin staining

This method is the same to that mentioned in section 3.2.6.

5.2.7 Expression of collagen

This method is the same to that mentioned in section 3.2.7.

5.2.8 Statistical analysis

All the data presented are expressed as mean ± standard deviation (SD) of the mean. Each experiment was repeated three times. Statistical differences were determined by Student's two-sample t test. Differences were considered statistically significant at $p \leq 0.05$.

5.3 Results and discussion

5.3.1 UV-vis spectra

Fig. 5.2 shows the UV-vis absorption spectra of PCL, PCL/P3HT(2), PCL/P3HT(10) and PCL/P3HT(20) in chloroform and methanol. No absorption peak was observed for PCL solution. Evidently, an increase in P3HT concentration resulted in an increase in the intensity of bands in the UV-vis spectra for PCL/P3HT(2), PCL/P3HT(10) and PCL/P3HT(20) solutions. The surface plasmon absorption bands for P3HT containing PCL solutions were centered around 410 nm, which is characteristic of the π–π* transition [274]. Moreover, the absorption wavelength of P3HT (410 nm) lies within the range of the visible light (390 to 750 nm). The most common visible light that we encounter daily in our life is the day light (sunlight) and half of its spectrum lies in the visible short-wave region of the electromagnetic spectrum. Human skin is the outer covering of the body and it is under the frequent exposure of sunlight. Photocurrent therapy with PCL/P3HT nanofibers for skin TE could be very feasible if carried out under the stimulation of light (sunlight).

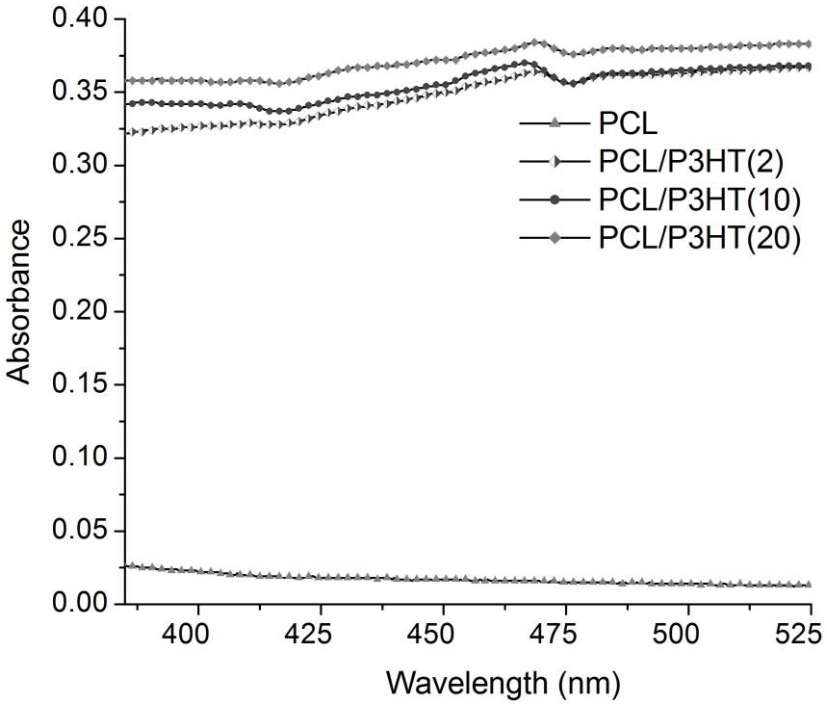

Fig. 5.2 UV-Visible absorption spectra of pure PCL, PCL/P3HT(2), PCL/P3HT(10), and PCL/P3HT(20) solutions dispersed in chloroform and methanol (75/25 v/v). The concentration of each solution was 9 % (w/v).

5.3.2 Morphology and characterization

SEM micrographs of the electrospun nanofibrous scaffolds revealed uniform, beadless, nano-scaled fibrous structures under the optimized spinning conditions utilized during this study (Fig. 5.3). Uniform nanofibers of PCL, PCL/P3HT(2), PCL/P3HT(10) and PCL/P3HT(20) with fiber diameters in the range of 608 ± 168, 503 ± 116, 424 ± 128 and 314 ± 101 nm, were respectively obtained. The diameters of PCL/P3HT nanofibers decreased with the increase of P3HT concentration in PCL solutions. P3HT is a photosensitive and conductive polymer and including P3HT in PCL solution will improve the conductivity of the solution [274]. The increase of P3HT concentration in PCL solution resulted in increased conductivity of the solutions and under the same electrospinning conditions, the high conductivity of the P3HT containing polymer solution favored the formation of fibers with smaller diameters [276, 277]. Hence the PCL/P3HT(20) had smaller fiber diameters compared to PCL/P3HT(10) than PCL/P3HT(2). The porosity of the electrospun scaffolds was studied by capillary flow

porometer (CFP-1200-A) and the pore size of PCL, PCL/P3HT(2), PCL/P3HT(10) and PCL/P3HT(20) was obtained as 4.3 µm, 3.0 µm, 2.1 µm and 1.9 µm, respectively. Capillary flow porometry can provide a simple and non-destructive technique to mesure pore size and distribution of electrospun nanofibrous scaffolds [217, 278]. It was found that fiber mass and diameter can significantly affect the pore diameter of the networks [218, 258]. In our study, the thickness of PCL, PCL/P3HT(2), PCL/P3HT(10) and PCL/P3HT(20) was kept identical (approximately 35 µm). The mean pore sizes obtained for the nanofibers were found inversely proportional to the diameter of the fibers and our results were also in accordance with the results reported by Li et al [258]. Uniform distribution of pore sizes was observed for PCL, PCL/P3HT(2), PCL/P3HT(10) and PCL/P3HT(20) (Fig. 5.3).

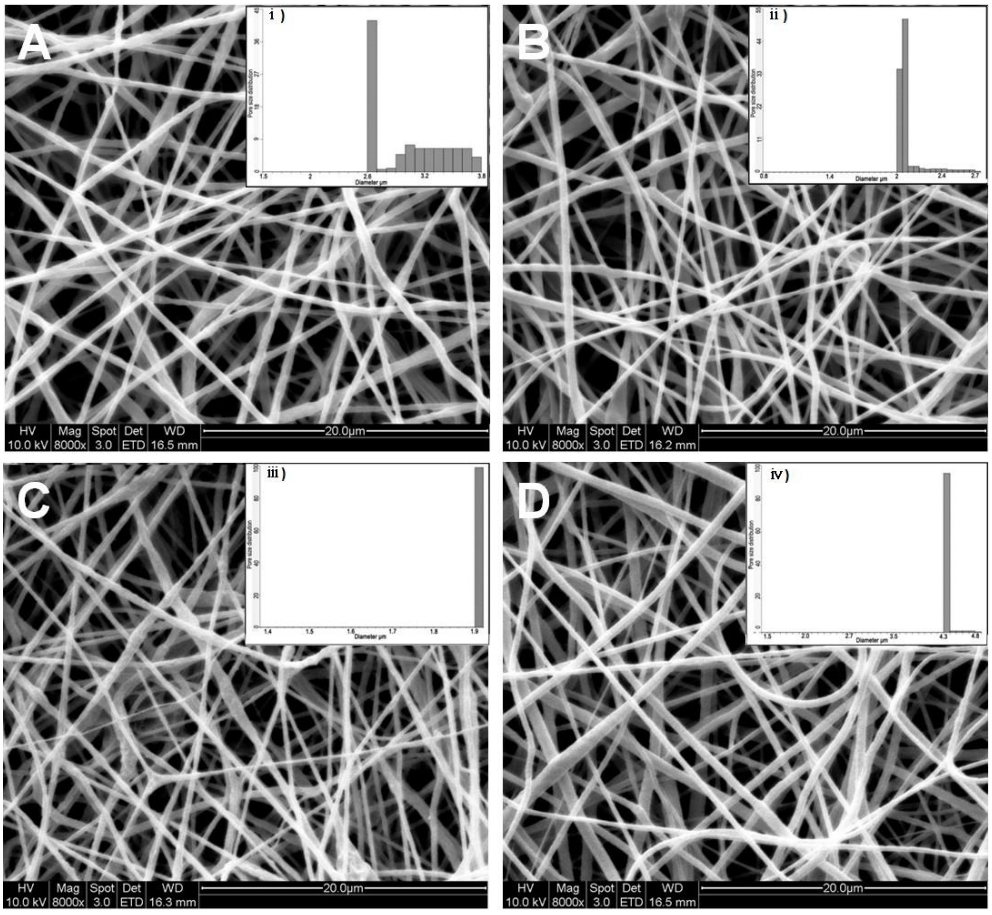

Fig. 5.3 SEM images of electrospun (A) PCL/P3HT(2), (B) PCL/P3HT(10), (C) PCL/P3HT(20) and (D) PCL nanofibers and pore size distribution of i) PCL/P3HT(2), ii) PCL/P3HT(10), iii) PCL/P3HT(20) and iv) PCL nanofibers.

Photoluminescence (PL) is a process in which a substance absorbs photons and then re-radiates photons. PL spectra of electrospun nanofibers were collected to probe into the electronic states of the P3HT present in the scaffolds. Fig. 5.4 shows the photoluminescence spectra of electrospun PCL, PCL/P3HT(2), PCL/P3HT(10) and PCL/P3HT(20) nanofibrous scaffolds. Spectra of every electrospun scaffolds containing P3HT indicated the same maximum emission intensity, at 699 nm. Chan et al. studied the structure of electrospun and casted P3HT membranes via PL spectroscopies and found the occurrence of blue shift in the PL spectra for electrospun P3HT membranes compared to cast film due to the presence of nano-voids in the electrospun fibers [279]. In our study, no blue or red shifts were observed. A broader peak was observed in the emission spectrum of PCL/P3HT(20) compared to PCL/P3HT(10) than PCL/P3HT(2). The broadening of the peak can be correlated to the existence of a large distribution of P3HT within PCL nanofibers.

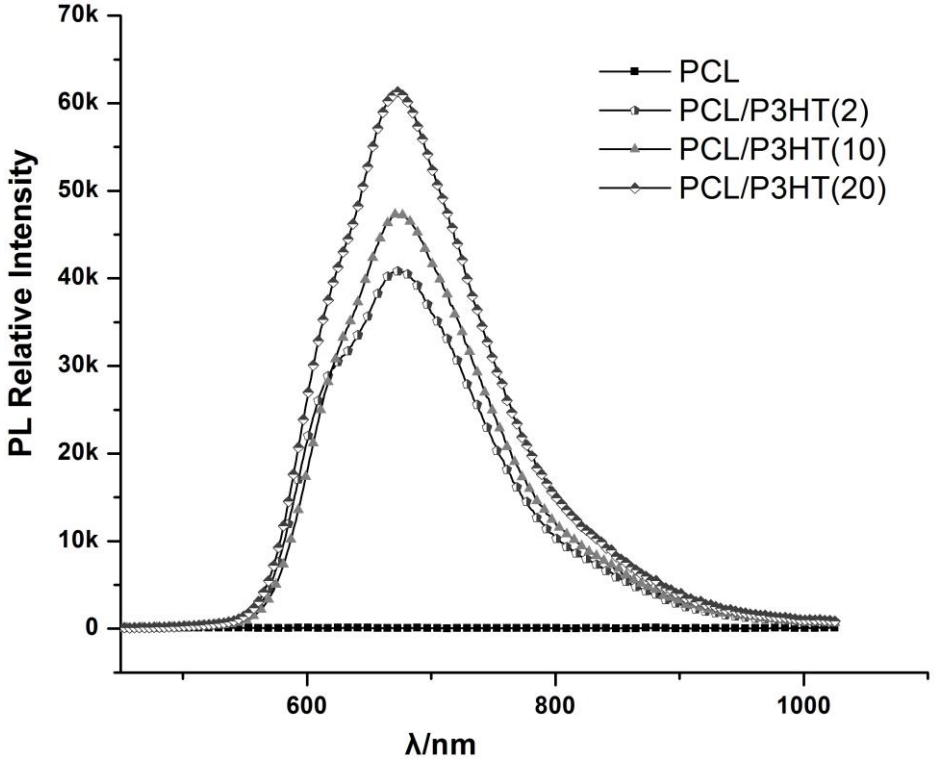

Fig. 5.4 PL spectra for PCL, PCL/P3HT(2), PCL/P3HT(10) and PCL/P3HT(20) under excitation beam of 380 - 400 nm.

The relative peak intensity of electrospun PCL/P3HT nanofibers was directly proportion to the amount of P3HT included in the PCL nanofibers. No emission intensity was however observed for electrospun PCL nanofibrous scaffolds. We therefore presumed that the P3HT was successfully conjugated with PCL within the nanofibers upon electrospinning.

5.3.3 Photovoltaic study

P3HT is a conjugated material with a band gap of 1.9-2.0 eV [280]. Upon illumination, certain electrons were generated due to the photosensitive properties of electrospun PCL/P3HT(2), PCL/P3HT(10) and PCL/P3HT(20), which was evaluated using a calibrated San-Ei XES-151 S (Japan) class A solar simulator. P3HT absorbs photons of light with appropriate wavelength (around 410 nm) and gets promoted to a higher energy level called the HOMO (highest occupied molecular orbital). The electrons getting to the HOMO level have high mobility in the delocalized orbitals of P3HT and they are free to move within a small space in P3HT chains based on the particle in a box model, similar to the movement of a particle free to move in a small space surrounded by impenetrable barriers. When the photoinduced electrons move within the P3HT chains, an electrical current is formed. Initial measurements of the current density versus voltage (J-V) of the PCL/P3HT(2), PCL/P3HT(10) and PCL/P3HT(20) were carried out under standard operating conditions (1 Sun, 1.5G) and showed in Fig. 5.5. The ‘efficiency’ which determines the amount of radiated quantity of light that is converted into useable electrical energy, as obtained for the PCL/P3HT(2), PCL/P3HT(10) and PCL/P3HT(20) were 2.0×10^{-6}, 1.6×10^{-5} and 2.9×10^{-5}, respectively. The efficiency of photosensitive nanofibrous scaffolds was proportion to the amount of P3HT incorporated in the PCL nanofibers (Fig. 5.5A). The low efficiency of the photosensitive nanofibers can be explained due to the structure change of P3HT chains. The P3HT polymer chains exist in two resonant structures [281]: aromatic (i) and quinoid (ii), as shown in Fig. 5.5B. When the polymer chains gets more disordered, the aromatic structure becomes more favorable compared to quinoid structure, because the adjacent rings in A are connected by a single bond making the chains more flexible and this was inferred during our studies too, when PCL was blended with P3HT polymer.

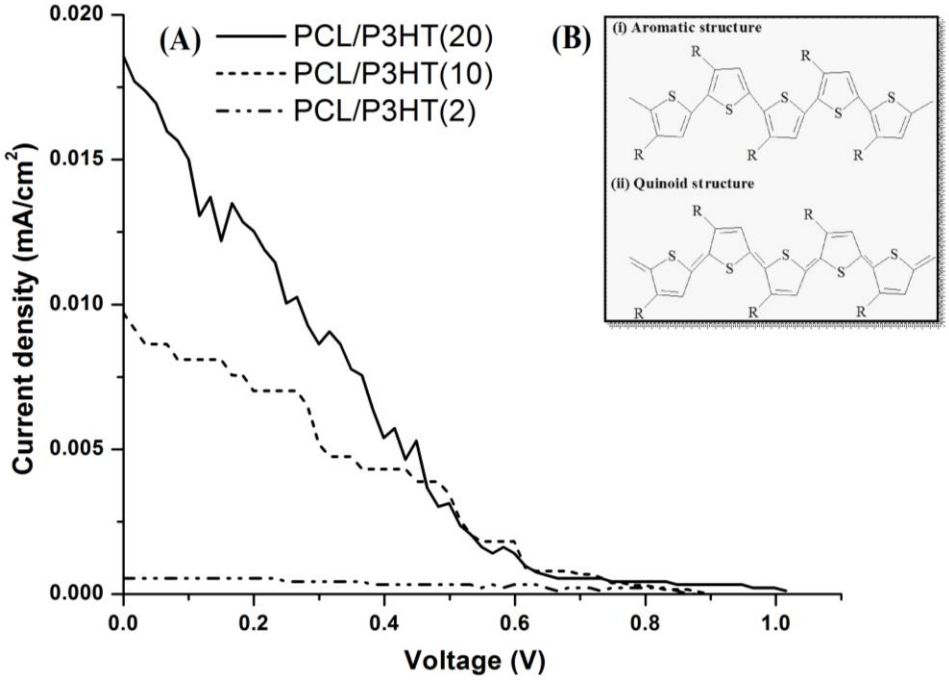

Fig. 5.5 (A) J-V graph of the PCL/P3HT(2), PCL/P3HT(10) and PCL/P3HT(20) photosensitive scaffolds measured under 1 Sun conditions. (B) the resonant structures, (i) aromatic and (ii) quinoid, of poly (3-alkylthiophenes) chains

This implies that even if the charge transfer occurs, the effect of disordering might overcome the effect of charge transfer [282] and as a result, less electrons might get transited to the electron acceptor. Photocurrent was thus generated in the fiber, though of low intensity and this amount was sufficient to meet the essential requirement for application of electrospun photosensitive scaffolds in photocurrent therapy.

5.3.4 Light stimulation

The effect of light stimulation as well as the effect of different amounts of P3HT incorporated within the PCL scaffolds towards the proliferation of HDFs was evaluated by MTS assay (Fig. 5.6). In non-stimulated (NS) conditions, the proliferation of HDFs on PCL nanofibrous scaffold showed higher fibroblast proliferation compared to the proliferation of HDFs on PCL/P3HT(2), PCL/P3HT(10) and PCL/P3HT(20). Moreover, the proliferation of HDFs on PCL/P3HT(20) non-stimulated showed the lowest proliferation of cells due to higher amounts of P3HT present in PCL/P3HT(20). Hence, it was clear that the biocompatibility of P3HT containing PCL naonfibrous scaffolds is not as

good as pure PCL nanofibrous scaffold.

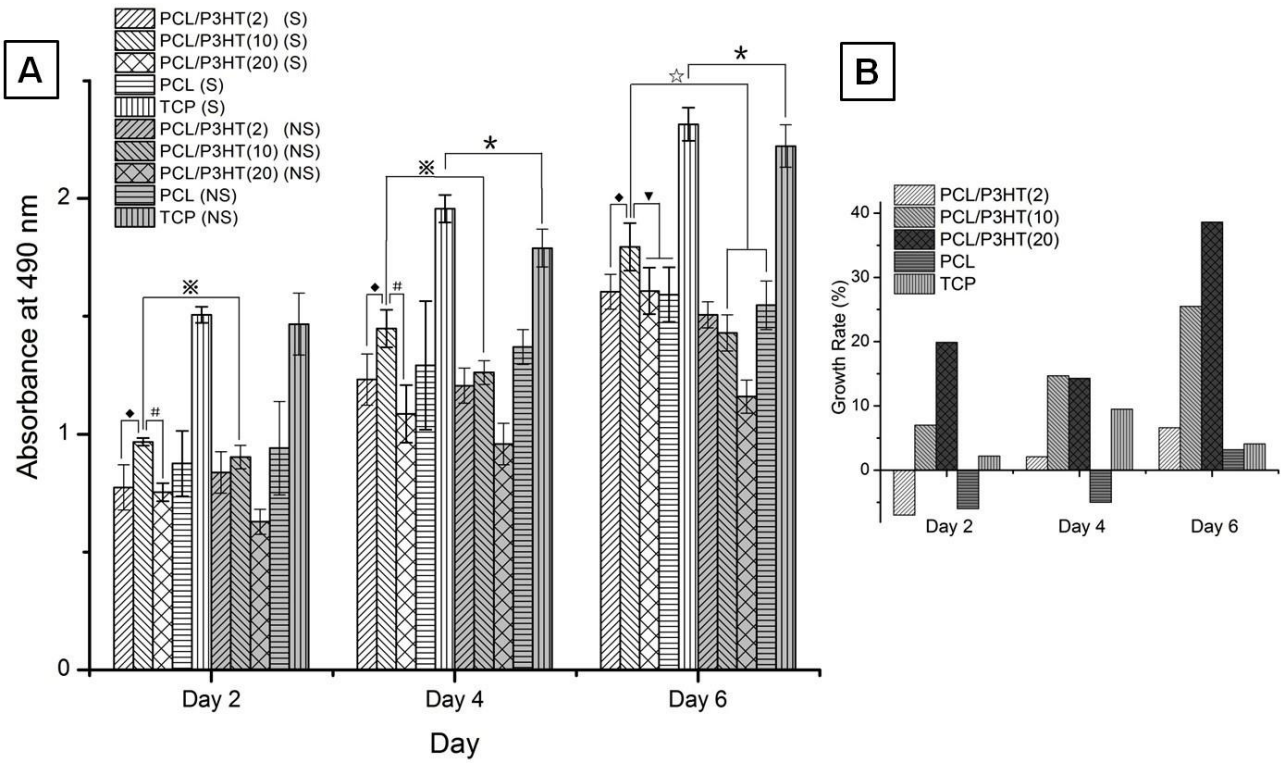

Fig. 5.6. (A) HDF proliferation on electrospun PCL, PCL/P3HT(2), PCL/P3HT(10) and PCL/P3HT(20) nanofibrous scaffolds stimulated (S) compared to HDF proliferation on electrospun PCL/P3HT(2), PCL/P3HT(10), PCL/P3HT(20) and PCL nanofibrous scaffolds non-stimulated (NS) by MTS assay. *Significant against cell proliferation on TCP (NS) at $p \leq 0.05$; $^{\blacklozenge}$Significant against cell proliferation on PCL/P3HT(2) (S) at $p \leq 0.05$. $^{\#}$Significant against cell proliferation on PCL/P3HT(20) (S) at $p \leq 0.05$. $^{※}$ Significant against cell proliferation on PCL/P3HT(10) (NS) at $p \leq 0.05$. $^{\blacktriangledown}$Significant against cell proliferation on PCL/P3HT(10) and PCL (S) at $p \leq 0.05$. $^{☆}$Significant against cell proliferation on PCL/P3HT(10) and PCL (NS) at $p \leq 0.05$. (B) Growth rate of cells on stimulated PCL/P3HT(2), PCL/P3HT(10), PCL/P3HT(20), PCL and TCP with respect to the non-stimulated scaffolds on day 2, day 4 and day 6.

However, the proliferation of HDFs under light stimulation (S) on PCL/P3HT(10) was significantly higher compared to the cell proliferation on other nanofibrous scaffolds. The ability of the photosensitive PCL/P3HT(10) in promoting the proliferation of HDFs was further confirmed after 6 days of MTS studies. It was demonstrated by Desmet et al. that light stimulation itself can promote cell proliferation [271]. However, the cell proliferation on TCP under light stimulation after 6 days, was merely 5.4 % ($p \leq 0.05$) higher compared

to cell proliferation on the non-stimulated TCP. On the other hand, the extent of cell proliferation was greatly improved by the combination of light stimulation with assistance of photosensitive P3HT containing scaffolds. Using PCL/P3HT(10) as the substrate, we found higher proliferation (25.5 %) of HDFs ($p \leq 0.05$) under stimulated conditions compared to cell proliferation in non-stimulated (NS) conditions. The significant increase in cell proliferation on PCL/P3HT(10) scaffold was due to the photosensitive ability of PCL/P3HT(10) nanofibers under light stimulation. Meanwhile, the cell proliferation on stimulated PCL/P3HT(10) scaffolds was 16.1 % higher compared to HDF proliferation on non-stimulated PCL. This result also supported the fact that the incorporation of optimized amount of P3HT in PCL/P3HT(10) favored cell proliferation through light stimulation. Furthermore, the proliferation of HDFs on PCL/P3HT(10) showed 12.8 % ,11.9 % and 11.6 % ($p \leq 0.05$) higher than the cell growth on PCL, PCL/P3HT(2) and PCL/P3HT(20) under light stimulated conditions, respectively (Fig. 5.6A). After 2, 4 and 6 days, the growth rate of cells on stimulated PCL/P3HT(2), PCL/P3HT(10), PCL/P3HT(20), PCL and TCP with respect to the non-stimulated scaffolds was also calculated (Fig. 5.6B). The proliferation of HDFs on day 2 and day 4 for light stimulated PCL scaffolds was less compared to HDFs proliferation on non-stimulated PCL. This could be because of the absence of P3HT (photosensitive material) within this scaffold. The inference was confirmed as we observed a similar effect on the scaffolds that contained minimum amounts of P3HT of our study, namely the PCL/P3HT(2) on day 2, which further picked up in its cell proliferation from day 4 onwards. By day 6, we observed that the growth of cells on all the stimulated scaffolds was higher compared to cells on corresponding non-stimulated scaffolds. Moreover, the cell proliferation on stimulated PCL/P3HT(10) scaffolds demonstrated both higher cell number and cell growth rate compared to the non-stimulated PCL. In conclusion, the amount of P3HT included in PCL/P3HT(10) was the optimized amount, most suitable scaffold for performing light stimulative regenerative experiments and regenerative medicine.

The morphology of HDFs on electrospun PCL and PCL/P3HT(10) nanofibrous scaffolds was studied after 6 days light stimulation and the results are shown in Fig. 5.7. Fibroblasts

attached on the scaffolds and stretched across the nanofibrous substrates upon proliferation. The number of cells that attached on PCL/P3HT(10) stimulated was higher than the number of cells attached on the same scaffold non-stimulated. Fibroblasts attached on PCL/P3HT(10) under light stimulation showed a characteristic spindle shape (Fig. 5.7A); however, fibroblasts attached on PCL and PCL/P3HT(10) nanofibrous scaffolds in non-stimulated conditions showed irregular morphology (Fig. 5.7D and 5.7E). From the SEM micrographs, we further established the non-toxicity of the PCL/P3HT(10) with successful adherence and proliferation of HDFs on PCL/P3HT(10) substrates under light stimulation, and confirmed their morphologies.

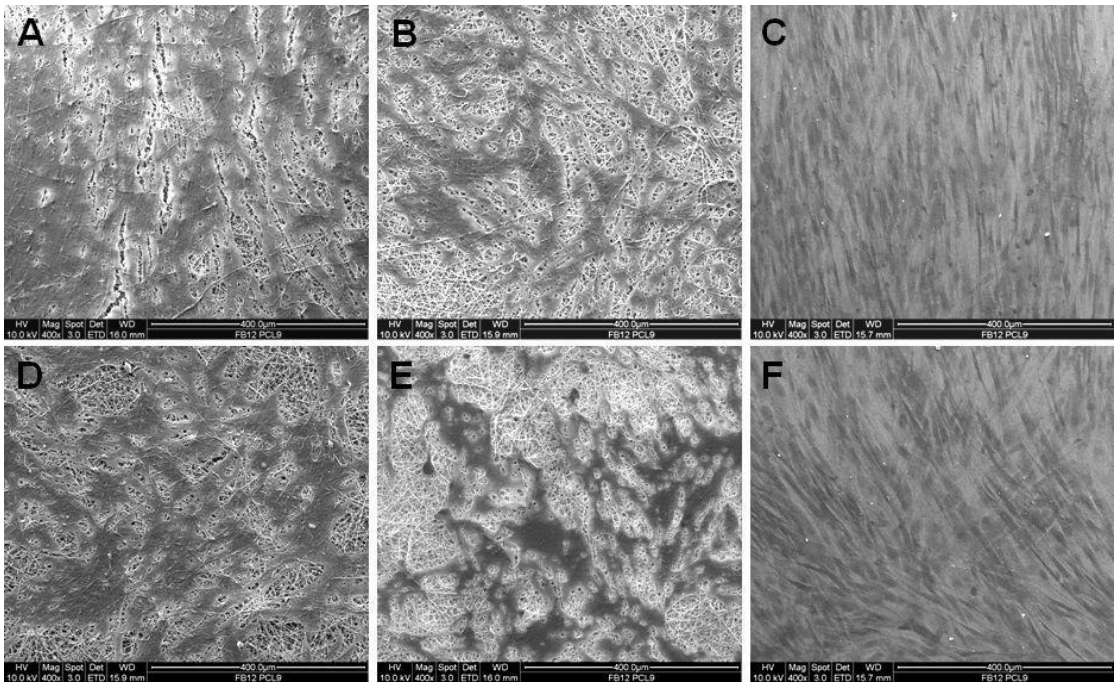

Fig. 5.7. SEM images of HDFs on electrospun (A) PCL/P3HT(10) (S), (B) PCL (S), (C) TCP (S), (D) PCL/P3HT(10) (NS), (E) PCL (NS) and (F) TCP (NS).

The explanatory mechanism of action could be such that the photosensitive polymer P3HT absorbs light (proved by UV-vis spectra), and photo-induced current was further generated in the P3HT containing PCL fibers (shown as J-V curve), while the electromagnetic field was created. When the cells were stimulated by the electromagnetic field, Ca^{2+} ions translocated through the cell-membrane voltage-gated calcium channels [283] and this led to an increase in cytosolic Ca^{2+}. The cytosolic Ca^{2+} would complex

with the low molecular weight protein calmodulin, which then activated several key intracellular processes leading to cell division [284]. Calmodulin was also thought to play a role in regulating the initiation of DNA synthesis. The increase in calmodulin-binding proteins in the nuclear fraction of cells stimulated cell proliferation [285]. As a result, the increase in cytosolic Ca^{2+} led to an increase in cell proliferation (Fig. 5.8 Green line). The effects of light (low power laser and light emitting diode) stimulation on cell behavior were studied during the past few years and many mechanisms were proposed and one such mechanism was that the light irradiation (He-Ne laser, 632.8 nm) could induce the phosphorylation of tyrosine protein kinase receptor (TPKR) such as c-Met, receptor of hepatocyte growth factor [286, 287]. After phosphorylation, TPKR will become an activated TPKR and it could promote the catalytic activity of phospholipase C (PLC)-gamma. The activated PLC c catalyzes the hydrolysis of some phospholipids which contain diacylglycerol (DAG) and inositol triphosphate (IP3). Further the concentration of DAG and IP3 increase in the cytoplasm and the IP3 encourage the endoplasmic reticulum (ER) to release Ca^{2+}, which works with DAG to activate protein kinase C (PKC) [288, 289]. These are the routes through which PKCs are involved in improving the cell proliferation [288, 290] (Fig. 5.8).

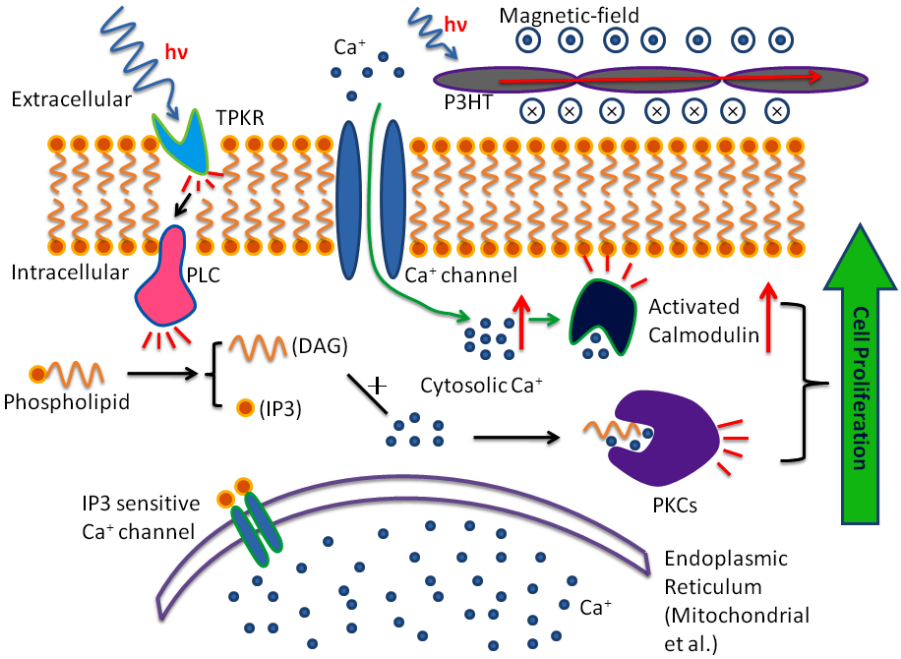

Fig. 5.8 Signal pathway involved in light stimulation induced cell proliferation (Black

line) and photocurrent induced cell proliferation (Green dotted line)

Minana et al. have previously shown that PKC inhibitors, namely H7 and calphostin C prevent the proliferation of primary cell cultures [291]. Similar results were also shown by Yoshimura et al. where they found that the proliferation of Schwann cells was significantly inhibited by staurosporine, a PKC inhibitor [292]. Instead of inhibiting PKC, light stimulation activated PKC and improved the cell proliferations and this was also confirmed in our study, where we found higher HDF proliferation on PCL/P3HT(10) after light stimulation by MTS assay. It was proved that the biocompatibility of P3HT containing PCL naonfibrous scaffolds were not as good as pure PCL nanofibrous scaffold. As a result, the amount of P3HT that might be optimum enough to be non-toxic to cells and support the proliferation of cells after light stimulation was considered necessary to be investigated in detail. Therefore, we followed a novel approach of incorporating various amounts of P3HT in PCL and studied the proliferation of fibroblasts cultured on P3HT containing nanofibrous scaffolds. Our results demonstrated that the PCL/P3HT(10) favored cell proliferation after light stimulation and could be a suitable substrate for wound healing. Therefore performed cell-scaffold interaction studies on PCL/P3HT(10) by SEM, F-actin staining and collagen expression and such studies were not carried out on PCL/P3HT(2) and PCL/P3HT(20).

5.3.5 F-actin staining

To understand the interaction of fibroblasts with PCL/P3HT(10) and PCL nanofibrous scaffolds under light stimulation, phalloidin staining was carried out. Phalloidin is a bicyclic peptide that belongs to a family of toxins isolated from the deadly Amanita phalloides “death cap” mushroom and is commonly used in imaging applications to selectively label filamentous actin in fixed cells [293]. Phalloidin staining was carried out after 6 days of light stimulation and the F-actin stains showed a cytoplasmic filamentous distribution under LSCM. It was found that the cell density of proliferated HDF under light stimulation (Fig. 5.9A-C) was higher compared to HDFs proliferated under non-stimulated conditions (Fig. 5.9D-F).

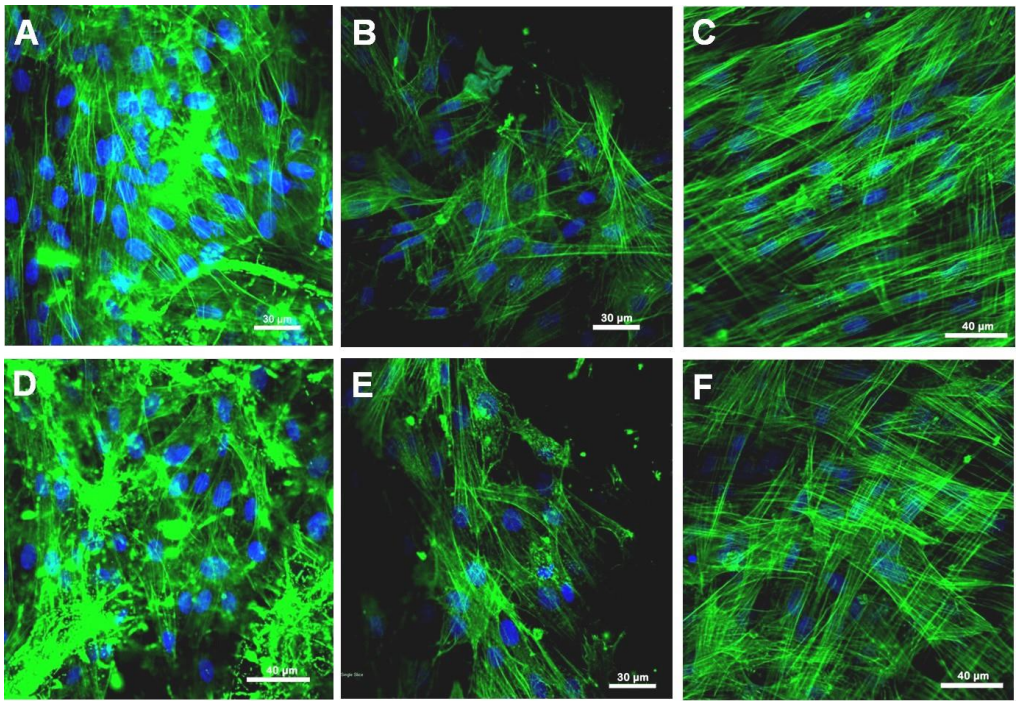

Fig. 5.9 Laser scanning confocal microscopic (LSCM) micrographs of HDFs grown on (A) PCL/P3HT(10) (S), (B) PCL (S), (C) TCP (S), (D) PCL/P3HT(10) (NS), (E) PCL (NS) and (F) TCP (NS), expressing F-actin.

We observed that the cell density and morphology was better on PCL/P3HT(10) under light stimulation compared to other electrospun nanofibrous scaffolds (Fig. 5.9). The spindle shaped morphology of the HDFs on PCL/P3HT(10) under light stimulation (Fig. 5.9A) was comparable to its phenotype on tissue culture plate (Fig. 5.9C). HDFs attached on PCL/P3HT(10) under light stimulation showed sufficient cell to cell communication. However, HDFs attached on PCL/P3HT(10) non-stimulated (Fig. 5.9D) showed limited cell-cell communication with limited distribution of cells. As a result, the cell density on PCL/P3HT(10) non-stimulated was lower than the cells proliferated on the same scaffold under light stimulation.

5.3.6 Collagen expression

Collagen staining with Picro-sirius red confirmed the secretion of ECM by the cells in culture. Fig. 5.10 shows the secretion of collagen on fibroblasts grown on PCL and PCL/P3HT(10) after 15 days of light stimulation.

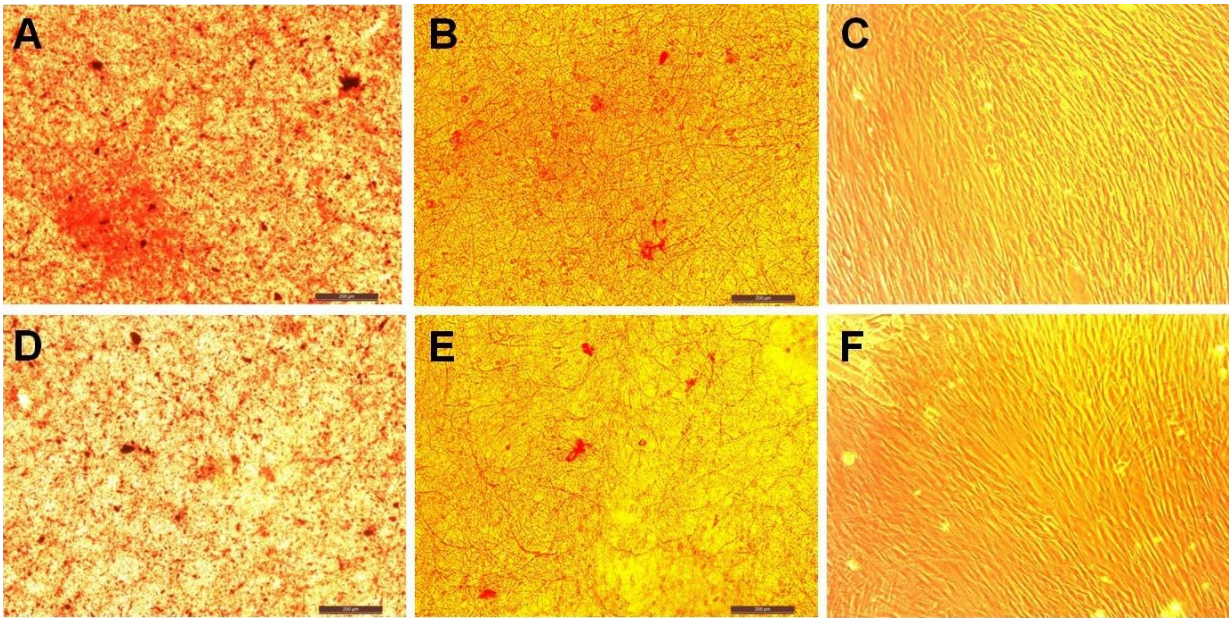

Fig. 5.10 Collagen staining on fibroblasts on nanofibrous scaffolds: A) PCL/P3HT(10) (S), (B) PCL (S), (C) TCP (S), (D) PCL/P3HT(10) (NS), (E) PCL (NS) and (F) TCP (NS).

Results showed that the secretion of collagen on PCL/P3HT(10) under light stimulation was better than other scaffolds. HDFs proliferated on PCL/P3HT(10) under light stimulation showed highest amount of collagen stains. Huang et al. evaluated the influence of LED photoirradiation (LED-PI) on fibroblast proliferation and collagen production *in vitro* and found that the collagen production increased significantly with LED-PI [294]. It was also found that electrical stimulation (ES) promoted collagen synthesis. Morris et al. developed the Ahn/Mustoe lapine wound model for systematic investigation of the effects of ES on ischemic wound therapy. Both type I collagen (COL-I) and type V collagen (COL-V) showed significantly higher expressions between day 7 and day 14 over a longer duration of electrical pulse treatment [130]. In our study we found that the higher cell proliferation on PCL/P3HT(10) under light stimulation contributed to increased collagen stains on these scaffolds. However, no obvious collagen stains were observed on TCP. The secretion of collagen on PCL/P3HT(10) proves the biocompatibility of PCL/P3HT(10) stimulated under light stimulation and its ability to induce cells for collagen expressions, thus potentially suitable as substrates for wound healing or skin tissue regeneration.

Polymeric nanofibers are studied individually for skin TE and the photovoltaic property of solar cells has also been separately investigated by various researchers. However, to the best of our knowledge, there are no studies that focused on the application of nanofibrous scaffold with photovoltaic ability for tissue regeneration. The photovoltaic ability of PCL/P3HT nanofiber scaffolds was demonstrated in this study by studying the current density versus voltage. The electrospun fiber can definitely absorb visible light and convert the optical energy to electrical energy causing the photocurrent effect. An optimized amount of P3HT was incorporated in PCL and our studies found higher HDF proliferation with collagen stains on PCL/P3HT(10) scaffolds after light stimulation. All these results proved that PCL/P3HT(10) could be a promising substrate for photocurrent therapy in skin TE.

5.4 Conclusions

Functional photosensitive P3HT containing PCL nanofibrous scaffolds were fabricated by electrospinning. Fibroblast proliferation on PCL, PCL/P3HT(2), PCL/P3HT(10) and PCL/P3HT(20) nanofibrous scaffolds under light stimulation was studied and the results of our study suggest that fibroblasts cultured on PCL/P3HT(10) after light stimulation had better proliferation and morphology than fibroblasts cultured on electrospun PCL, PCL/P3HT(2) and PCL/P3HT(20) nanofibers. Electrospun PCL/P3HT(10) nanofibrous scaffold was capable of supporting cell proliferation and favoring cell ECM secretion. We concluded that the electrospun PCL/P3HT(10) nanofibers are suitable substrates for wound healing applications.

Chapter 6

Electrospun biomimetic and photosensitive core-shell nanofibrous scaffolds for skin regeneration

6.1 Introduction

Burn injuries, chronic wounds (pressure and leg ulcers), tumors and excision of skin are the main forms of skin damage [1, 190]. Burn injuries cause damage to blood vessels in the immediate area of the wound and lead to restriction or cessation of blood flow at the site of injury [235]. According to WHO, 300,000 deaths are annually reported in hospitals due to burn injuries, while 6 million patients worldwide suffer from burns every year [3]. For patients with very large total body surface area wounds, insufficient donor sites for autografting complicate wound closure, and this increase the risk of invasive wound infection and mortality [9]. The need for permanent wound closure in burn patients has driven the development of bio-engineered skin replacements [10]. The ideal skin graft shall encompass several strategies such as the use of functional cellular components, biodegradable scaffolds with analogous extracellular matrix (ECM) structures and other biological factors. Rho and colleagues produced a cross-linked nanofibrous matrix of type I collagen via electrospinning to develop natural protein based biomimetic scaffolds. They examined the effect of collagen nanofibers on open wound healing in rats and found that collagen nanofibrous matrices promote cell adhesion and were effective as wound-healing accelerators in early-stage wound healing [194]. However, the poor mechanical properties and high cost limit the application of collagen in skin tissue engineering. Unlike collagen, gelatin is a natural biopolymer derived from collagen by controlled hydrolysis and it has been widely used in pharmaceutical and medical fields because of its biological origin, biodegradability, biocompatibility, commercial availability and due to its relatively low cost [195]. Chong and colleagues developed a cost-effective substrate by directly electrospinning

poly(ε-caprolactone)/gelatin (PCL/gelatin) nanofibers onto a commercially available polyurethane (PU) dressing (Tegaderm^{TM}, 3M Medical) for application as a dermal wound healing scaffold. The presence of PCL/gelatin on PU was suggested to promote cell adhesion and proliferation capacity of the Tegaderm^{TM} [191]. Similarly, electrospun polyurethane/gelatin (PU/Gel) nanofibers were also found to enhance the regeneration of burn-wounds [213]. Most of these researchers focused on the development of skin grafts which mimic the natural ECM of skin to realize wound healing and skin regeneration. Unlike these researchers, Zhao and his colleagues studied wound healing in a different way where they used electrical signals to regulate wound re-epithelialization. In every species studied, the disruption of an epithelial layer instantaneously generated endogenous electric fields, which is crucial in wound healing [119, 120]. It was observed that with percolation of an electric field with a polarity that opposed the default healing direction, the movement of the epithelium followed the direction of the electric signal and the wound opened up. By reversal of the electrical polarity the wound got closed [121]. Oscillatory electric fields are known to induce human macrophage migration on glass substrate, whereby macrophages exposed to 1 Hz, 2 V/cm field showed an induced migration velocity of $5.2 \pm 0.4 \times 10^{-2}$ μm/min [295]. Macrophages are phagocytic cells that originate in the bone marrow, and they act as scavengers of cell debris and extracellular material in the wound site [48]. Electrical stimulation shows promising results in wound healing, and phototherapy is also gaining recognition for immediate relief of acute and chronic pain, for treatment of inflammatory conditions, and to promote wound healing. Light irradiation was found to significantly influence wound healing. In one such study, the treatment of the wounds in rat models using blue light demonstrated a significant decrease in the wound area [116]. On the other hand, a significantly higher number of fibroblasts were found under green light-emitting diode (LED) irradiation compared with fibroblasts irradiated with infrared LED light ($p < 0.001$) [117]. Previously in our labs, we performed electrospinning of a blend of poly(3-hexylthiophene) (P3HT) and PCL to prepare a photosensitive scaffold PCL/P3HT, to study the biocompability of the scaffolds [296]. In the current study, we incorporated photosensitive polymer P3HT and EGF in Gel/PLLCL core-shell nanofibers and studied the potential application of this core-shell nanofibers as a novel skin graft.

6.2 Materials and Methods

6.2.1 Materials

ASCs were obtained from Lonza (Portsmouth, NH). HDF were purchased from American Type Culture Collection, USA. DMEM/F12, FBS, penicillin-streptomycinsolution, Alexa Fluor 594, Alexa Fluor 488 and DAPI, were all purchased from Invitrogen (Carlsbad, CA). P3HT, gelatin, chloroform, methanol, and HFP, EGF and bovine serum albumin were all purchased from Sigma-Aldrich (Singapore) and mouse anti-human keratin 10 (Ker 10) antibody was obtained from Thermo Fisher Scientific (Singapore). CD 105 was purchased from Abcam (USA). PLLCL with ratio of 70:30 was obtained from Boehringer Ingelheim Pharma GmbH (Ingelheim, Germany).

6.2.2 Electrospinning of nanofibers

8% (w/v) of PLLCL solution was prepared by dissolving block copolymer in HFP. Gelatin and PLLCL were dissolved in HFP at a ratio of 60:40 (wt.%) to obtain 10% (w/v) solution and stirred overnight. The solutions were individually placed in a 3 ml standard syringe attached with blunted steel needles with 27 G inner diameters. Then, the solution loaded syringe was located in a syringe pump (KDS 100, KD Scientific, Holliston, MA) at a flow rate of 1.0 ml h^{-1}. Nanofibers were fabricated via electrospinning at 15 kV (Gamma High Voltage Research, Ormond Beach, FL) and collected on an aluminum foil wrapped flat grounded steel plate at a distance of 12 cm from the needle tip. A vacuum desiccator was used to evaporate residual solution of the nanofibers collected on 15 mm coverslips.

To fabricate EGF encapsulated core-shell nanofibers, 1.7 μg EGF was diluted into 1 ml solution with 5% bovine serum albumin (BSA) and was used as the core solution. The amount of loaded EGF was calculated based on the study by Jiang et al. [248]. To fabricate EGF and P3HT encapsulated core-shell nanofibers, 1.7 μg EGF and 18 mg P3HT were dissolved in 1 ml chloroform/methanol (3:1 v/v) solution and was used as the core solution. The amount of the P3HT used in this study was optimized based on our previous study [296].

A coaxial spinneret was applied for electrospinning, where the inner needle had an inner diameter of 0.8 mm and an outer diameter of 1 mm; the outer needle has an inner diameter of 1.8 mm. The fluids of the core and shell remained immiscible before exiting the coaxial spinneret. Two syringe pumps were provided to pump a constant volume flow rate of 0.3 mL/h for the core solution and 1.0 mL/h for the shell solution. The core-shell structured fibers were electrospun at a high-voltage of 15 kV. The distance between the tip of spinneret and collector was 12 cm. Hereafter, in this manuscript P3HT, EGF encapsulated nanofibers and EGF encapsulated nanofibers will be represented as Gel/PLLCL/P3GF(cs) and Gel/PLLCL/GF(cs), respectively.

6.2.3 Characterization of electrospun nanofibers

FESEM (FEI-QUANTA 200F, Netherlands) was used to study the morphology of the electrospun nanofibers at an accelerating voltage of 10 kV, after sputter coating with gold (JEOL JFC-1200 fine coater, Japan). The obtained SEM images were applied to obtain the diameters of the electrospun fibers using image analysis software (Image J, National Institutes of Health, USA). The core-shell structure of Gel/PLLCL/P3GF(cs) and Gel/PLLCL/GF(cs) was examined using a JEOL JEM-2010F transmission electron microscopy (TEM). VCA Optima Surface Analysis system (AST products, Billerica, MA) was applied to measure the hydrophilic/hydrophobic properties of the electrospun nanofibrous scaffolds. Functional groups of the electrospun nanofibrous scaffolds were evaluated by attenuated total reflectance fourier transform infrared (ATR-FTIR) spectroscopic analysis in a Nicolet Avatar 380 spectrometer (Thermo Nicolet, Waltham, MA) over the range 600-3800 cm^{-1} at a resolution of 4 cm^{-1}. A tabletop tensile tester (Instron x345, Canton, MA) was applied to determine the tensile properties of the electrospun nanofibrous scaffolds at a load cell capacity of 10 N. Specimens with dimensions 10 mm × 20 mm were used for tensile test at a rate of 10 mm min^{-1}. The tensile stress-strain curves were plotted from the data recorded by the instrument at ambient conditions. As a minimum, five specimens from each scaffold were tested.

6.2.4 Light stimulation conditions

To evaluate the effect of light stimulation on HDF proliferation, *in vitro* wound healing

and ASC epidermal differentiation, illumination of cells on the electrospun nanofibrous scaffolds was performed using white color light emitting diodes (LEDs) (DIODER Lighting strip, IKEA, Singapore). USB 2000 spectrometer (Ocean optics, USA) was used to perform the calibration of LEDs. The wavelength of white LED is 421 to 670 nm, within the range of visible light (390 – 750 nm). After seeding cells, the cell-scaffold composites were directly located under LEDs and irradiated for 1 hour once every 24 hours. The effect of light stimulation on HDF proliferation and *in vitro* wound healing was performed for 9 days and the effect on ASC epidermal differentiation was carried out for 15 days.

6.2.5 Culture of HDFs and proliferation

DMEM supplemented with 10% FBS and 1% antibiotic and antimycotic solutions were used to culture human dermal fibroblasts (HDFs) in a 75 cm^2 cell culture flask. Cells were incubated for 6 days in an incubator at 37 °C, containing 5% CO_2 and the culture medium was changed once every 3 days. Nanofibrous scaffolds were placed in 24 well plate and pressed by a stainless steel ring. The specimens were exposed to UV radiation for 2 h, washed thrice with phosphate-buffered saline (PBS) and incubated overnight in DMEM. HDFs were seeded on the scaffolds at a density of 10×10^3 cells/well. The comparative proliferation capacity of fibroblasts on Gel/PLLCL/P3GF(cs), Gel/PLLCL/GF(cs), Gel/PLLCL and PLLCL nanofibrous scaffolds under light stimulation was evaluated following the parameters as described in section 6.2.4. The cell proliferation was evaluated by colorimetric MTS assay (CellTiter 96 AQueous One solution, Promega, Madison, WI). After culturing the cells for a period of 3, 6 and 9 days, the culture medium was removed and cell-scaffold composites were washed 3 times with PBS to remove unattached cells. Then, the composites were incubated for a period of 3 hrs at 37 °C with 20 % MTS reagent in serum free medium. A spectrophotometric plate reader (FLUOstar OPTIMA, BMG lab Technologies) was applied to measure the absorbance of the obtained dye at 490 nm. The amount of formazan crystals formed is directly proportional to the number of live cells, which was also directly proportional to the absorbance values obtained. As a control, cells were also cultured on the scaffolds under non-stimulative conditions to understand the specific effect of light stimulation

towards cell proliferation after seeding cells on the same scaffolds.

6.2.6 *In vitro* wound healing on Gel/PLLCL/P3GF(cs) nanofibrous scaffold

In vitro wounds were induced to study the capability of photosensitive Gel/PLLCL/P3GF(cs) in promoting wound healing. Before seeding cells, a sterilized 0.5 × 0.5 cm^2 glass slide was located in the center of the scaffold. After 9 days, when HDFs were grown to confluency, the glass slide on each scaffold was removed to induce the wound. The *in vitro* wound and scaffold constructs in the light stimulated group were irradiated for 1 hour once every 24 hours. The appearances of *in vitro* wounds closure in stimulated and non-stimulated groups were obtained by SEM. After periods of 3 and 9 days, the cell-scaffold constructs were fixed in 2.5% glutaraldehyde for 2 h. The scaffolds were further rinsed in DI water, dehydrated with increasing concentrations of ethanol (50%, 75% 95%, 100%) for 10 min each. Finally the cell-scaffold constructs were air-dried in fume hood overnight and observed under the SEM.

6.2.7 Epidermal differentiation of ASCs on photosensitive scaffolds

To study the potential of photosensitive nanofibrous scaffolds towards the epidermal differentiation of ASCs under light stimulation, illumination of ASCs on Gel/PLLCL/P3GF(cs) and Gel/PLLCL/GF(cs) was performed using the LED and light stimulation parameters as described in section 6.2.4. ASCs were seeded on the scaffolds at 5 ×10^3 cells/well in 24-well plates using medium comprising of DMEM and Ham's F12 medium (3:1) containing10% FBS, 100 IU ml^{-1} penicillin and 100 μg ml^{-1} streptomycin. All samples were incubated under standard culture conditions and the culture medium was changed every 3 days.

6.2.8 Immunostaining analysis of differentiated ASCs

To confirm the differentiation of ASCs along the epidermal lineage, double immunostaining was performed. After 15 days, the cell-scaffold composites were washed with PBS, fixed with 2.5% paraformaldehyde. The ASCs on Gel/PLLCL/P3GF(cs) and Gel/PLLCL/GF(cs) were blocked for nonspecific staining using 2% BSA then immunostained with ASC-specific marker CD 105 for 2 h at room temperature.

Subsequently, the cell-scaffold composites were revealed with Alexa Fluor 594 (red) secondary antibody for 60 min at room temperature. After that, the samples were washed three times with PBS and treated with diluted Ker 10 (1:100) for 2 h at room temperature. Then, the secondary antibody Alexa Fluor 488 (green) was added for 60 min at room temperature. Finally, the samples were treated with DAPI after washing thrice with PBS and incubated for 30 min at room temperature. The stained samples were mounted on a glass slide and examined under confocal microscope (LSM 700, ZEISS).

6.2.9 Statistical analysis

All the experiments were repeated 3 times to calculate the mean ± standard deviation (SD). Statistical differences were determined by Student's two-sample *t*-test. Differences were considered statistically significant at $p \leq 0.05$.

6.3 Results and discussion

Over the last few decades innovations in biomaterials and medical technology have had a sustainable impact on the development of biomimetic scaffolds for regenerative medicine. To realize skin regeneration, researchers use stem cells, growth factors and smart bioactive materials to develop artificial extracellular matrix (ECM) (20). However, these tissue engineered composites still suffer certain drawbacks such as short shelf-life, high cost and the clinical performance of many of these scaffolds are poor due to low adhesion to lesion, difficulty in reproducing skin appendages and inability to replace the lost tissue, particularly the dermis, after severe burns [1, 297]. Hence, it was necessary to conquer wound healing directions via a different path such as the 'photocurrent therapy'. Photocurrent is generated when photovoltaic device such as a photodiode gets irradiated with certain wavelength of light and absorbs energy from the light. While electrotherapy and phototherapy have shown promising results in skin regeneration, photocurrent therapy combines these two therapies and it could be more appropriate in regenerative medicine [134]. In order to improve the biocompatibility of the photosensitive P3HT, we electrospun core-shell structured nanofibers and encapsulated P3HT and EGF within the core and studied the ability of the core-shell nanofibers in promoting cell proliferation, *in vitro* wound healing and further utilized the scaffolds to study their potential for

epidermal differentiation of stem cells.

6.3.1 Morphology, chemical and mechanical characterization of electrospun nanofibers

Nanofibers of Gel/PLLCL/P3GF(cs), Gel/PLLCL/GF(cs), Gel/PLLCL and PLLCL were fabricated by electrospinning under the optimized spinning conditions. SEM images (Fig. 6.1) shows beadless, nano-scaled fibrous structures with interconnected pores.

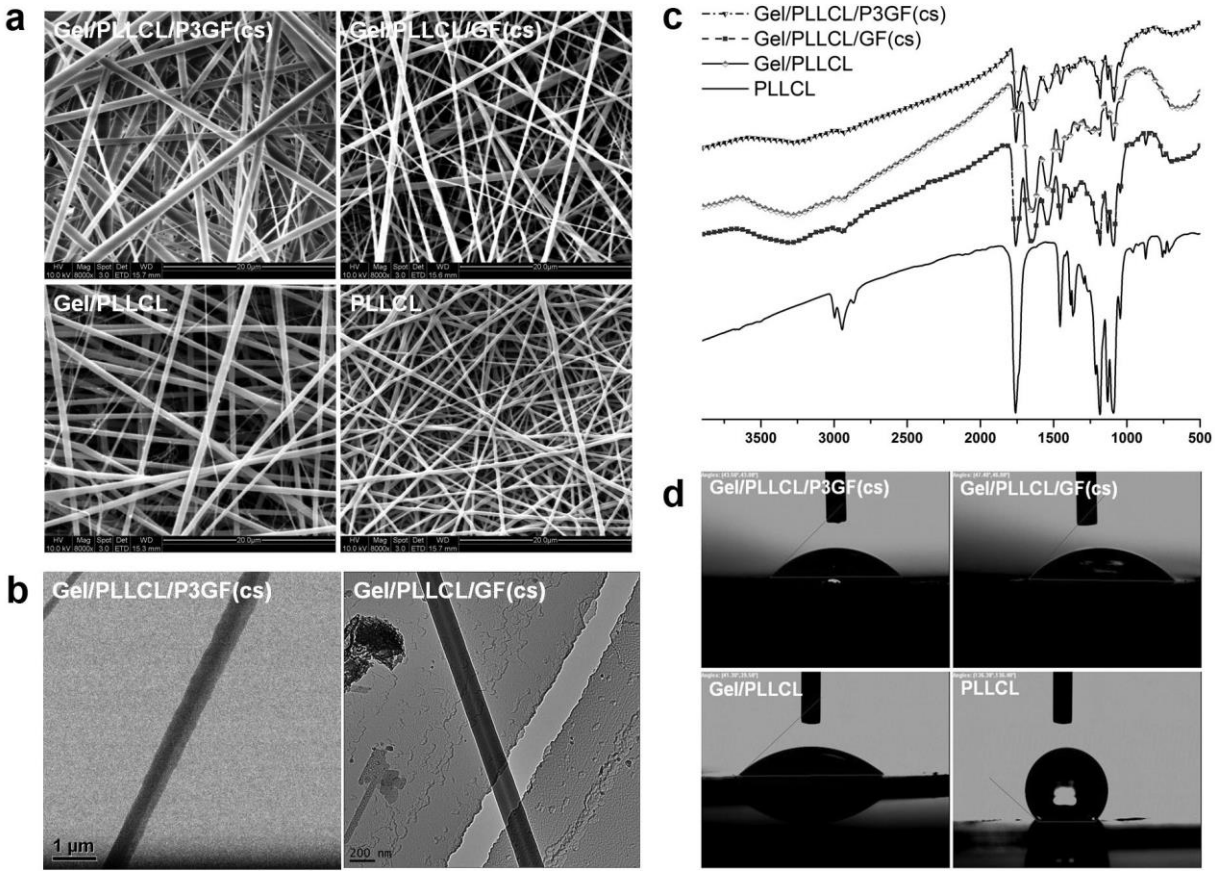

Fig. 6.1 Characterizations of electrospun nanofibers. a. SEM morphology of Gel/PLLCL/P3GF(cs), Gel/PLLCL/GF(cs) , Gel/PLLCL and PLLCL nanofibers. **b**. TEM morphology of core-shell nanofibers. **c**. FTIR spectra of Gel/PLLCL/P3GF(cs), Gel/PLLCL/GF(cs), Gel/PLLCL and PLLCL nanofibers. **d**. Water contact angle of electrospun nanofibers.

Uniform nanofibers of Gel/PLLCL/P3GF(cs), Gel/PLLCL/GF(cs), Gel/PLLCL and PLLCL with fiber diameters of 804 ± 264, 751 ± 171, 702 ± 105, 392 ± 47 nm were respectively, obtained. The TEM images (Fig. 6.1b) demonstrate the core-shell structure of Gel/PLLCL/P3GF(cs) and Gel/PLLCL/GF(cs) scaffolds. The dark gray colored P3HT

was clearly distinguishable from the shell (light gray) due to the high electron density of P3HT molecules. On the other hand, the TEM image of Gel/PLLCL/GF(cs) shows a reverse color distribution with light grey in the core and dark grey in the shell. Fourier transform infrared spectroscopy was applied to analyze functional groups present in nanofibers (Fig. 6.1c). Ester absorption peak at 1760 cm^{-1} was observed as the characteristic peak of PLLCL. Meanwhile peaks at 1097, 1133 and 1187 cm^{-1} were observed as the C-O-C stretching vibrations of PLLCL. Characteristic bands of gelatin were observed in Gel/PLLCL/P3GF(cs), Gel/PLLCL/GF(cs) and Gel/PLLCL scaffolds. Bands of amide group are present in the spectra of gelatin containing nanofibrous scaffolds. In addition to the characteristic peaks of PLLCL, carbonyl stretch and N–H bend coupled with a C–N stretch were observed at 1650 cm^{-1} and 1550 cm^{-1}, respectively. The water contact angle of pure PLLCL nanofibers was 136 ± 30, which reveals the highly hydrophobic property of PLLCL. However, the hydrophilicity of the Gel/PLLCL/P3GF(cs), Gel/PLLCL/GF(cs) and Gel/PLLCL nanofibers was greatly improved with incorporation of gelatin. The contact angle of Gel/PLLCL/P3GF(cs), Gel/PLLCL/GF(cs) and Gel/PLLCL was 43 ± 40, 45 ± 60 and 40 ± 20, respectively.

The stress-strain curves of the fibers are shown in Fig. 6.2. A linear segment up to the proportionality limit was observed for all scaffolds, followed by a non-linear curve. The changes of fiber arrangement in the mat under loaded stress were mainly attributed to this feature. It was demonstrated that fibers tend to align in the direction of applied force before getting thinner and finally the breaking occurred [223]. The elastic modulus of Gel/PLLCL/P3GF(cs), Gel/PLLCL/GF(cs), Gel/PLLCL and PLLCL nanofibers was 70.71 ± 2.62, 87.14 ± 3.37, 93.57 ± 5.28 and 29.75 ± 3.42 MPa, respectively. Table 6.1 summarizes the tensile properties of different electrospun nanofibers. Comparing the stress-strain curves of gelatin containing nanofibrous scaffolds with those of the stress-strain curve of PLLCL, we found that the incorporation of gelatin to PLLCL led to a significant increase in elastic modulus and decrease in ductility of Gel/PLLCL scaffolds.

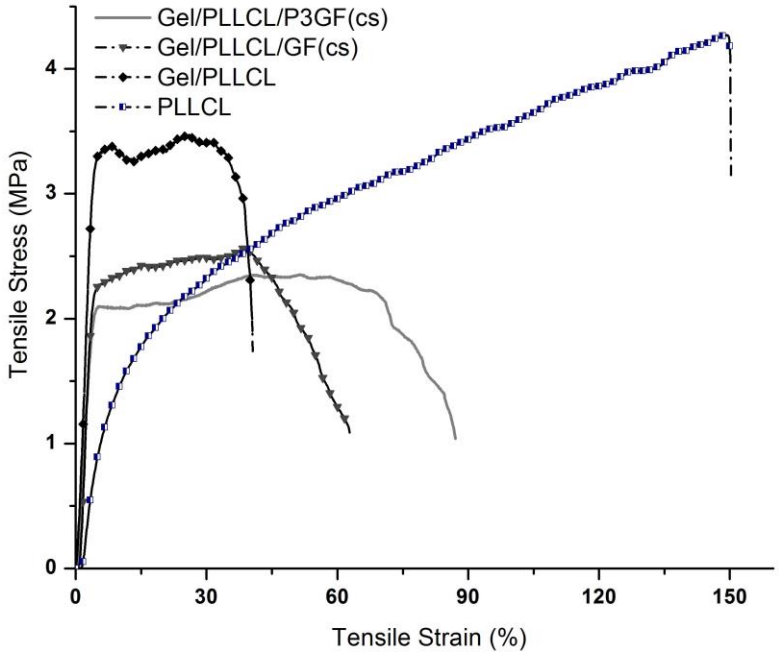

Fig. 6.2 Stress-strain curve of electrospun Gel/PLLCL/P3GF(cs), Gel/PLLCL/GF(cs), Gel/PLLCL and PLLCL nanofibers.

Table 6.1 Tensile properties of the electrospun nanofibers

Property	Gel/PLLCL/P3GF(cs)	Gel/PLLCL/GF(cs)	Gel/PLLCL	PLLCL
Elastic Modulus (MPa)	70.71 ± 2.62	87.14 ± 3.37	93.57 ± 5.28	29.75 ± 3.42
Tensile Stress (MPa)	2.33 ± 0.02	2.52 ± 0.03	3.40 ± 0.12	4.23 ± 0.03
Strain at break (%)	76.05 ± 8.78	46.14 ± 6.94	37.70 ± 3.07	149.13 ± 1.84

This is due to the influence of gelatin, introducing crystallinity to the gelatin containing scaffolds and the crystallinity of the electrospun nanofibers was found to strongly influence the mechanical properties of scaffolds [220-222]. Fibers with higher crystallinity are more likely to have higher molecular orientation which will result in higher resistance to axial tensile force [222] and hence the gelatin containing nanofibers had higher elastic modulus with low ductility. Among the gelatin containing scaffolds, Gel/PLLCL showed the highest ultimate tensile stress (followed by Gel/PLLCL/GF(cs) and Gel/PLLCL/P3GF(cs)). Wong et al. studied the effect of fiber diameter towards the tensile properties of electrospun fibers and they found that fiber diameter mainly affect tensile strength when the fiber diameter is less than ~700 nm [259]. Similarly our

Gel/PLLCL scaffold with the smallest diameter had the highest ultimate tensile stress. The elastic modulus of Gel/PLLCL/P3GF(cs) scaffold (70.71 ± 2.62 MPa) is comparable to the elastic modulus of human skin (15-150 MPa) (28). The tensile modules of Gel/PLLCL/P3GF(cs) provides the scaffold with good resilience and compliance as a skin graft, especially for flexible skin movement.

6.3.2 Light stimulative effect

Previously we have demonstrated that the photosensitive PCL/P3HT nanofibers promoted the proliferation of HDFs after light irradiation. The cell proliferation was greatly improved by the combination of light stimulation with assistance of photosensitive P3HT containing scaffolds [296]. However, due to the toxicity of P3HT, the proliferation of HDF on PCL/P3HT was extremely limited. In the current study, we encapsulated P3HT and EGF together within the Gel/PLLCL/P3GF(cs) core-shell nanofibers and studied the extend of cell proliferation under light stimulation and the results are given in Fig. 6.3. On day 6, the proliferation of HDFs on Gel/PLLCL/P3GF(cs) and Gel/PLLCL/GF(cs) was significantly higher compared to the cell proliferation on Gel/PLLCL and PLLCL nanofibrous scaffolds (under both light stimulated and dark conditions). This is because of the sustained release of EGF from core-shell nanofiber [298] and the released EGF helped to promote the proliferation of HDFs. EGF is known to promote the proliferation of various cell types and it has also been applied to skin wounds [299-301]. Matsumoto and Kuroyanagi designed a spongy sheet of hyaluronic acid containing EGF and evaluated its potential application in wound healing. They found that EGF in the wound dressing were sufficient to facilitate fibroblast proliferation and promote wound healing by inducing moderate inflammation [302]. At the same time, the proliferation of HDFs on stimulated Gel/PLLCL/P3GF(cs) was 1.6% higher compared to HDF proliferation on stimulated Gel/PLLCL/GF(cs). This higher amount of proliferation on stimulated Gel/PLLCL/P3GF(cs) is caused by the stimulative photosensitive effect of P3HT within the core of the fibers. Using Gel/PLLCL/P3GF(cs) as the substrate, we found higher proliferation (13.7%) of HDFs ($p \leq 0.05$) under stimulated conditions compared to cell proliferation in non-stimulated (NS) conditions after 9 days. Moreover, the proliferation of fibroblasts on Gel/PLLCL/P3GF(cs) was

found 3.4%, 28.2% and 51.8% ($p \leq 0.05$) higher than the cell growth on Gel/PLLCL/GF(cs), Gel/PLLCL and PLLCL, respectively under light stimulated conditions, (Fig. 6.3). From the obtained results, it was clear that the EGF mainly contributed towards the proliferation of HDFs and additionally the photosensitive P3HT under light radiation enhanced the ability of Gel/PLLCL/P3GF(cs) to promote the cell proliferation even better.

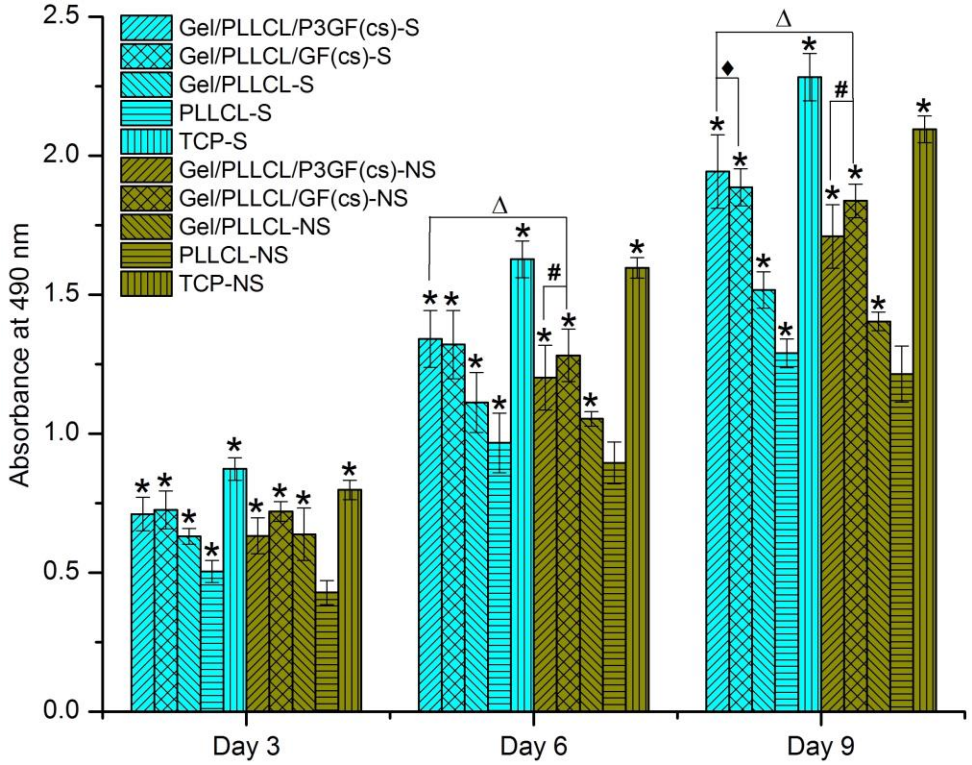

Fig. 6.3 HDF proliferation on electrospun Gel/PLLCL/P3GF(cs), Gel/PLLCL/GF(cs), Gel/PLLCL and PLLCL nanofibrous scaffolds stimulated (S) compared to HDF proliferation on electrospun Gel/PLLCL/P3GF(cs), Gel/PLLCL/GF(cs), Gel/PLLCL and PLLCL nanofibrous scaffolds non-stimulated (NS) by MTS assay. *Significant against cell proliferation on PLLCL (NS) at $p \leq 0.05$. $^{\Delta}$Significant against cell proliferation on Gel/PLLCL/P3GF(cs) (NS) and Gel/PLLCL/GF(cs) (NS) at $p \leq 0.05$. $^{\#}$Significant against cell proliferation on Gel/PLLCL/P3GF(cs) (NS) at $p \leq 0.05$.$^{\blacklozenge}$Significant against cell proliferation on Gel/PLLCL/GF(cs) (S) at $p \leq 0.05$.

6.3.3 *In vitro* wound healing

The potential application of Gel/PLLCL/P3GF(cs) nanofibrous scaffold for wound healing was evaluated using an *in vitro* wound model. As shown in Fig. 6.4, fibroblasts

under light stimulation migrated from the boundary of the wound towards the centre of the wound after 3 days and a few cells also showed elongated morphology towards wound. However, the migration of fibroblasts in the dark condition was limited and few cells showed elongated morphology, while most of the fibroblasts remained at the wound boundary. Cells could cover the entire surface of the stimulated Gel/PLLCL/P3GF(cs) nanofibrous scaffold in 9 days. In contrast, a void was observed after the same period of time for non-stimulated scaffold (red arrows).

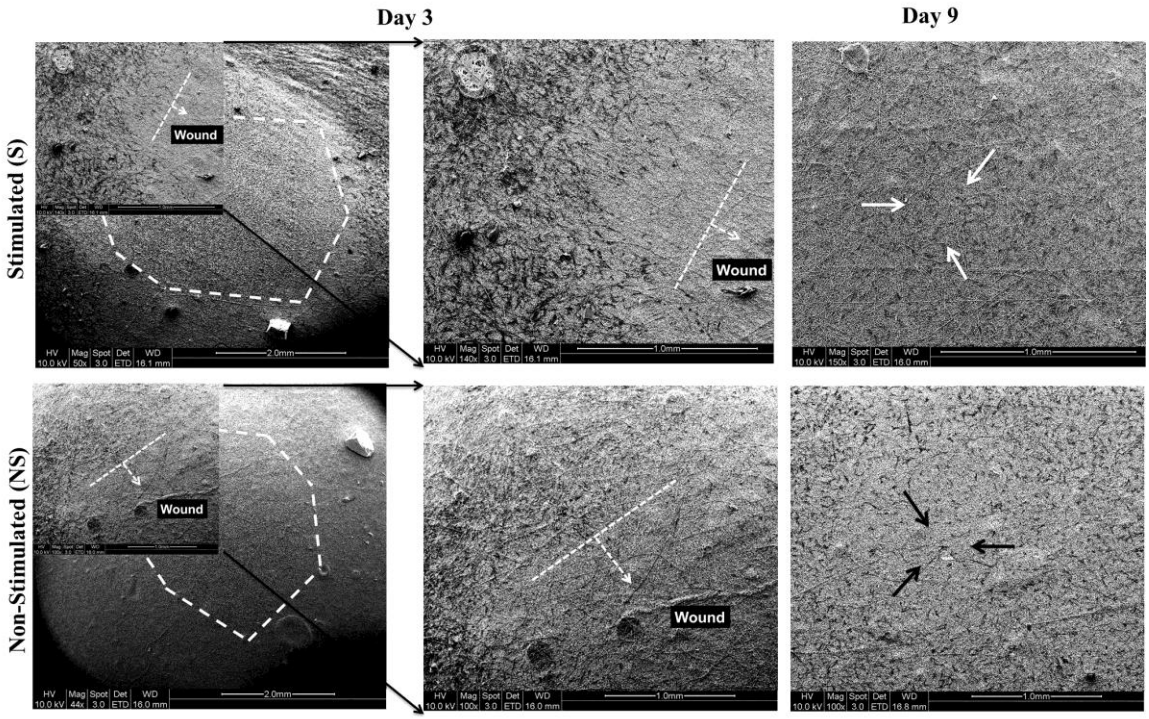

Fig. 6.4 *In vitro* wound healing on stimulated and non-stimulated Gel/PLLCL/P3GF(cs) nanofibrous scaffold for 9 days.

The faster wound healing on Gel/PLLCL/P3GF(cs) under light stimulation could be due to the higher cell proliferation on this scaffold under light irradiation as obvious from the results of the cell proliferation study. Higher number of fibroblasts on the stimulated Gel/PLLCL/P3GF(cs) improves the efficacy of cell communication. Moreover, the shell portion of the nanofibers (Gelatin/PLLCL) provided hydrophilicity to the scaffolds, and it could assist in cell communication via promoting the circulation of bioactive molecules, thereby enabling faster wound closure. When light irradiated on the wound site of

Gel/PLLCL/P3GF(cs) fibers, electrons were generated by the core P3HT polymer molecules and when the electrons flow in the same direction, an electrical current was generated [134, 296]. Meanwhile, an electrical field gets created which guide the fibroblasts in migrating towards the wound site. Studies performed by Zhao and Nishimura et al. utilizing keratinocytes and corneal epithelial cells, were also found to migrate directionally towards the cathode in an electrical field as low as ~25 mV/mm [121, 303]. Our *in vitro* wound healing result suggests that Gel/PLLCL/P3GF(cs) nanofibers could be applied as a wound healing graft for preclinical studies.

6.3.4 Epidermal differentiation of ASCs on photosensitive core-shell nanofibers

With the success of using the EGF and P3HT containing scaffolds for HDF proliferation, the epidermal differentiation capacity of ASCs was performed on electrospun Gel/PLLCL/P3GF(cs) and Gel/PLLCL/GF(cs) nanofibrous scaffolds for a period of 15 days (Fig. 6.5). ASCs are a heterogeneous group of multipotent progenitor cells that can be readily derived from adipose tissue of adult humans in very large quantities by lipoaspiration [304] and the isolation of ASCs yields higher amount of stem cells, that are required for most of the stem cell-based therapies or accompanied tissue regeneration [262]. ASCs are multipotent stem cells and can differentiate into adipogenic, osteogenic, chondrogenic and myogenic cell lineages [160, 305]. Here we studied the plasticity of ASCs towards epidermal cell lineages on electrospun nanofibers. The epidermal differentiation capacity of ASCs on EGF incorporated Gel/PLLCL/P3GF(cs) and Gel/PLLCL/GF(cs) core-shell nanofibrous scaffolds were studied under light stimulation after 15 days and analyzed by immunostaining studies. Cells were stained for ASC-specific marker CD 105 and early epidermal differentiation marker Ker 10. The distinguishable phenotypical features of keratinocyte-like cells were observed on Gel/PLLCL/P3GF (cs) under light stimulation (highlighted with red boundary in Fig. 6.5). However, ASCs on Gel/PLLCL/GF(cs) nanofibers and non-stimulated Gel/PLLCL/P3GF (cs) showed undifferentiated fibroblastic morphology (Fig. 6.5).

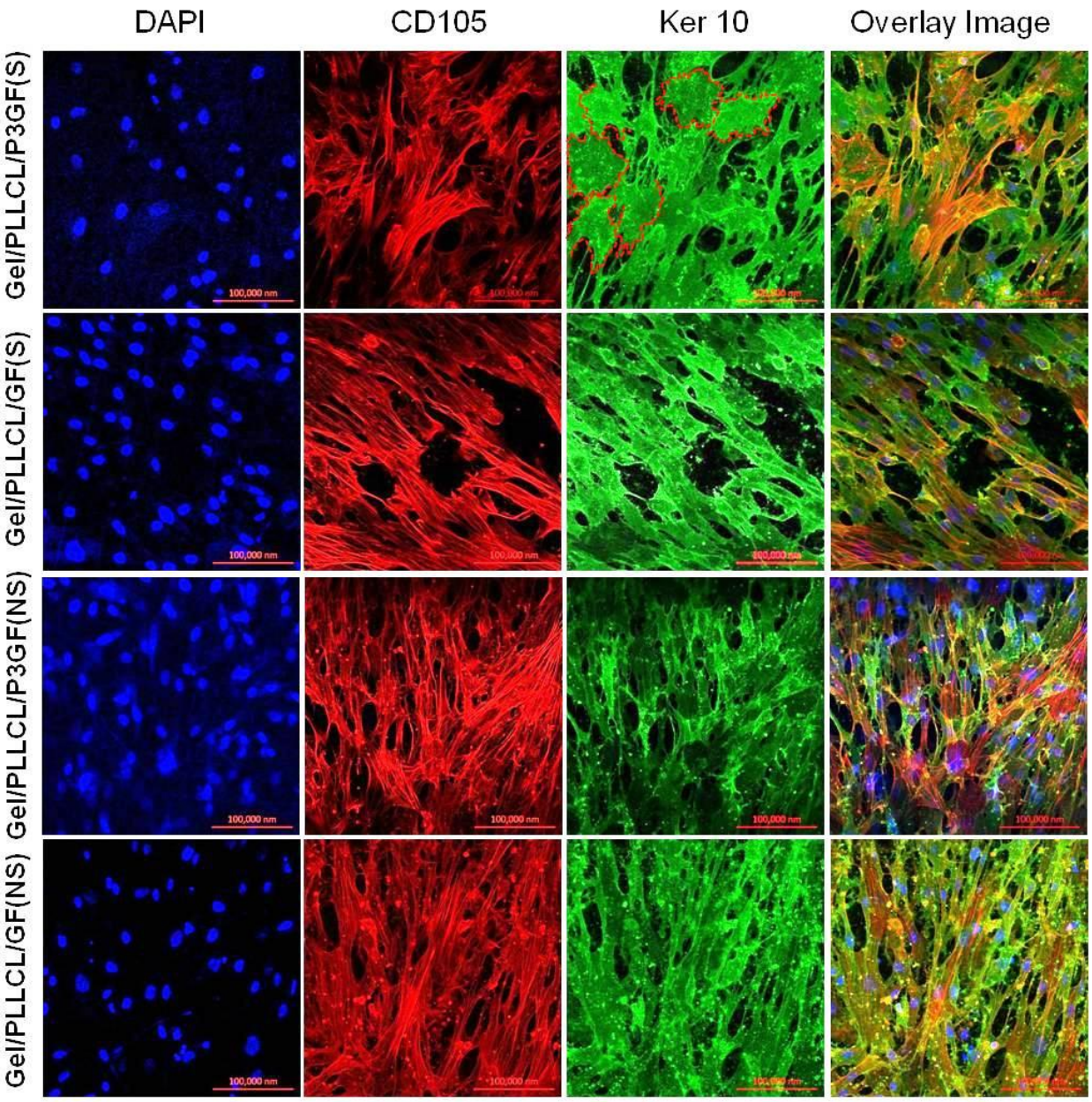

Fig. 6.5 Dual immunocytochemical analysis for the expression of Ker 10, CD 105 and merged image showing the dual expression of both CD 105 and Ker 10 on stimulated Gel/PLLCL/P3GF(cs), Gel/PLLCL/GF(cs) nanofibers and non-stimulated Gel/PLLCL/P3GF(cs), Gel/PLLCL/GF(cs) nanofibers at 20 × magnification.

Adamskaya and colleagues [116] found that blue light significantly influenced wound healing based on rat animal models. The keratin-10 mRNA level of the rats irradiated with blue (470 nm) and red (629 nm) LED was significantly elevated compared to control. Meanwhile, Liebmann et al. found that blue LED up to 453 nm induced differentiation of

primary keratinocytes [39]. Keratinocytes are produced in the deepest layer of the epidermis (basal layer) during cell division and they are carried towards the skin surface. In the meantime, they undergo a complex series of morphological and biochemical changes known as keratinocyte differentiation [53]. Results of their study demonstrated that the irradiated primary keratinocytes significantly increased the mRNA levels of involucrin by up to threefold relative to the non-irradiated control. Involucrin is increasingly expressed by differentiating keratinocytes and it is a marker of keratinocyte terminal differentiation [306]. Recently, Arai and colleagues investigated the keratinocyte differentiation under mono-directional pulsed electric stimulation. Cultured keratinocytes were exposed to an electric field of 3 V (ca. 100 mV/mm) or 5 V (ca. 166 mV/mm) at a frequency of 4,800 Hz for 5 min a day for a period of 5 days. They found that the expression of mRNAs encoding keratinocyte differentiation markers such as keratin 10, involucrin, transglutaminase 1, and filaggrin was significantly increased in response to the 5 V stimulation [307]. Both light and electrical stimulation were shown to promote the differentiation of keratinocyte. Similarly the epidermal differentiation of ASCs on the stimulated Gel/PLLCL/P3GF(cs) might have been induced by the sustained release of EGF and photosensitive ability of Gel/PLLCL/P3GF(cs) nanofibrous scaffold. Our immunocytochemical results proved that the electrospun Gel/PLLCL/P3GF(cs) under light stimulation could act as a suitable substrate for epidermal differentiation of ASCs. The studies open up new opportunities for transplantation of wound healing mediators containing nanofibrous scaffold as skin graft for skin tissue engineering.

6.4 Conclusion

EGF incorporated Gel/PLLCL nanofibers were prepared by core-shell spinning, either alone or with additional incorporation of a photosensitive polymer P3HT, within Gel/PLLCL nanofibers by coaxial electrospinning. Fibroblast proliferation was significantly improved with incorporation of EGF; while P3HT assist the proliferation of fibroblast on Gel/PLLCL/P3GF(cs) nanofibers under light stimulation. Moreover, the stimulated Gel/PLLCL/P3GF(cs) was found to accelerate the *in vitro* wound healing. The effect of the photosensitive Gel/PLLCL/P3GF(cs) on epidermal differentiation of ASCs was further explored and keratinocyte-like cells were only found on the stimulated

Gel/PLLCL/P3GF(cs) scaffolds. We propose here that the biomimetic and photosensitive Gel/PLLCL/P3GF(cs) nanofibers could be a novel scaffold that could be applied in photocurrent therapy for wound healing and skin construction.

Chapter 7

Conclusions and Recommendations

The scope of this research encompasses the fabrication of cost-effective NFS for *in vivo* wound healing, and the *in vitro* differentiation of human ASCs into epidermal lineage under an artificial skin-specific environment constructed by multiple EIF encapsulated core-shell NFS. In addition, the potential application of photosensitive P3HT containing NFS for skin tissue engineering was study. The final product is a biomimetic and photosensitve core-shell NSF/ASCs composite for skin graft application. This product has shown superior effects on promoting cell proliferation, differentiation and *in vitro* wound healing.

7.1 Main conclusions

- The epidermal differentiation potential of stem cells was confirmed and achieved by manipulating the biochemical cues combined with the environmental and physical factors of culture substrate (NFS). We found that the regional differentiation was greatly reduced by using electrospun NFS as a substrate instead of such differentiations on TCP.

- The electrospun Gel/PLLCL(60) nanofibers which had sufficient mechanical properties in both dry and wet conditions, along with the highest cell proliferation was the optimized NFS for skin tissue engineering. The capability of Gel/PLLCL(60) in promoting wound healing was confirmed in a mouse model. *In vivo* wounds treated with NFS complete closure within 14 dyas and 4 days earlier than the control groups.

- The core-shell structured NFS, which encapsulated multiple EIF, achieved

sustained release without burst release. The expression of early and intermediate epidermal differentiation markers was observed by performing the differentiation of ASCs to epidermal lineages on the core-shell NFS. With sustained release of EIF from core-shell NFS, the percentage of epidermally differentiated ASCs on core-shell nanofibers was significantly higher (62%) than that on EIF blended NFS (43%).

- Photosensitive P3HT containing nanofibrous scaffolds were fabricated by electrospinning. Fibroblast proliferation on PCL, PCL/P3HT(2), PCL/P3HT(10) and PCL/P3HT(20) nanofibrous scaffolds under light stimulation was studied and the results of our study suggest that fibroblasts cultured on PCL/P3HT(10) after light stimulation had better proliferation and morphology than fibroblasts cultured on electrospun PCL, PCL/P3HT(2) and PCL/P3HT(20) nanofibers. Electrospun PCL/P3HT(10) nanofibrous scaffold was capable of supporting cell proliferation and favoring cell ECM secretion.

- The feasibility of EGF and P3HT encapsulated core-shell NFS as skin graft was confirmed. Fibroblast proliferation was significantly improved with incorporation of EGF; while P3HT assist the proliferation of fibroblast on Gel/PLLCL/P3GF(cs) nanofibers under light stimulation. Moreover, the stimulated Gel/PLLCL/P3GF(cs) was found to accelerate the *in vitro* wound healing. The effect of the photosensitive Gel/PLLCL/P3GF(cs) on epidermal differentiation of ASCs was further explored and keratinocyte-like cells were only found on the stimulated Gel/PLLCL/P3GF(cs) scaffolds.

7.2 Recommendations for future work

The biomimetic and photosensitive core-shell NFS described herein has showed promising results in promoting ASCs epidermal differentiation and *in vitro* wound healing. Further study on the capability of NFS/ASCs composite *in vivo* wound healing is needed to be evaluated in anmal model. Moreover, investigations are required to understand the growth factor and gene expression profiles of ASCs under *in vivo*

wounding environment as well as to identify the functions of differentiated ASCs within wounding milieu and the underlying molecular mechanisms of ASCs transdifferentiation.

Uniaxially aligned arrays of nanofibers can be electrospun under certain conditions such as use of an air-gap collector or a mandrel rotating at a high speed [308, 309]. Aligned core-shell NFS which includes growth factors and photosensitive polymer could be more efficient in promoting cell proliferation and migration compared to the random NFS. The photocurrent generated in aligned nanofibers is uniaxial and this uniaxial photocurrent will promoted cell migration along the direction of the electrical field to accelerate wound healing [121]. Furthermore, radially aligned nanofibers can be electrospun by utilizing a collector composed of a central point electrode and a peripheral ring electrode [310]. The photosensitive core-shell NFS constructed with radially aligned nanofibers could promote cell migration from the surrounding tissue to the center of a defect and shorten the time for healing and regeneration of wound.

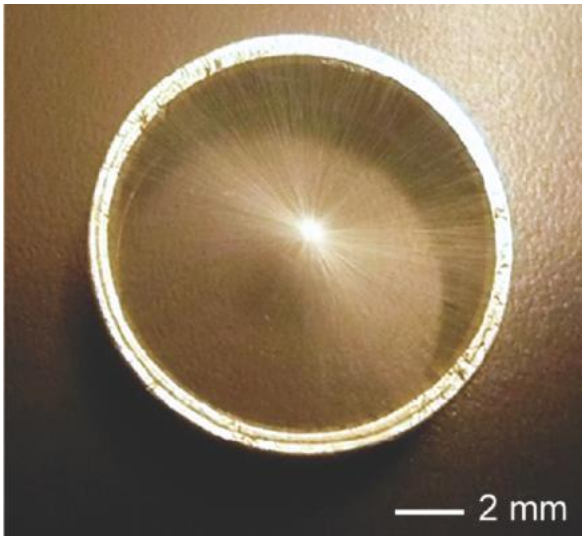

Fig. 7.1 Photograph of a scaffold of radically aligned nanofibers directly deposited on the ring collector [310].

The main advantage of the electrospun fibrous scaffold is the ability to mimic the native ECM of human skin, due to its fibrous structure, suitable mechanical properties and the ability in incorporating bioactive factors (e.g., growth factors). Moreover, the flexibility of the scaffold makes it can easily integrate with the skin wound. However, the high cost,

short-term shelf-time and complexity in using still impede the wide applications as tissue engineered scaffold. As a result, more studies are expected to address these issues of current tissue engineered scaffolds.

Reference

[1] Groeber F, Holeiter M, Hampel M, Hinderer S, Schenke-Layland K. Skin tissue engineering - In vivo and in vitro applications. Advanced Drug Delivery Reviews. 2011;63:352-66.
[2] Supp DM, Boyce ST. Engineered skin substitutes: practices and potentials. Clinics in Dermatology. 2005;23:403-12.
[3] Yildirimer L, Thanh NTK, Seifalian AM. Skin regeneration scaffolds: a multimodal bottom-up approach. Trends in Biotechnology. 2012;30:638-48.
[4] Jones I, Currie L, Martin R. A guide to biological skin substitutes. British journal of plastic surgery. 2002;55:185-93.
[5] Bottcher-Haberzeth S, Biedermann T, Reichmann E. Tissue engineering of skin. Burns. 2010;36:450-60.
[6] Metcalfe AD, Ferguson MWJ. Bioengineering skin using mechanisms of regeneration and repair. Biomaterials. 2007;28:5100-13.
[7] Chiang B, Essick E, Ehringer W, Murphree S, Hauck MA, Li M, et al. Enhancing skin wound healing by direct delivery of intracellular adenosine triphosphate. American Journal of Surgery. 2007;193:213-8.
[8] Song C, Chua A. Epidemiology of burn injuries in Singapore from 1997 to 2003. Burns. 2005;31:S18-S26.
[9] Wu X-W, Herndon DN, Spies M, Sanford AP, Wolf SE. Effects of delayed wound excision and grafting in severely burned children. Archives of Surgery. 2002;137:1049-54.
[10] Klingenberg JM, McFarland KL, Friedman AJ, Boyce ST, Aronow BJ, Supp DM. Engineered human skin substitutes undergo large-scale genomic reprogramming and normal skin-like maturation after transplantation to athymic mice. Journal of Investigative Dermatology. 2009;130:587-601.
[11] Martins-Green M, Bissell MJ. Cell-ECM interactions in development. Seminars in Developmental Biology. 1995;6:149-59.
[12] Patel S, Kurpinski K, Quigley R, Gao H, Hsiao BS, Poo M-M, et al. Bioactive nanofibers: Synergistic effects of nanotopography and chemical signaling on cell guidance. Nano Letters. 2007;7:2122-8.
[13] Huebsch N, Mooney DJ. Inspiration and application in the evolution of biomaterials. Nature. 2009;462:426-32.
[14] Murugan R, Huang ZM, Yang F, Ramakrishna S. Nanofibrous scaffold engineering using electrospinning. Journal of Nanoscience and Nanotechnology. 2007;7:4595-603.
[15] Hromadka M, Collins JB, Reed C, Han L, Kolappa KK, Cairns BA, et al. Nanofiber applications for burn care. J Burn Care Res. 2008;29:695-703.
[16] Venugopal J, Low S, Choon AT, Ramakrishna S. Interaction of cells and nanofiber scaffolds in tissue engineering. Journal of Biomedical Materials Research Part B: Applied Biomaterials. 2008;84B:34-48.
[17] Zhang YZ, Su B, Venugopal J, Ramakrishna S, Lim CT. Biomimetic and bioactive nanofibrous scaffolds from electrospun composite nanofibers. International Journal of Nanomedicine. 2007;2:623-38.

[18] Rho KS, Jeong L, Lee G, Seo BM, Park YJ, Hong SD, et al. Electrospinning of collagen nanofibers: Effects on the behavior of normal human keratinocytes and early-stage wound healing. Biomaterials. 2006;27:1452-61.
[19] Zhang YZ, Venugopal J, Huang ZM, Lim CT, Ramakrishna S. Characterization of the surface biocompatibility of the electrospun PCL-Collagen nanofibers using fibroblasts. Biomacromolecules. 2005;6:2583-9.
[20] Choi JS, Lee SJ, Christ GJ, Atala A, Yoo JJ. The influence of electrospun aligned poly(epsilon-caprolactone)/collagen nanofiber meshes on the formation of self-aligned skeletal muscle myotubes. Biomaterials. 2008;29:2899-906.
[21] Bigi A, Cojazzi G, Panzavolta S, Roveri N, Rubini K. Stabilization of gelatin films by crosslinking with genipin. Biomaterials. 2002;23:4827-32.
[22] Zhang YZ, Venugopal J, Huang ZM, Lim CT, Ramakrishna S. Crosslinking of the electrospun gelatin nanofibers. Polymer. 2006;47:2911-7.
[23] Panzavolta S, Gioffrè M, Focarete ML, Gualandi C, Foroni L, Bigi A. Electrospun gelatin nanofibers: Optimization of genipin cross-linking to preserve fiber morphology after exposure to water. Acta Biomaterialia. 2011;7:1702-9.
[24] Su Y, Su Q, Liu W, Lim M, Venugopal JR, Mo X, et al. Controlled release of bone morphogenetic protein 2 and dexamethasone loaded in core–shell PLLACL–collagen fibers for use in bone tissue engineering. Acta Biomaterialia. 2012;8:763-71.
[25] Medrado ARAP, Pugliese LS, Reis SRA, Andrade ZA. Influence of low level laser therapy on wound healing and its biological action upon myofibroblasts. Lasers in Surgery and Medicine. 2003;32:239-44.
[26] Whelan HT, Smits RL, Buchman EV, Whelan NT, Turner SG, Margolis DA, et al. Effect of NASA light-emitting diode irradiation on wound healing. Journal of Clinical Laser Medicine & Surgery. 2001;19:305-14.
[27] Kipshidze N, Nikolaychik V, Keelan MH, Shankar LR, Khanna A, Kornowski R, et al. Low-power helium: neon laser irradiation enhances production of vascular endothelial growth factor and promotes growth of endothelial cells in vitro. Lasers Surg Med. 2001;28:355-64.
[28] Reddy GK, Stehno-Bittel L, Enwemeka CS. Laser photostimulation accelerates wound healing in diabetic rats. Wound Repair and Regeneration. 2001;9:248-55.
[29] Kesava Reddy G. Comparison of the photostimulatory effects of visible He-Ne and infrared Ga-As lasers on healing impaired diabetic rat wounds. Lasers in Surgery and Medicine. 2003;33:344-51.
[30] Petrofsky J, Lawson D, Prowse M, Suh HJ. Effects of a 2-, 3- and 4-electrode stimulator design on current dispersion on the surface and into the limb during electrical stimulation in controls and patients with wounds. Journal of Medical Engineering & Technology. 2008;32:485-97.
[31] Im MJ, Lee WPA, Hoopes JE. Effect of electrical stimulation on survival of skin flaps in pigs. Physical Therapy. 1990;70:37-40.
[32] Stromberg BV. Effects of electrical currents on wound contraction. Annals of Plastic Surgery. 1988;21:121-3.
[33] Alvarez OM, Mertz PM, Smerbeck RV, Eaglstein WH. The healing of superficial skin wounds is stimulated by external electrical current. J Investig Dermatol. 1983;81:144-8.
[34] Cruz NI, Bayrón FE, Suárez AJ. Accelerated healing of full-thickness burns by the

use of high-voltage pulsed galvanic stimulation in the pig. Annals of Plastic Surgery. 1989;23:49-55.
[35] Puissant B, Barreau C, Bourin P, Clavel C, Corre J, Bousquet C, et al. Immunomodulatory effect of human adipose tissue-derived adult stem cells: comparison with bone marrow mesenchymal stem cells. British Journal of Haematology. 2005;129:118-29.
[36] Yañez R, Lamana ML, García-Castro J, Colmenero I, Ramírez M, Bueren JA. Adipose tissue-derived mesenchymal stem cells have in vivo immunosuppressive properties applicable for the control of the graft-versus-host disease. Stem Cells. 2006;24:2582-91.
[37] Zhu Y, Liu T, Song K, Fan X, Ma X, Cui Z. Adipose-derived stem cell: a better stem cell than BMSC. Cell Biochemistry and Function. 2008;26:664-75.
[38] Cianfarani F, Toietta G, Di Rocco G, Cesareo E, Zambruno G, Odorisio T. Diabetes impairs adipose tissue–derived stem cell function and efficiency in promoting wound healing. Wound Repair and Regeneration. 2013;21:545-53.
[39] Gimble JM, Guilak F. Adipose-derived adult stem cells: isolation, characterization, and differentiation potential. Cytotherapy. 2003;5:362-9.
[40] Oedayrajsingh-Varma M, van Ham S, Knippenberg M, Helder M, Klein-Nulend J, Schouten T, et al. Adipose tissue-derived mesenchymal stem cell yield and growth characteristics are affected by the tissue-harvesting procedure. Cytotherapy. 2006;8:166-77.
[41] Lee RH, Kim B, Choi I, Kim H, Choi H, Suh K, et al. Characterization and expression analysis of mesenchymal stem cells from human bone marrow and adipose tissue. Cellular Physiology and Biochemistry. 2004;14:311-24.
[42] Kim W-S, Park B-S, Sung J-H, Yang J-M, Park S-B, Kwak S-J, et al. Wound healing effect of adipose-derived stem cells: A critical role of secretory factors on human dermal fibroblasts. Journal of Dermatological Science. 2007;48:15-24.
[43] Margorie F. Yang VVT, Anna N. Yaroslavsky. Principles of light-Skin interactions. In: Baron ED, editor. Light-Based Therapies for skin of color. New York: Springer; 2009.
[44] Madison KC. Barrier function of the skin: "La Raison d'Etre" of the epidermis. J Investig Dermatol. 2003;121:231-41.
[45] Guan CP, Zhou MN, Xu AE, Kang KF, Liu JF, Wei XD, et al. The skin: an indispensable barrier. Experimental Dermatology. 2008;17:1059-62.
[46] MacNeil S. Progress and opportunities for tissue-engineered skin. Nature. 2007;445:874-80.
[47] Gawkrodger DJ. Dermatology: An Illustrated Colour Text. In: Horne T, editor. Dermatology: An Illustrated Colour Text: Churchill Livingstone; 2002. p. 2-3.
[48] Graham-Brown R, Burns T. Lecture Notes: Dermatology. In: Graham-Brown R, Burns T, editors. Lecture Notes: Dermatology: Blackwell; 2007. p. 1-9.
[49] Streilein JW, Bergstresser PR. Langerhans cells: Antigen presenting cells of the epidermis. Immunobiology. 1984;168:285-300.
[50] Jones P, Simons BD. OPINIONEpidermal homeostasis: do committed progenitors work while stem cells sleep? Nat Rev Mol Cell Biol. 2008;9:82-8.
[51] Alonso L, Fuchs E. Stem cells of the skin epithelium. Proceedings of the National Academy of Sciences of the United States of America. 2003;100:11830-5.
[52] Hudson DL. Keratins as markers of epithelial cells. In: Wise C, editor. Epithelial

Cell Culture Protocols, Methods in Molecular Biology: Humana Press 2002. p. 157-68.
[53] Proksch E, Brandner JM, Jensen J-M. The skin: an indispensable barrier. Experimental Dermatology. 2008;17:1063-72.
[54] Carroll JM, Albers KM, Garlick JA, Harrington R, Taichman LB. Tissue- and stratum-specific expression of the human involucrin promoter in transgenic mice. Proceedings of the National Academy of Sciences. 1993;90:10270-4.
[55] Simon M. The epidermal cornified envelope and its precursors. In: Leigh IM, Lane EB, Watt FM, editors. The Keratinocyte Handbook: Cambridge University Press 1994. p. 275-92.
[56] Mitsiadis TA, Barrandon O, Rochat A, Barrandon Y, De Bari C. Stem cell niches in mammals. Experimental Cell Research. 2007;313:3377-85.
[57] Guo S, DiPietro LA. Factors affecting wound healing. Journal of Dental Research. 2010;89:219-29.
[58] Gosain A, DiPietro LA. Aging and wound healing. World J Surg. 2004;28:321-6.
[59] Broughton G, Janis JE, Attinger CE. The basic science of wound healing. Plastic and Reconstructive Surgery. 2006;117:12S-34S.
[60] Campos AC, Groth AK, Branco AB. Assessment and nutritional aspects of wound healing. Current Opinion in Clinical Nutrition & Metabolic Care. 2008;11:281-8.
[61] Hübner G, Brauchle M, Smola H, Madlener M, Fässler R, Werner S. Differentiatial regulation of pro-inflammatory cytokines druing wound healing in normal and glucocorticoid-treated mice. Cytokine. 1996;8:548-56.
[62] Opalenik SR, Davidson JM. Fibroblast differentiation of bone marrow-derived cells during wound repair. The FASEB Journal. 2005.
[63] Mast BA. The skin. In: Cohen IK, Diegelmann RF, Lindblad WJ, editors. Wound healing: biochemical & clinical aspects. Philadelphia, PA, USA,: W.B. Saunders Company; 1992. p. 344.
[64] Diegelmann RF, Evans MC. Wound healing: an overview of acute, fibrotic and delayed healing. Front Biosci. 2004;9:283-9.
[65] Shevchenko RV, James SL, James SE. A review of tissue-engineered skin bioconstructs available for skin reconstruction. Journal of The Royal Society Interface. 2010;7:229-58.
[66] Sen CK, Gordillo GM, Roy S, Kirsner R, Lambert L, Hunt TK, et al. Human skin wounds: A major and snowballing threat to public health and the economy. Wound Repair and Regeneration. 2009;17:763-71.
[67] Atiyeh B, Gunn SW, Hayek S. State of the art in burn treatment. World J Surg. 2005;29:131-48.
[68] Nwomeh BC, Liang H-X, Diegelmann RF, Cohen IK, Yager DR. Dynamics of the matrix metalloproteinases MMP-1 and MMP-8 in acute open human dermal wounds. Wound Repair and Regeneration. 1998;6:127-34.
[69] Nwomeh BC, Liang HX, Cohen IK, Yager DR. MMP-8 is the predominant collagenase in healing wounds and nonhealing ulcers. The Journal of surgical research. 1999;81:189-95.
[70] Yager DR, Zhang L-Y, Liang H-X, Diegelmann RF, Cohen IK. Wound fluids from human pressure ulcers contain elevated matrix metalloproteinase levels and activity compared to surgical wound fluids. Journal of Investigative Dermatology. 1996;107:743-8.

[71] Robson MC, Mustoe TA, Hunt TK. The future of recombinant growth factors in wound healing. The American Journal of Surgery. 1998;176:80S-2S.
[72] Falanga V. Growth factors and wound healing. Dermatol Clin. 1993;11:667-75.
[73] Papini R. Management of burn injuries of various depths. BMJ. 2004;329:158-60.
[74] Andreassi A, Bilenchi R, Biagioli M, D'Aniello C. Classification and pathophysiology of skin grafts. Clinics in Dermatology. 2005;23:332-7.
[75] Eisenbud D, Huang NF, Luke S, Siberklang M. Skin substitutes and wound healing: current status and challenges. Wounds. 2004;16:2-17.
[76] Metcalfe AD, Ferguson MWJ. Tissue engineering of replacement skin: the crossroads of biomaterials, wound healing, embryonic development, stem cells and regeneration. Journal of The Royal Society Interface. 2007;4:413-37.
[77] Hrabchak C, Flynn L, Woodhouse KA. Biological skin substitutes for wound cover and closure. Expert Review of Medical Devices. 2006;3:373-85.
[78] Griffiths M, Livingstone R, Price R, Navsaria H. Survival of Apligraf in acute human wounds. Tissue Engineering. 2004;10:1180-95.
[79] Eaglstein WH, Alvarez OM, Auletta M, Leffel D, Rogers GS, Zitelli JA, et al. Acute excisional wounds treated with a tissue-engineered skin (Apligraf). Dermatologic Surgery. 1999;25:195-201.
[80] Ehrenreich M, Ruszczak Z. Update on tissue-engineered biological dressings. Tissue Engineering. 2006;12:2407-24.
[81] Clark RAF, Ghosh K, Tonnesen MG. Tissue engineering for cutaneous wounds. Journal of Investigative Dermatology. 2007;127:1018-29.
[82] Xiao yl, Riesle J, Blitterswijk CAV. Static and dynamic fibroblast seeding and cultivation in porous PEO/PBT scaffolds. Journal of Materials Science: Materials in Medicine. 1999;10:773-7.
[83] El Ghalbzouri A, Lamme EN, van Blitterswijk C, Koopman J, Ponec M. The use of PEGT/PBT as a dermal scaffold for skin tissue engineering. Biomaterials. 2004;25:2987-96.
[84] Yannas IV, Burke JF. Design of an artificial skin. I. Basic design principles. Journal of Biomedical Materials Research. 1980;14:65-81.
[85] Anthony ET, Syed M, Myers S, Moir G, Navsaria H. The development of novel dermal matrices for cutaneous wound repair. Drug Discovery Today: Therapeutic Strategies. 2006;3:81-6.
[86] Kim PJ, Dybowski KS, Steinberg JS. A closer look at bioengieered alternative tissues. Podiatry Today. 2006;19:38-55.
[87] Hansbrough JF, Doré C, Hansbrough WB. Clinical trials of a living dermal tissue replacement placed beneath meshed, split-thickness skin grafts on excised burn wounds. Journal of Burn Care & Research. 1992;13:519-29.
[88] Pham C, Greenwood J, Cleland H, Woodruff P, Maddern G. Bioengineered skin substitutes for the management of burns: A systematic review. Burns. 2007;33:946-57.
[89] Horch RE, Kopp J, Kneser U, Beier J, Bach AD. Tissue engineering of cultured skin substitutes. Journal of Cellular and Molecular Medicine. 2005;9:592-608.
[90] Moustafa M, Simpson C, Glover M, Dawson RA, Tesfaye S, Creagh FM, et al. A new autologous keratinocyte dressing treatment for non-healing diabetic neuropathic foot ulcers. Diabetic Medicine. 2004;21:786-9.
[91] Clark RAF, Ghosh K, Tonnesen MG. Tissue Engineering for Cutaneous Wounds. J

Invest Dermatol. 2007;127:1018-29.
[92] Nunery WR. Risk of prion transmission with the use of xenografts and allografts in surgery. Ophthalmic Plastic & Reconstructive Surgery. 2001;17:389-94.
[93] Enoch S, Shaaban H, Dunn KW. Informed consent should be obtained from patients to use products (skin substitutes) and dressings containing biological material. Journal of Medical Ethics. 2005;31:2-6.
[94] Yu W, Naim JO, Lanzafame RJ. Effects of photostimulation on wound healing in diabetic mice. Lasers in Surgery and Medicine. 1997;20:56-63.
[95] Hopkins JT, McLoda TA, Seegmiller JG, Baxter GD. Low-level laser therapy facilitates superficial wound healing in humans: a triple-blind, sham-controlled study. J Athl Train. 2004;39:223-9.
[96] Maiya GA, Kumar P, Rao L. Effect of low intensity helium-neon (He-Ne) laser irradiation on diabetic wound healing dynamics. Photomedicine and Laser Surgery. 2005;23:187-90.
[97] Mendez T, Pinheiro ALB, Pacheco MTT, Nascimento PM, Ramalho LMP. Dose and wavelength of laser light have influence on the repair of cutaneous wounds. Journal of Clinical Laser Medicine & Surgery. 2004;22:19-25.
[98] Bisht D, Mehrotra R, Singh PA, Atri SC, Kumar A. Effect of helium-neon laser on wound healing. Indian journal of experimental biology. 1999;37:187-9.
[99] Lyons RF, Abergel RP, White RA, Dwyer RM, Castel JC, Uitto J. Biostimulation of wound healing in vivo by a helium-neon laser. Annals of Plastic Surgery. 1987;18:47-50.
[100] Hemvani N, Chitnis DS, Bhagwanani NS. Effect of helium-neon laser on cultured human macrophages. Laser Ther. 1998;10:159-64.
[101] Agaiby A, Ghali L, Dyson M. Laser modulation of T-lymphocyte proliferation in vitro. . Laser Ther. 1998;10:153-8.
[102] Hrnjak M, Kuljić-Kapulica N, Budisin A, Giser A. Stimulatory effect of low-power density He-Ne laser radiation on human fibroblasts in vitro. Vojnosanit Pregl. 1995;52:539-46.
[103] Yu H-S, Chang K-L, Yu C-L, Chen J-W, Chen G-S. Low-energy helium-neon laser irradiation stimulates interleukin-1[agr] and interleukin-8 release from cultured human keratinocytes. J Investig Dermatol. 1996;107:593-6.
[104] Horwitz LR, Burke TJ, Carnegie D. Augmentation of wound healing using monochromatic infrared energy: Exploration of a new technology for wound management. . Adv Wound Care. 1999;12:35-40.
[105] Karu TI, Piatibrat LV, Kalendo GS, Serebriakov NG. Changes in the amount of ATP in HeLa cells under the action of He-Ne laser radiation. Biulleten' eksperimental'noi biologii i meditsiny. 1993;115:617-8.
[106] Morimoto Y, Aral T, Kikuchi M, Nakajima S, Nakamura H. Effect of low-intensity argon laser irradiation on mitochondrial respiration. Lasers in Surgery and Medicine. 1994;15:191-9.
[107] Funk JO, Kruse A, Kirchner H. Cytokine production after helium-neon laser irradiation in cultures of human peripheral blood mononuclear cells. Journal of Photochemistry and Photobiology B: Biology. 1992;16:347-55.
[108] Pourreau-Schneider N, Ahmed A, Soudry M, Jacquemier J, Kopp F, Franquin JC, et al. Helium-neon laser treatment transforms fibroblasts into myofibroblasts. . Am J Pathol. 1990;137:171-8.

[109] Lam TS, Abergel RP, Meeker CA, Castel JC, Dwyer RM, Uitto J. Laser stimulation of collagen synthesis in human skin fibroblast cultures. Lasers Life Sci. 1986;1:61-77.
[110] Karu T. Photobiology of low-power laser effects. Health Phys. 1989;56:691-704.
[111] Damante C, Micheli G, Miyagi S, Feist I, Marques M. Effect of laser phototherapy on the release of fibroblast growth factors by human gingival fibroblasts. Lasers Med Sci. 2009;24:885-91.
[112] Fujisawa K, Miyamoto Y, Nagayama M. Basic fibroblast growth factor and epidermal growth factor reverse impaired ulcer healing of the rabbit oral mucosa. Journal of Oral Pathology & Medicine. 2003;32:358-66.
[113] de Sousa APC, Santos JN, dos Reis JA, Ramos TA, de Souza J, Cangussu MCT, et al. Effect of LED phototherapy of three distinct wavelengths on fibroblasts on wound healing: A histological study in a rodent model. Photomedicine and Laser Surgery. 2010;28:547-52.
[114] Tada K, Ikeda K, Tomita K. Effect of polarized light emitting diode irradiation on wound healing. The Journal of Trauma and Acute Care Surgery. 2009;67:1073-9.
[115] Erdle BJ, Brouxhon S, Kaplan M, Vanbuskirk J, Pentland AP. Effects of continuous-wave (670-nm) red light on wound healing. Dermatologic Surgery. 2008;34:320-5.
[116] Adamskaya N, Dungel P, Mittermayr R, Hartinger J, Feichtinger G, Wassermann K, et al. Light therapy by blue LED improves wound healing in an excision model in rats. Injury. 2011;42:917-21.
[117] Vinck EM, Cagnie BJ, Cornelissen MJ, Declercq HA, Cambier DC. Increased fibroblast proliferation induced by light emitting diode and low power laser irradiation. Lasers Med Sci. 2003;18:95-9.
[118] Al-Watban FAH, Andres BL. Polychromatic LED in oval full-thickness wound healing in non-diabetic and diabetic rats. Photomedicine and Laser Surgery. 2006;24:10-6.
[119] McCaig CD, Rajnicek AM, Song B, Zhao M. Controlling cell behavior electrically: Current views and future potential. Physiological Reviews. 2005;85:943-78.
[120] Foulds IS, Barker AT. Human skin battery potentials and their possible role in wound healing. British Journal of Dermatology. 1983;109:515-22.
[121] Zhao M, Song B, Pu J, Wada T, Reid B, Tai G, et al. Electrical signals control wound healing through phosphatidylinositol-3-OH kinase-[gamma] and PTEN. Nature. 2006;442:457-60.
[122] Huo R, Ma Q, Wu JJ, Chin-Nuke K, Jing Y, Chen J, et al. Noninvasive electromagnetic fields on keratinocyte growth and migration. Journal of Surgical Research. 2010;162:299-307.
[123] Quattrini C, Jeziorska M, Malik RA. Small fiber neuropathy in diabetes: Clinical consequence and assessment. The International Journal of Lower Extremity Wounds. 2004;3:16-21.
[124] Lee PY, Chesnoy S, Huang L. Electroporatic delivery of TGF-b1 gene works synergistically with electric therapy to enhance diabetic wound healing in db/db mice. Journal of Investigative Dermatology. 2004;123:791-8.
[125] Thawer HA, Houghton PE. Effects of electrical stimulation on the histological properties of wounds in diabetic mice. Wound Repair and Regeneration. 2001;9:107-15.
[126] Petrofsky JS, Lawson D, Berk L, Suh H. Enhanced healing of diabetic foot ulcers

using local heat and electrical stimulation for 30 min three times per week. Journal of Diabetes. 2010;2:41-6.
[127] Houghton PE, Kincaid CB, Lovell M, Campbell KE, Keast DH, Woodbury MG, et al. Effect of electrical stimulation on chronic leg ulcer size and appearance. Physical Therapy. 2003;83:17-28.
[128] Karba R, Šemrov D, Vodovnik L, Benko H, Sˇavrin R. DC electrical stimulation for chronic wound healing enhancement Part 1. Clinical study and determination of electrical field distribution in the numerical wound model. Bioelectrochemistry and Bioenergetics. 1997;43:265-70.
[129] Stefanovska A, Vodovnik L, Benko H, Turk R. Treatment of chronic wounds by means of electric and electromagnetic fields. Med Biol Eng Comput. 1993;31:213-20.
[130] Morris K, McGee M, Jasper J, Bogie K. Evaluation of electrical stimulation for ischemic wound therapy: a feasibility study using the lapine wound model. Arch Dermatol Res. 2009;301:323-7.
[131] Goudarzi I, Hajizadeh S, Salmani ME, Abrari K. Pulsed electromagnetic fields accelerate wound healing in the skin of diabetic rats. Bioelectromagnetics. 2010;31:318-23.
[132] Young S, Hampton S, Tadej M. Study to evaluate the effect of low-intensity pulsed electrical currents on levels of oedema in chronic non-healing wounds. J Wound Care. 2011;20:368, 70-73.
[133] Vanhaesebroeck B. Charging the batteries to heal wounds through PI3K. Nat Chem Biol. 2006;2:453-5.
[134] Jin G, Prabhakaran MP, Liao S, Ramakrishna S. Photosensitive materials and potential of photocurrent mediated tissue regeneration. Journal of Photochemistry and Photobiology B: Biology. 2011;102:93-101.
[135] Reya T, Morrison SJ, Clarke MF, Weissman IL. Stem cells, cancer, and cancer stem cells. Nature. 2001;414:105-11.
[136] Bajada S, Mazakova I, Richardson JB, Ashammakhi N. Updates on stem cells and their applications in regenerative medicine. Journal of Tissue Engineering and Regenerative Medicine. 2008;2:169-83.
[137] Thomson JA, Itskovitz-Eldor J, Shapiro SS, Waknitz MA, Swiergiel JJ, Marshall VS, et al. Embryonic stem cell lines derived from human blastocysts. Science. 1998;282:1145-7.
[138] Martin GR. Isolation of a pluripotent cell line from early mouse embryos cultured in medium conditioned by teratocarcinoma stem cells. Proceedings of the National Academy of Sciences. 1981;78:7634-8.
[139] Cowan CM, Shi Y-Y, Aalami OO, Chou Y-F, Mari C, Thomas R, et al. Adipose-derived adult stromal cells heal critical-size mouse calvarial defects. Nat Biotech. 2004;22:560-7.
[140] Rodbell M. The Metabolism of Isolated Fat Cells: IV. Regulation of release of protein by lipolytic hormones and insulin. Journal of Biological Chemistry. 1966;241:3909-17.
[141] Rodbell M. Metabolism of Isolated Fat Cells: II. The similar effects of phospholipase c (Clostridium perfringens α toxin) and of insulin on glucose and amino acid metabolism. Journal of Biological Chemistry. 1966;241:130-9.
[142] Van RLR, Bayliss CE, Roncari DAK. Cytological and enzymological

characterization of adult human adipocyte precursors in culture. Journal of Clinical Investigation. 1976;58:699-704.
[143] Björntorp P, Karlsson M, Pertoft H, Pettersson P, Sjöström L, Smith U. Isolation and characterization of cells from rat adipose tissue developing into adipocytes. Journal of Lipid Research. 1978;19:316-24.
[144] Deslex S, Negrel R, Vannier C, Etienne J, Ailhaud G. Differentiation of human adipocyte precursors in a chemically defined serum-free medium. International Journal of Obesity. 1987;11:19-27.
[145] Hauner H, Wabitsch M, Pfeiffer EF. Differentiation of adipocyte precursor cells from obese and nonobese adult women and from different adipose tissue sites. Hormone and metabolic research Supplement series. 1988;19:35-9.
[146] Aust L, Devlin B, Foster SJ, Halvorsen YDC, Hicok K, du Laney T, et al. Yield of human adipose-derived adult stem cells from liposuction aspirates. Cytotherapy. 2004;6:7-14.
[147] Zuk PA, Zhu M, Ashjian P, De Ugarte DA, Huang JI, Mizuno H, et al. Human adipose tissue is a source of multipotent stem cells. Molecular Biology of the Cell. 2002;13:4279-95.
[148] Kristine MS, Henry ER. Stem cell therapy for neurologic disorders: Therapeutic potential of adipose-derived stem cells. Current Drug Targets. 2005;6:57-62.
[149] Katz AJ, Tholpady A, Tholpady SS, Shang H, Ogle RC. Cell surface and transcriptional characterization of human adipose-derived adherent stromal (hADAS) cells. Stem Cells. 2005;23:412-23.
[150] McIntosh K, Zvonic S, Garrett S, Mitchell JB, Floyd ZE, Hammill L, et al. The immunogenicity of human adipose-derived cells: Temporal changes in vitro. Stem Cells. 2006;24:1246-53.
[151] Pittenger MF, Mackay AM, Beck SC, Jaiswal RK, Douglas R, Mosca JD, et al. Multilineage potential of adult human mesenchymal stem cells. Science. 1999;284:143-7.
[152] Gimble JM, Katz AJ, Bunnell BA. Adipose-derived stem cells for regenerative medicine. Circulation Research. 2007;100:1249-60.
[153] Huang JI, Beanes SR, Zhu M, Lorenz PH, Hedrick MH, Benhaim P. Rat extramedullary adipose tissue as a source of osteochondrogenic progenitor cells. Plastic and Reconstructive Surgery. 2002;109:1033-41.
[154] Hicok KC, Du Laney TV, Zhou YS, Halvorsen YDC, Hitt DC, Cooper LF, et al. Human adipose-derived adult stem cells produce osteoid in vivo. Tissue Engineering. 2004;10:371-80.
[155] Winter A, Breit S, Parsch D, Benz K, Steck E, Hauner H, et al. Cartilage-like gene expression in differentiated human stem cell spheroids: A comparison of bone marrow–derived and adipose tissue–derived stromal cells. Arthritis & Rheumatism. 2003;48:418-29.
[156] Dragoo JL, Samimi B, Zhu M, Hame SL, Thomas BJ, Lieberman JR, et al. Tissue-engineered cartilage and bone using stem cells from human infrapatellar fat pads. Journal of Bone & Joint Surgery, British Volume. 2003;85-B:740-7.
[157] Miranville A, Heeschen C, Sengenès C, Curat CA, Busse R, Bouloumié A. Improvement of postnatal neovascularization by human adipose tissue-derived stem cells. Circulation. 2004;110:349-55.
[158] Ebrahimian TG, Pouzoulet F, Squiban C, Buard V, André M, Cousin B, et al. Cell

therapy based on adipose tissue-derived stromal cells promotes physiological and pathological wound healing. Arteriosclerosis, Thrombosis, and Vascular Biology. 2009;29:503-10.
[159] Nie C, Yang D, Xu J, Si Z, Jin X, Zhang J. Locally administered adipose-derived stem cells accelerate wound healing through differentiation and vasculogenesis. Cell Transplantation. 2011;20:205-16.
[160] Bunnell BA, Flaat M, Gagliardi C, Patel B, Ripoll C. Adipose-derived stem cells: Isolation, expansion and differentiation. Methods. 2008;45:115-20.
[161] Meruane MA, Rojas M, Marcelain K. The use of adipose tissue-derived stem cells within a dermal substitute improves skin regeneration by increasing neoangiogenesis and collagen synthesis. Plast Reconstr Surg. 2012;130:53-63.
[162] Davis GB, Ragina NP, Lee SH, Nguyen DT, Hill CK, Senagore AJ, et al. Abstract 12: Adipose Derived Stem Cell Therapy Rescues Delayed Wound Healing in Chronic Radiation Injury. Plastic and Reconstructive Surgery.130.
[163] Nambu M, Kishimoto S, Nakamura S, Mizuno H, Yanagibayashi S, Yamamoto N, et al. Accelerated wound healing in healing-impaired db/db mice by autologous adipose tissue-derived stromal cells combined with atelocollagen matrix. Annals of Plastic Surgery. 2009;62:317-21.
[164] Kadler KE, Holmes DF, Trotter JA, Chapman JA. Collagen fibril formation. Biochemical Journal. 1996;316:1-11.
[165] Krishnan J, Kotaki M, Yanzhong Z, Xiumei M, Ramakrishna S. Recent advances in polymer nanofibers. Journal of Nanoscience and Nanotechnology. 2004;4:52-65.
[166] Zhang S. Fabrication of novel biomaterials through molecular self-assembly. Nat Biotech. 2003;21:1171-8.
[167] Ma ZW, Kotaki M, Inai R, Ramakrishna S. Potential of nanofiber matrix as tissue-engineering scaffolds. Tissue Engineering. 2005;11:101-9.
[168] Greiner A, Wendorff JH. Electrospinning: A fascinating method for the preparation of ultrathin fibers. Angewandte Chemie International Edition. 2007;46:5670-703.
[169] Deitzel JM, Kleinmeyer JD, Hirvonen JK, Beck Tan NC. Controlled deposition of electrospun poly(ethylene oxide) fibers. Polymer. 2001;42:8163-70.
[170] Fong H, Reneker DH. Electrospinning and formation of nanofibers. In: Salem DR, editor. Structure formation in polymeric fibers. Munich: Hanser; 2001. p. 225-46.
[171] Murugan R, Ramakrishna S. Design strategies of tissue engineering scaffolds with controlled fiber orientation. Tissue Engineering. 2007;13:1845-66.
[172] Zeleny J. The electrical discharge from liquid points, and a hydrostatic method of measuring the electric intensity at their surfaces. Physical Review. 1914;3:69-91.
[173] Dhandayuthapani B, Krishnan UM, Sethuraman S. Fabrication and characterization of chitosan-gelatin blend nanofibers for skin tissue engineering. Journal of Biomedical Materials Research Part B: Applied Biomaterials. 2010;94B:264-72.
[174] Han I, Shim KJ, Kim JY, Im SU, Sung YK, Kim M, et al. Effect of poly(3-hydroxybutyrate-co-3-hydroxyvalerate) nanofiber matrices cocultured with hair follicular epithelial and dermal cells for biological wound dressing. Artificial Organs. 2007;31:801-8.
[175] Sethuraman S, Nair LS, El-Amin S, Nguyen M-T, Singh A, Greish YE, et al. Development and characterization of biodegradable nanocomposite injectables for orthopaedic applications based on polyphosphazenes. Journal of Biomaterials Science,

Polymer Edition. 2011;22:733-52.
[176] Jin G, Prabhakaran MP, Ramakrishna S. Stem cell differentiation to epidermal lineages on electrospun nanofibrous substrates for skin tissue engineering. Acta Biomaterialia. 2011;7:3113-22.
[177] Ma K, Liao S, He LM, Lu J, Ramakrishna S, Chan CK. Effects of nanofiber/stem cell composite on wound healing in acute full-thickness skin wounds. Tissue Engineering Part A. 2011;17:1413-24.
[178] Wnek GE, Carr ME, Simpson DG, Bowlin GL. Electrospinning of nanofiber fibrinogen structures. Nano Letters. 2002;3:213-6.
[179] Kang M, Jung R, Kim H-S, Youk JH, Jin H-J. Silver nanoparticles incorporated electrospun silk fibers. Journal of Nanoscience and Nanotechnology. 2007;7:3888-91.
[180] Catherine PB, Matthew JS, Gary LB, Scott AS, Teresa T, Jamil AM, et al. Feasibility of electrospinning the globular proteins hemoglobin and myoglobin. Journal of Engineered Fibers and Fabrics. 2006;1:16-29.
[181] Khil M-S, Cha D-I, Kim H-Y, Kim I-S, Bhattarai N. Electrospun nanofibrous polyurethane membrane as wound dressing. Journal of Biomedical Materials Research Part B: Applied Biomaterials. 2003;67B:675-9.
[182] Chen G, Ushida T, Tateishi T. Scaffold design for tissue engineering. Macromolecular Bioscience. 2002;2:67-77.
[183] Katti DS, Lakshmi S, Langer R, Laurencin CT. Toxicity, biodegradation and elimination of polyanhydrides. Advanced Drug Delivery Reviews. 2002;54:933-61.
[184] Kolambkar YM, Peister A, Ekaputra AK, Hutmacher DW, Guldberg RE. Colonization and osteogenic differentiation of different stem cell sources on electrospun nanofiber meshes. Tissue Engineering Part A. 2010;16:3219-30.
[185] Ma J, He X, Jabbari E. Osteogenic differentiation of marrow stromal cells on random and aligned electrospun poly(l-lactide) nanofibers. Annals of Biomedical Engineering. 2011;39:14-25.
[186] Mukherjee S, Reddy Venugopal J, Ravichandran R, Ramakrishna S, Raghunath M. Evaluation of the biocompatibility of PLACL/Collagen nanostructured matrices with cardiomyocytes as a model for the regeneration of infarcted myocardium. Advanced Functional Materials. 2011;21:2291-300.
[187] Nair LS, Laurencin CT. Biodegradable polymers as biomaterials. Progress in Polymer Science. 2007;32:762-98.
[188] Grijpma DW, Pennings AJ. (Co)polymers of L-lactide, 2. Mechanical properties. Macromol Chem Phys. 1994;195:1649-63.
[189] Yan S, Xiaoqiang L, Lianjiang T, Chen H, Xiumei M. Poly(l-lactide-co-ε-caprolactone) electrospun nanofibers for encapsulating and sustained releasing proteins. Polymer. 2009;50:4212-9.
[190] Dai NT, Williamson MR, Khammo N, Adams EF, Coombes AGA. Composite cell support membranes based on collagen and polycaprolactone for tissue engineering of skin. Biomaterials. 2004;25:4263-71.
[191] Chong EJ, Phan TT, Lim IJ, Zhang YZ, Bay BH, Ramakrishna S, et al. Evaluation of electrospun PCL/gelatin nanofibrous scaffold for wound healing and layered dermal reconstitution. Acta Biomaterialia. 2007;3:321-30.
[192] Jeong SI, Lee A-Y, Lee YM, Shin H. Electrospun gelatin/poly(L-lactide-co-ε-caprolactone) nanofibers for mechanically functional

tissue-engineering scaffolds. Journal of Biomaterials Science, Polymer Edition. 2008;19:339-57.
[193] Monaco JL, Lawrence WT. Acute wound healing an overview. Clin Plast Surg 2003;30:1-2.
[194] Rho KS, Jeong L, Lee G, Seo B-M, Park YJ, Hong S-D, et al. Electrospinning of collagen nanofibers: Effects on the behavior of normal human keratinocytes and early-stage wound healing. Biomaterials. 2006;27:1452-61.
[195] Zhang Y, Ouyang H, Lim CT, Ramakrishna S, Huang Z-M. Electrospinning of gelatin fibers and gelatin/PCL composite fibrous scaffolds. Journal of Biomedical Materials Research Part B: Applied Biomaterials. 2005;72B:156-65.
[196] Kim SE, Heo DN, Lee JB, Kim JR, Park SH, Jeon S, et al. Electrospun gelatin/polyurethane blended nanofibers for wound healing. Biomedical Materials. 2009;4.
[197] Kang YO, Yoon I-S, Lee SY, Kim D-D, Lee SJ, Park WH, et al. Chitosan-coated poly(vinyl alcohol) nanofibers for wound dressings. Journal of Biomedical Materials Research Part B: Applied Biomaterials. 2010;92B:568-76.
[198] Schneider A, Wang XY, Kaplan DL, Garlick JA, Egles C. Biofunctionalized electrospun silk mats as a topical bioactive dressing for accelerated wound healing. Acta Biomaterialia. 2009;5:2570-8.
[199] Choi JS, Choi SH, Yoo HS. Coaxial electrospun nanofibers for treatment of diabetic ulcers with binary release of multiple growth factors. Journal of Materials Chemistry. 2011;21:5258-67.
[200] Zhang Q, Sun Y, Xu W, Zhu D. Thermoelectric energy from flexible P3HT films doped with a ferric salt of triflimide anions. Energy & Environmental Science. 2012;5:9639-44.
[201] Manceau M, Rivaton A, Gardette J-L, Guillerez S, Lemaître N. The mechanism of photo- and thermooxidation of poly(3-hexylthiophene) (P3HT) reconsidered. Polymer Degradation and Stability. 2009;94:898-907.
[202] Lee Y, Russell TP, Jo WH. Synthesis and photovoltaic properties of low-bandgap alternating copolymers consisting of 3-hexylthiophene and [1,2,5]thiadiazolo[3,4-g]quinoxaline derivatives. Organic Electronics. 2010;11:846-53.
[203] Souto Maior RM, Hinkelmann K, Eckert H, Wudl F. Synthesis and characterization of two regiochemically defined poly(dialkylbithiophenes): A comparative study. Macromolecules. 1990;23:1268-79.
[204] Sirringhaus H, Tessler N, Friend RH. Integrated optoelectronic devices based on conjugated polymers. Science. 1998;280:1741-4.
[205] Yaszemski MJ, Payne RG, Hayes WC, Langer R, Mikos AG. Evolution of bone transplantation: molecular, cellular and tissue strategies to engineer human bone. Biomaterials. 1996;17:175-85.
[206] Kumbar SG, James R, Nukavarapu SP, Laurencin CT. Electrospun nanofiber scaffolds: engineering soft tissues. Biomedical Materials. 2008;3.
[207] Bhattarai N, Edmondson D, Veiseh O, Matsen FA, Zhang M. Electrospun chitosan-based nanofibers and their cellular compatibility. Biomaterials. 2005;26:6176-84.
[208] Dieckmann C, Renner R, Milkova L, Simon JC. Regenerative medicine in dermatology: biomaterials, tissue engineering, stem cells, gene transfer and beyond.

Experimental Dermatology. 2010;19:697-706.
[209] Lin J, Li C, Zhao Y, Hu J, Zhang L-M. Co-electrospun Nanofibrous Membranes of Collagen and Zein for Wound Healing. ACS Applied Materials & Interfaces. 2012;4:1050-7.
[210] Kim G, Ahn S, Kim Y, Cho Y, Chun W. Coaxial structured collagen-alginate scaffolds: fabrication, physical properties, and biomedical application for skin tissue regeneration. Journal of Materials Chemistry. 2011;21:6165-72.
[211] Liu SJ, Kau YC, Chou CY, Chen JK, Wu RC, Yeh WL. Electrospun PLGA/collagen nanofibrous membrane as early-stage wound dressing. Journal of Membrane Science. 2010;355:53-9.
[212] Balin A, Vilenchik M. Connective tissue. . In: Schulz R, Noelker L, Rockwood K, Sprott R, editors. The Encyclopedia of aging. New York: Springer; 2006. p. 260-1.
[213] Heo DN, Yang DH, Lee JB, Bae MS, Kim JH, Moon SH, et al. Burn-wound healing effect of gelatin/polyurethane nanofiber scaffold containing silver-sulfadiazine. Journal of Biomedical Nanotechnology. 2013;9:511-5.
[214] Lee SJ, Oh SH, Liu J, Soker S, Atala A, Yoo JJ. The use of thermal treatments to enhance the mechanical properties of electrospun poly(ε-caprolactone) scaffolds. Biomaterials. 2008;29:1422-30.
[215] Baguneid MS, Seifalian AM, Salacinski HJ, Murray D, Hamilton G, Walker MG. Tissue engineering of blood vessels. British Journal of Surgery. 2006;93:282-90.
[216] Mano JF, Silva GA, Azevedo HS, Malafaya PB, Sousa RA, Silva SS, et al. Natural origin biodegradable systems in tissue engineering and regenerative medicine: present status and some moving trends. Journal of The Royal Society Interface. 2007;4:999-1030.
[217] Jena A, Gupta K. Characterization of pore structure of filtration media. Fluid/Part Sep J. 2002;14:227-41.
[218] Li D, Frey MW, Joo YL. Characterization of nanofibrous membranes with capillary flow porometry. J Memb Sci. 2006;286:104-14.
[219] Drury JL, Mooney DJ. Hydrogels for tissue engineering: scaffold design variables and applications. Biomaterials. 2003;24:4337-51.
[220] Linh NTB, Min YK, Song H-Y, Lee B-T. Fabrication of polyvinyl alcohol/gelatin nanofiber composites and evaluation of their material properties. Journal of Biomedical Materials Research Part B: Applied Biomaterials. 2010;95B:184-91.
[221] Liu Y, Pellerin C. Highly oriented electrospun fibers of self-assembled inclusion complexes of poly(ethylene oxide) and urea. Macromolecules. 2006;39:8886-8.
[222] Lim CT, Tan EPS, Ng SY. Effects of crystalline morphology on the tensile properties of electrospun polymer nanofibers. Applied Physics Letters. 2008;92:141908--3.
[223] Lu J-W, Zhang Z-P, Ren X-Z, Chen Y-Z, Yu J, Guo Z-X. High-elongation fiber mats by electrospinning of polyoxymethylene. Macromolecules. 2008;41:3762-4.
[224] Bottino MC, Thomas V, Janowski GM. A novel spatially designed and functionally graded electrospun membrane for periodontal regeneration. Acta Biomaterialia. 2011;7:216-24.
[225] Kwon IK, Kidoaki S, Matsuda T. Electrospun nano- to microfiber fabrics made of biodegradable copolyesters: structural characteristics, mechanical properties and cell adhesion potential. Biomaterials. 2005;26:3929-39.
[226] Christopherson GT, Song H, Mao H-Q. The influence of fiber diameter of

electrospun substrates on neural stem cell differentiation and proliferation. Biomaterials. 2009;30:556-64.
[227] Burridge K, Fath K, Kelly T, Nuckolls G, Turner C. Focal adhesions: transmembrane junctions between the extracellular matrix and the cytoskeleton. Annu Rev Cell Biol. 1988;4:487-525.
[228] Barnes MJ, Morton LF, Bennett RC, Bailey AJ, Sims TJ. Presence of type III collagen in guinea-pig dermal scar. Biochem J. 1976;157:263-6.
[229] Jin G, Prabhakaran MP, Kai D, Annamalai SK, Arunachalam KD, Ramakrishna S. Tissue engineered plant extracts as nanofibrous wound dressing. Biomaterials. 2013;34:724-34.
[230] Jayakumar R, Prabaharan M, Sudheesh Kumar PT, Nair SV, Tamura H. Biomaterials based on chitin and chitosan in wound dressing applications. Biotechnology Advances. 2011;29:322-37.
[231] Charernsriwilaiwat N, Opanasopit P, Rojanarata T, Ngawhirunpat T. Lysozyme-loaded, electrospun chitosan-based nanofiber mats for wound healing. International Journal of Pharmaceutics. 2012;427:379-84.
[232] Hettiaratchy S, Dziewulski P. Introduction. BMJ. 2004;328:1366-8.
[233] Torpy JM, Lynm C, Glass RM. Burn Injuries. JAMA: The Journal of the American Medical Association. 2009;302:1828.
[234] Siemionow M, Zor F. Burn reconstruction — Future perspectives: Facial transplantation
Handbook of Burns. In: Kamolz L-P, Jeschke MG, Horch RE, Küntscher M, Brychta P, editors.: Springer Vienna; 2012. p. 303-9.
[235] Shakespeare P. Burn wound healing and skin substitutes. Burns. 2001;27:517-22.
[236] Hutchinson RW, Broughton D, Barbolt TA, Poandl T, Muench T, Rockar R, et al. Hemostatic effectiveness of fibrin pad after prtial nephrectomy in swine. Journal of Surgical Research. 2011;167:e291-e8.
[237] Ma K, Laco F, Ramakrishna S, Liao S, Chan CK. Differentiation of bone marrow-derived mesenchymal stem cells into multi-layered epidermis-like cells in 3D organotypic coculture. Biomaterials. 2009;30:3251-8.
[238] Burdick JA, Murphy WL. Moving from static to dynamic complexity in hydrogel design. Nat Commun. 2012;3:1269.
[239] Behm B, Babilas P, Landthaler M, Schreml S. Cytokines, chemokines and growth factors in wound healing. Journal of the European Academy of Dermatology and Venereology. 2012;26:812-20.
[240] Barrandon Y, Green H. Cell migration is essential for sustained growth of keratinocyte colonies: The roles of transforming growth factor-± and epidermal growth factor. Cell. 1987;50:1131-7.
[241] Knauer DJ, Wiley HS, Cunningham DD. Relationship between epidermal growth factor receptor occupancy and mitogenic response. Quantitative analysis using a steady state model system. Journal of Biological Chemistry. 1984;259:5623-31.
[242] Pierre EJ, Barrow RE, Hawkins HK, Nguyen TT, Sakurai Y, Desai M, et al. Effects of Insulin on Wound Healing. The Journal of Trauma and Acute Care Surgery. 1998;44:342-5.
[243] Formanek M, Millesi W, Willheim M, Scheiner O, Kornfehl J. Optimized growth medium for primary culture of human oral keratinocytes. International Journal of Oral

and Maxillofacial Surgery. 1996;25:157-60.
[244] Brzoska M, Geiger H, Gauer S, Baer P. Epithelial differentiation of human adipose tissue-derived adult stem cells. Biochemical and Biophysical Research Communications. 2005;330:142-50.
[245] Meng ZX, Xu XX, Zheng W, Zhou HM, Li L, Zheng YF, et al. Preparation and characterization of electrospun PLGA/gelatin nanofibers as a potential drug delivery system. Colloids and Surfaces B: Biointerfaces. 2011;84:97-102.
[246] Sill TJ, von Recum HA. Electrospinning: Applications in drug delivery and tissue engineering. Biomaterials. 2008;29:1989-2006.
[247] Gandhi M, Srikar R, Yarin AL, Megaridis CM, Gemeinhart RA. Mechanistic examination of protein release from polymer nanofibers. Molecular Pharmaceutics. 2009;6:641-7.
[248] Jiang X, Cao HQ, Shi LY, Ng SY, Stanton LW, Chew SY. Nanofiber topography and sustained biochemical signaling enhance human mesenchymal stem cell neural commitment. Acta Biomaterialia. 2012;8:1290-302.
[249] Kim K, Luu YK, Chang C, Fang D, Hsiao BS, Chu B, et al. Incorporation and controlled release of a hydrophilic antibiotic using poly(lactide-co-glycolide)-based electrospun nanofibrous scaffolds. Journal of Controlled Release. 2004;98:47-56.
[250] Meng ZX, Zheng W, Li L, Zheng YF. Fabrication, characterization and in vitro drug release behavior of electrospun PLGA/chitosan nanofibrous scaffold. Materials Chemistry and Physics. 2011;125:606-11.
[251] Davis G, Ragina N, Lee S, Nguyen D, Hill C, Senagore A, et al. Abstract 12: Adipose derived stem cell therapy rescues delayed wound healing in chronic radiation injury. Plastic and Reconstructive Surgery. 2012;130:19.
[252] Hori K, Sotozono C, Hamuro J, Yamasaki K, Kimura Y, Ozeki M, et al. Controlled-release of epidermal growth factor from cationized gelatin hydrogel enhances corneal epithelial wound healing. Journal of Controlled Release. 2007;118:169-76.
[253] Liu Y, Cai S, Shu XZ, Shelby J, Prestwich GD. Release of basic fibroblast growth factor from a crosslinked glycosaminoglycan hydrogel promotes wound healing. Wound Repair and Regeneration. 2007;15:245-51.
[254] Zeugolis DI, Khew ST, Yew ESY, Ekaputra AK, Tong YW, Yung L-YL, et al. Electro-spinning of pure collagen nano-fibres – Just an expensive way to make gelatin? Biomaterials. 2008;29:2293-305.
[255] Plowman J, Deb-Choudhury S, Dyer J. Fibrous Protein Nanofibers. In: Gerrard JA, editor. Protein Nanotechnology: Humana Press; 2013. p. 61-76.
[256] Jena A, Gupta K. Characterization of Pore Structure of Filter Media. Fluid/Part Sep J. 2002;14:227-41.
[257] Jena A, Gupta K. Pore volume of nanofiber nonvwovens. Int Nonwovens J. 2005;14:25-30.
[258] Eichhorn SJ, Sampson WW. Statistical geometry of pores and statistics of porous nanofibrous assemblies. J R Soc Interface. 2005;2:309-18.
[259] Wong S-C, Baji A, Leng S. Effect of fiber diameter on tensile properties of electrospun poly(ε-caprolactone). Polymer. 2008;49:4713-22.
[260] Ulubayram K, Cakar AN, Korkusuz P, Ertan C, Hasirci N. EGF containing gelatin-based wound dressings. Biomaterials. 2001;22:1345-56.
[261] Zhang YZ, Wang X, Feng Y, Li J, Lim CT, Ramakrishna S. Coaxial electrospinning

of (Fluorescein isothiocyanate-conjugated bovine serum albumin)-encapsulated poly(ε-caprolactone) nanofibers for sustained release. Biomacromolecules. 2006;7:1049-57.
[262] Baer PC. Adipose-derived stem cells and their potential to differentiate into the epithelial lineage. Stem Cells and Development. 2011;20:1805-16.
[263] Hettiaratchy S, Dziewulski P. ABC of burns. Introduction. BMJ. 2004;328:1366-8.
[264] Guo R, Xu S, Ma L, Huang A, Gao C. The healing of full-thickness burns treated by using plasmid DNA encoding VEGF-165 activated collagen–chitosan dermal equivalents. Biomaterials. 2011;32:1019-31.
[265] Beachley V, Wen XJ. Fabrication of nanofiber reinforced protein structures for tissue engineering. Materials Science & Engineering C-Materials for Biological Applications. 2009;29:2448-53.
[266] Friedmann H, Lubart R, Laulicht I, Rochkind S. A possible explanation of laser-induced stimulation and damage of cell cultures. Journal of Photochemistry and Photobiology B: Biology. 1991;11:87-91.
[267] Bai H, McCaig CD, Forrester JV, Zhao M. DC electric fields induce distinct preangiogenic responses in microvascular and macrovascular cells. Arteriosclerosis, Thrombosis, and Vascular Biology. 2004;24:1234-9.
[268] Feedar JA, Kloth LC, Gentzkow GD. Chronic dermal ulcer healing enhanced with monophasic pulsed electrical stimulation. Physical Therapy. 1991;71:639-49.
[269] Brighton C, Wang W, Srldes R, Zhang G, Pollack S. Single transduction in electrically stimulated bone cells. J Bone Joint Surg Am. 2001;83-A:1514-23.
[270] Conlan MJ, Rapley JW, Cobb CM. Biostimulation of wound healing by low-energy laser irradiation A review. Journal of Clinical Periodontology. 1996;23:492-6.
[271] Desmet KD, Paz DA, Corry JJ, Eells JT, Wong-Riley MTT, Henry MM, et al. Clinical and experimental applications of NIR-LED photobiomodulation. Photomedicine and Laser Surgery. 2006;24:121-8.
[272] Cannon JP, Bearden SD, Gold SA. Effect of wetting solvent on poly(3-hexylthiophene) (P3HT) nanotubles fabricated via template wetting. Synthetic Metals. 2010;160:2623-7.
[273] Santos A, Forment P, Pallar J, Ferr?Borrull J, Marsal LF. Fabrication and characterization of high-density arrays of P3HT nanopillars on ITO/glass substrates. Solar Energy Materials and Solar Cells. 2010;94:1247-53.
[274] Sundarrajan S, Murugan R, Nair AS, Ramakrishna S. Fabrication of P3HT/PCBM solar cloth by electrospinning technique. Materials Letters. 2010;64:2369-72.
[275] Cheng M, Deng J, Yang F, Gong Y, Zhao N, Zhang X. Study on physical properties and nerve cell affinity of composite films from chitosan and gelatin solutions. Biomaterials. 2003;24:2871-80.
[276] Ramakrishna S, Fujihara K, Teo WE, LIn TC, Ma Z. Electrospinning process. Electrospinning and Nanofibres. An introduction to electrospinning and nanofibers. Singapore: World scientific publishing; 2005. p. 98-9.
[277] Jin GR, Prabhakaran MP, Nadappuram BP, Singh G, Kai D, Ramakrishna S. Electrospun poly(L-Lactic Acid)-co-poly(epsilon-caprolactone) nanofibres containing silver nanoparticles for skin-tissue engineering. Journal of Biomaterials Science-Polymer Edition. 2012;23:2337-52.
[278] Jena A, Gupta K. Pore volume of nanofiber nonwovens. Int Nonwovens J.

2005;14:25-30.
[279] Chan KHK, Yamao T, Kotaki M, Hotta S. Unique structural features and electrical properties of electrospun conjugated polymer poly(3-hexylthiophene) (P3HT) fibers. Synthetic Metals. 2010;160:2587-95.
[280] McCullough PCERD. Handbook of conducting polymers. New York1998.
[281] Bredas JL. Relationship between band-gap and bond length alternation in organic conjugated polymers. Journal of Chemical Physics. 1985;82:3808-11.
[282] Shrotriya V, Ouyang J, Tseng RJ, Li G, Yang Y. Absorption spectra modification in poly(3-hexylthiophene):methanofullerene blend thin films. Chemical Physics Letters. 2005;411:138-43.
[283] Brighton CT, Wang W, Seldes R, Zhang G, Pollack SR. Signal Transduction in Electrically Stimulated Bone Cells. The Journal of Bone & Joint Surgery. 2001;83:1514-23.
[284] Tomlinson S, MacNeil S, Walker S, Ollis C, Merrit J, Brown B. Calmodulin and cell function. Clin Sci. 1984;66:497-507.
[285] Bachs O, Lanini L, Serratosa J, Coll MJ, Bastos R, Aligue R, et al. Calmodulin-binding proteins in the nuclei of quiescent and proliferatively activated rat liver cells. Journal of Biological Chemistry. 1990;265:18595-600.
[286] Shefer G, Oron U, Irintchev A, Wernig A, Halevy O. Skeletal muscle cell activation by low-energy laser irradiation: A role for the MAPK/ERK pathway. Journal of Cellular Physiology. 2001;187:73-80.
[287] Gao X, Xing D. Molecular mechanisms of cell proliferation induced by low power laser irradiation. Journal of Biomedical Science. 2009;16:1-16.
[288] Braun DC, Garfield SH, Blumberg PM. Analysis by fluorescence resonance energy transfer of the interaction between ligands and protein kinase Cδ in the intact cell. Journal of Biological Chemistry. 2005;280:8164-71.
[289] Rhee SG, Bae YS. Regulation of Phosphoinositide-specific Phospholipase C Isozymes. Journal of Biological Chemistry. 1997;272:15045-8.
[290] Musashi M, Ota S, Shiroshita N. The role of protein kinase C isoforms in cell proliferation and apoptosis. Int J Hematol. 2000;72:12.
[291] Minana M, Cabedo H, Felipo V, Grisolia S. Inhibition of the proliferation of primary cell cultures and of L-132 cells by protein kinase C inhibitors. Cancer J. 1993;6:136-41.
[292] Yoshimura T, Goda S, Kobayashi T, Goto I. Involvement of protein kinase C in the proliferation of cultured Schwann cells. Brain Research. 1993;617:55-60.
[293] Cooper J. Effects of cytochalasin and phalloidin on actin. J Cell Biol. 1987;105:1473-8.
[294] Huang PJ, Huang YC, Su MF, Yang TY, Huang JR, Jiang CP. In vitro observations on the influence of copper peptide aids for the LED photoirradiation of fibroblast collagen synthesis. Photomedicine and Laser Surgery. 2007;25:183-90.
[295] Cho M, Thatte H, Lee R, Golan D. Integrin-dependent human macrophage migration induced by oscillatory electrical stimulation. Annals of Biomedical Engineering. 2000;28:234-43.
[296] Jin G, Prabhakaran MP, Kai D, Kotaki M, Ramakrishna S. Electrospun photosensitive nanofibers: potential for photocurrent therapy in skin regeneration. Photochemical & Photobiological Sciences. 2013;12:124-34.

[297] Günter CI, Machens HG. New strategies in clinical care of skin wound healing. European Surgical Research. 2012;49:16-23.
[298] Jin G, Prabhakaran MP, Kai D, Ramakrishna S. Controlled release of multiple epidermal induction factors through core–shell nanofibers for skin regeneration. European Journal of Pharmaceutics and Biopharmaceutics.
[299] Carpenter G, Cohen S. Epidermal Growth Factor. Annual Review of Biochemistry. 1979;48:193-216.
[300] Hong JP, Kim YW, Jung HD, Jung KI. The effect of various concentrations of human recombinant epidermal growth factor on split-thickness skin wounds. International Wound Journal. 2006;3:123-32.
[301] Lee A-R. Enhancing dermal matrix regeneration and biomechanical properties of 2nd degree-burn wounds by EGF-impregnated collagen sponge dressing. Arch Pharm Res. 2005;28:1311-6.
[302] Matsumoto Y, Kuroyanagi Y. Development of a wound dressing composed of hyaluronic acid sponge containing arginine and epidermal growth factor. Journal of Biomaterials Science, Polymer Edition. 2010;21:715-26.
[303] Nishimura KY, Isseroff RR, Nuccitelli R. Human keratinocytes migrate to the negative pole in direct current electric fields comparable to those measured in mammalian wounds. Journal of Cell Science. 1996;109:199-207.
[304] Sun N, Panetta NJ, Gupta DM, Wilson KD, Lee A, Jia F, et al. Feeder-free derivation of induced pluripotent stem cells from adult human adipose stem cells. Proceedings of the National Academy of Sciences of the United States of America. 2009;106:15720-5.
[305] Guilak F, Lott KE, Awad HA, Cao Q, Hicok KC, Fermor B, et al. Clonal analysis of the differentiation potential of human adipose-derived adult stem cells. Journal of cellular physiology. 2006;206:229-37.
[306] Watt FM, Green H. Involucrin synthesis is correlated with cell size in human epidermal cultures. The Journal of Cell Biology. 1981;90:738-42.
[307] Arai K, Nakamura Y, Hachiya Y, Tsuchiya H, Akimoto R, Hosoki K, et al. Pulsed electric current induces the differentiation of human keratinocytes. Mol Cell Biochem. 2013:1-7.
[308] Li D, Wang Y, Xia Y. Electrospinning of polymeric and ceramic nanofibers as uniaxially aligned arrays. Nano Letters. 2003;3:1167-71.
[309] Li D, Xia Y. Electrospinning of nanofibers: Reinventing the wheel? Advanced Materials. 2004;16:1151-70.
[310] Xie JW, MacEwan MR, Ray WZ, Liu WY, Siewe DY, Xia YN. Radially aligned, electrospun nanofibers as dural substitutes for wound closure and tissue regeneration applications. Acs Nano. 2010;4:5027-36.